The Dynamics of Turbulent Fountains in Homogeneous and Stratified Fluids

Lynn J Bloomfield

A thesis submitted for the degree of

Doctor of Philosophy at

The Australian National University

November 1999

Except where otherwise indicated, this thesis is my own original work.

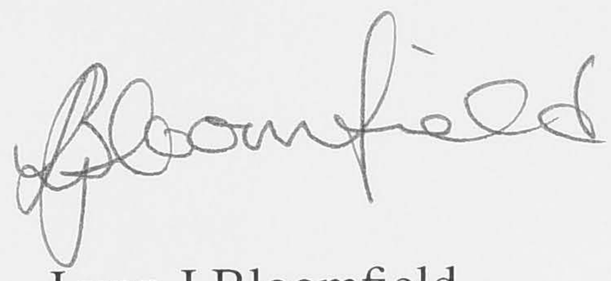

Lynn J Bloomfield

15 November 1999

For Grandad

Acknowledgements

The scientist does not study nature because it is useful;

he studies it because he delights in it,

and he delights in it because it is beautiful.

If nature were not beautiful,

it would not be worth knowing,

and if nature were not worth knowing,

life would not be worth living.

Henri Poincaré (1854 - 1912)

French Mathematician

Acknowledgements

Throughout the past three and a half years, many people have offered me their support, guidance and friendship.

First and foremost, I must thank my supervisors: Dr Ross Kerr, Prof. Ross Griffiths and Emer. Prof. Stewart Turner. The fact that much of my work has already been published is due to the support and encouragement of Ross Kerr, both in motivating me to write up my work and in the editing of draft manuscripts. Both Ross Griffiths and Stewart Turner have also provided considerable support during the course of my Ph.D, and their help and advice are gratefully acknowledged.

I also wish to thank Tony Beasely, Derek Corrigan and Ross Wylde-Brown for their technical assistance with the experiments, and all of the people in the Geophysical Fluid Dynamics group for creating a friendly working atmosphere and stimulating working environment. I'd particularly like to thank those who weren't able to run away fast enough when I was looking for prospective proof-readers (Graham Hughes, Mathew Wells and David Osmond).

I am forever grateful to my family for their long-distance support and, more importantly, for their continued belief in me and in my abilities to achieve all that I have.

Finally, I am grateful to all my friends for making Canberra a home away from home. To Jacki, for always being there for me when I needed a friend, right from the start of my honours year. To Jan, for her friendship and for her television and X-files video collection. To Jason, for understanding all the trials and tribulations, and for taking the time to proof-read this thesis. Lastly, to Matt, for his friendship from day one, and for his love and support throughout this final year.

Abstract

An experimental and theoretical investigation of the dynamics of turbulent fountains in homogeneous and stratified surroundings is presented. Experiments show that a dense fluid injected upwards into a lighter environment rises to an initial height above the source before the flow comes to rest and then reverses direction. The initial height is reduced to a final height as the upflow interacts turbulently with the subsequently formed downflow. The downflow then either spreads along the base of the tank or intrudes at an intermediate height in the environment. Whether basal or intermediate spreading occurs depends on the value of a dimensionless parameter, σ, which is related to the strength of the ambient density stratification and the fluxes of momentum and buoyancy at the source. It is shown that basal spreading occurs when $\sigma < \sigma_c$ and intermediate intrusion occurs when $\sigma > \sigma_c$, where σ_c is determined experimentally for axisymmetric and line fountains. The initial, final and spreading heights of the fountain are measured as a function of σ, and dimensional arguments are used in combination with experimental measurements to determine expressions for the fountain heights in the limits of $\sigma = 0$ and $\sigma \to \infty$.

In an environment of finite extent, the continued addition of dense fluid upward through either a point or line source results in the spreading layer increasing in thickness. For $\sigma < \sigma_c$ the density stratification that is established in the basal spreading layer is comparable to, or stronger than, the ambient density gradient. Conversely, the intermediate spreading layer that forms when $\sigma > \sigma_c$ becomes almost homogeneous. Expressions are developed to quantify the motion of the ascending and descending fronts that mark the vertical extent of the spreading layer, and it is shown that an ambient density stratification has a negligible effect on the motion of these fronts. The motion of the ascending front does, however, depend on the fountain height, which increases as the environment becomes homogeneously mixed. The evolution of the ambient density profile from linearly stratified to homogeneous is accurately predicted using a numerical model.

The turbulent mixing that occurs between the upflow and downflow of an axisymmetric

fountain is examined theoretically for fountains in both homogeneous and stratified surroundings. The theoretical model quantifies the entrainment of ambient fluid into the fountain upflow, as well as the entrainment of fluid from both the upflow and the environment into the downflow. Four different variations of the model are considered, comprising the two most reasonable formulations of the body forces acting on the 'double' structure and two formulations of the rate of entrainment between the flows. The best agreement between the calculated and experimentally measured fountain properties is obtained when the rates of entrainment into the upflow and downflow are proportional to the velocity of the respective flows, and the buoyancy of the upflow is measured relative to the accelerating downflow. Similar theoretical models are also developed to describe line fountains in a stratified fluid with both symmetric and asymmetric profiles. The results calculated from the symmetric model give better agreement with experimental measurements than the results from the asymmetric model.

Finally, the results of the experimental and theoretical investigation have been used to analyse two physical problems: the replenishment of magma chambers and the heating or cooling of a room.

Contents

Acknowledgements v

Abstract vi

1 Overview 1

1.1 Turbulent jets, plumes and fountains 2

1.2 Previous work 3

1.3 Aims and outline 6

2 Turbulent Fountains in an Unbounded Stratified Fluid 7

2.1 Qualitative observations 8

2.2 Axisymmetric fountains 11

2.2.1 Experimental techniques 11

2.2.2 Theoretical techniques 14

2.2.3 Homogeneous fluid 15

2.2.4 Zero buoyancy flux at the source 16

2.2.5 Non-zero buoyancy flux at the source 18

2.3 Line fountains 23

2.3.1 Experimental techniques 23

2.3.2 Homogeneous fluid 24

2.3.3 Zero buoyancy flux at the source 26

2.3.4 Non-zero buoyancy flux at the source 27

2.4 Conclusions 31

3 Turbulent Fountains in a Confined Stratified Fluid 32

3.1 Qualitative observations 33

3.2 Axisymmetric fountains 37

3.2.1 The descending front 37
3.2.2 The ascending front 39
3.2.3 The fountain height 40
3.2.4 Outflow dynamics — the assumption of instantaneous spreading 44
3.2.5 Experimental results 47
3.2.6 The ambient density profile 49
3.3 Line fountains 51
3.3.1 The descending front 51
3.3.2 The ascending front 52
3.3.3 The fountain height 53
3.3.4 Outflow dynamics 54
3.3.5 Experimental results 55
3.3.6 The ambient density profile 58
3.4 Conclusions 59

4 Theoretical Models of Turbulent Fountains **61**

4.1 Previous theoretical investigations 62
4.2 An axisymmetric turbulent fountain in a homogeneous fluid 62
4.2.1 Entrainment 69
4.2.1.1 Entrainment formulation I 69
4.2.1.2 Entrainment formulation II 69
4.2.2 The numerical method 70
4.2.3 Results and comparison with experiments 71
4.3 An axisymmetric fountain in a stratified fluid 77
4.3.1 Results 79
4.3.1.1 Theoretical results for $\sigma \to \infty$ 79
4.3.1.2 Theoretical results for $0 < \sigma < \infty$ 80
4.4 A line fountain in a stratified fluid 82
4.4.1 Symmetric profile 82
4.4.1.1 Results and comparison with experiment 86
4.4.2 Asymmetric profile 87

4.4.2.1 Results and comparison with experiments 88
4.5 Conclusions 90

5 Applications **92**
5.1 Introduction 93
5.2 Fountains to heat or cool buildings 94
5.2.1 A fountain of cold air in a warm room 94
5.2.2 Fountains of hot air in an aircraft hanger 96
5.3 Fountains in magma chambers 99
5.3.1 Magma chamber evolution and replenishment 101
5.3.2 Rapid replenishment by a dense parent magma 101
5.3.2.1 Homogeneous magma 103
5.3.2.2 Stratified magma 105
5.3.3 Double-diffusive fountains 107
5.3.3.1 Homogeneous magma 107
5.3.3.2 Stratified magma: $0 < \sigma^* < \infty$ 108
5.3.3.3 Stratified magma: $\sigma^* \to \infty$ 109
5.3.4 Effects of viscosity 109
5.3.5 Geological interpretation and implications 110
5.4 Conclusions 111

6 Conclusions **112**
6.1 Summary of results 113
6.2 Further work 113

Bibliography **116**

List of Figures

1.1 Illustrations of the turbulent plumes and fountains that have been investigated in the past. 5

2.1 Photographs of an axisymmetric fountain in a stratified fluid with a zero buoyancy flux at the source. 9

2.2 Photographs of a line fountain in a stratified fluid with a zero buoyancy flux at the source. 10

2.3 The experimental setup. 11

2.4 The measured position of the front formed by an axisymmetric jet in a homogeneous environment. 13

2.5 Experimental measurements of the initial and final heights of an axisymmetric fountain in a homogeneous fluid. 16

2.6 Experimental measurements of the initial, final and spreading heights of an axisymmetric fountain in a stratified fluid with a zero buoyancy flux at the source. 17

2.7 Dimensionless initial and final heights of an axisymmetric fountain in a stratified fluid. 20

2.8 Ratio of the initial to final height of an axisymmetric fountain showing the decrease in the ratio as the spreading height increases. 21

2.9 Dimensionless spreading height of an axisymmetric fountain in a stratified fluid. 22

2.10 Experimental data showing the two regimes of axisymmetric fountain behaviour represented by basal and intermediate spreading. 22

2.11 The measured position of the front formed by a line jet in a homogeneous environment. 24

2.12 Experimental measurements of the initial, final symmetric and final asymmetric heights of a line fountain in a homogeneous fluid. 25

2.13 Experimental measurements of the initial, final symmetric, final asymmetric and spreading heights of a line fountain in a stratified fluid with a zero buoyancy flux at the source. 26

2.14 Dimensionless initial, final symmetric, final asymmetric and spreading heights of a line fountain in a stratified fluid. 29

2.15 Experimental data showing the two regimes of line fountain behaviour represented by basal and intermediate spreading. 30

3.1 Photographs of an axisymmetric fountain in a confined stratified fluid with a zero buoyancy flux at the source. 34

3.2 Photographs of a line fountain in a confined stratified fluid with a zero buoyancy flux at the source. 36

3.3 Comparison between the calculated volume flux in the upflow of a fountain and the volume flux in a jet. 38

3.4 Experimental measurements of the evolving ambient density profile produced by an axisymmetric fountain. 41

3.5 Geometry illustrating the outflow of fluid into the spreading layer. 45

3.6 A comparison between the theoretical predictions and the experimental measurements of the positions of the axisymmetric fountain height, ascending front and descending front as a function of time. 48

3.7 Measurements of the ambient density profile produced by an axisymmetric fountain, in comparison with numerical predictions. 51

3.8 A comparison between the theoretical predictions and the experimental measurements of the positions of the line fountain height, ascending front and descending front as a function of time. 56

3.9 Measurements of the ambient density profile produced by a line fountain, in comparison with numerical predictions. 59

4.1 A schematic illustration of an axisymmetric turbulent fountain. 63

4.2 Comparison between two methods of finding the fountain height. 64

4.3 Model of a turbulent fountain, indicating the quantities and properties that are included in the equations. 65

4.4 Comparison between the numerical results and the experimental data of Mizushina *et al.* (1982). 73

4.5 Numerical calculations of the (a) velocity and (b) buoyancy in the downflow for each of the four formulations. 76

4.6 Three possible methods to determine the spreading height of an axisymmetric fountain in a stratified fluid. 78

4.7 Comparison between the numerical predictions and the experimental measurements of $f(\sigma)$ for the initial, final and spreading heights of an axisymmetric fountain. 81

4.8 Schematic illustration of a line fountain when the profile is (a) symmetric and (b) asymmetric. 83

5.1 Schematic illustration of a room that is cooled by the injection of a fountain of cold air through a vent in the floor. 95

5.2 Schematic illustration of an aircraft hanger that is heated by the injection of multiple fountains of hot air through vents in the ceiling. 97

5.3 Calculated time taken for the ascending front to reach the floor of an aircraft hanger, plotted against the final homogeneous air temperature. 99

5.4 Schematic illustration of a magma chamber. 100

5.5 The evolution of a MORB chamber during the process of fractionation. 102

List of Tables

1.1 Some major contributions to the study of turbulent fountains and plumes. . . . 3

2.1 Dimensionless values of the initial and final fountain heights in a homogeneous fluid that were measured in several experimental investigations. 15

4.1 Calculated results for the final height of an axisymmetric fountain in a homogeneous fluid. 72

4.2 Calculated values of the constants in the expression $z = C \times M_o^{1/4} N^{-1/2}$ for the final and spreading heights of an axisymmetric fountain as $\sigma \to \infty$. 80

4.3 Calculated results for the final symmetric and spreading heights of a line fountain as $\sigma^* \to \infty$. 86

4.4 Comparison between the symmetric and asymmetric heights of a line fountain calculated as $\sigma^* \to \infty$. 89

5.1 Assumed values of the parameters used in the calculations for a warm room cooled by a fountain of cold air. 95

5.2 Properties of the fountain and the ambient temperature profile produced when a fountain cools an initially stratified room. 96

5.3 Assumed values of the parameters used in the calculations for a cold aircraft hanger heated by a series of fountains of hot air. 97

5.4 Properties of line fountains injected into a magma chamber at various stages in the fractionation sequence 104

Chapter 1

Overview

"The beginning of knowledge is the discovery of something we do not understand."

Frank Herbert (1920 - 1986)

American Author

The fluid motions that are driven by buoyant convection are widespread and varied (Turner 1973). This investigation focuses on the dynamics of turbulent fountains – flows which are formed when heavy fluid is injected rapidly upwards into a lighter ambient fluid. Turbulent jets, plumes and fountains are introduced in §1.1, and some previous investigations into these flows are summarized in §1.2. In §1.3 I present the aims of this investigation and outline the work presented in this thesis.

1.1 Turbulent jets, plumes and fountains

The cloud of smoke and ash from a volcanic eruption, the rise of cigarette smoke, sewerage outfalls and large scale ocean mixing are just a few manifestations of turbulent buoyant flows. These flows exhibit a variety of behaviours, depending on the momentum of the injected fluid and on any differences in density between the injected and ambient fluids. One feature that is common to all of these examples is that the shear between the flow and the environment leads to the formation of large eddies on the edge of the flow, which randomly engulf the ambient fluid, folding it into the flow where it is thoroughly mixed by turbulence at smaller scales. This mixing, or *entrainment*, of ambient fluid into the turbulent flow results in the volume flux in the flow increasing with distance from the source. The subsequent dynamics of the flow depend on any density differences between the two fluids and on the momentum of the injected fluid. Depending on the fluxes of buoyancy and momentum at the source, the flow is classified as either a jet, plume or fountain.

A *turbulent jet* is a momentum-driven flow which arises when the source fluid is injected into an identical ambient fluid. In the absence of any density differences, the momentum flux of the flow remains constant, while the entrainment of ambient fluid increases the volume flux.

If source fluid is released from rest into an ambient fluid of different density, the resulting buoyancy-driven flow is called a *turbulent plume*. The buoyancy forces acting on the flow result in an increase in the momentum flux with height while the entrainment of ambient fluid decreases the density difference between the plume and its surroundings. While a plume is a source of buoyancy only, a *forced plume* is driven by both momentum and buoyancy. If the momentum and buoyancy act in the same direction (when a lighter fluid is injected upwards into a heavy ambient fluid, for example), the flow undergoes a transition from the initial jet-like flow to a plume-like flow at greater heights. When the initial momentum is opposed by the buoyancy force, the resulting flow is called a *turbulent fountain*.

The turbulent fountains that are formed by injecting dense fluid upwards into a lighter environment experience a decrease in the density difference between the flow and environment due to the entrainment of lighter ambient fluid. At the same time, the opposing buoyancy causes the momentum flux to decrease until the flow eventually comes to rest. The heavy fluid then reverses direction and falls back around the central upflow.

1.2 Previous work

Our current understanding of turbulent plumes and fountains has arisen from a series of theoretical and experimental investigations (table 1.1) which span the past forty years (detailed reviews are presented by Fischer *et al.* (1979), List (1982) and Turner (1973, 1986)). Most of the theoretical studies have relied on a basic assumption, first conceptualized by G.I. Taylor and published by Batchelor (1954), that quantifies the rate of entrainment of ambient fluid into the flow. This *entrainment assumption* – that the velocity with which ambient fluid is entrained into a turbulent flow at any height is proportional to a characteristic velocity of the flow at that height – first arose from dimensional considerations of a turbulent plume, but has been applied with equal success to other turbulent flows.

Environment	Plumes	Fountains
Unbounded homogeneous	Morton, Taylor & Turner (1956)	Morton (1959a); Turner (1966)
Unbounded stratified	Morton, Taylor & Turner (1956)	Morton (1959a); **This study**
Confined homogeneous	Baines & Turner (1969)	Baines, Turner & Campbell (1990)
Confined stratified	Cardoso & Woods (1992)	**This study**

Table 1.1: Some major contributions to the study of turbulent fountains and plumes.

Taylor's entrainment assumption was extended in the pioneering work of Morton, Taylor & Turner (1956), which is the commonly stated starting point of this subject. They used the entrainment assumption to derive a set of *entrainment equations* which quantify the conservation of the fluxes of volume, momentum and buoyancy in a turbulent flow. Solutions of the equations were presented for plumes in both homogeneous and stratified environments (figure 1.1a,b). In a linearly stratified fluid, the solution of the entrainment equations quantified the decreasing density difference between the plume fluid and the environment as the ambient density becomes lighter with height and the plume fluid becomes heavier due to the entrainment of ambient fluid. The density difference eventually vanishes at a height of neutral buoyancy, although the plume continues to rise some distance above this height. As the flow is now heavier than the environment, the momentum flux decreases until the rising fluid comes to rest. The plume fluid then falls back a small distance towards the source before intrud-

ing laterally into the environment. Hence, while a plume rises indefinitely in homogeneous surroundings, the rise of the plume in a stratified fluid is restricted by the ambient density gradient. To complement their theoretical analysis of plumes rising in an unbounded stratified environment, Morton *et al.* (1956) also performed some experiments in which fresh water was released into a large tank of stratified salt water. These experimental results were combined with a dimensional argument to give expressions for both the terminal height of the plume and the height of intrusion.

Morton (1959a) then continued to extend the work of Morton *et al.* (1956) to include a theoretical analysis of forced plumes, of which turbulent fountains are one example (figure 1.1c). He used the entrainment equations to quantify the dynamics of the dense fluid injected upwards into both homogeneous and stratified surroundings. However, these equations are only valid until the velocity of the first element of fluid in the flow is reduced to zero at the initial fountain height. To investigate the flow after the fluid has reversed direction, laboratory experiments are needed. Experiments in a homogeneous environment (Turner 1966) showed that the turbulent interactions between the upflow and downflow restrict the rise of any further fluid and thus immediately reduce the initial fountain height to a smaller final height. This observed final height was related to the momentum and buoyancy fluxes at the source using dimensional arguments, and the relevant constant was found experimentally.

In each of the studies discussed so far, only the initial flow was investigated. In the numerous situations where these turbulent flows arise, however, the presence of confining boundaries results in the accumulation of source fluid in the environment. This addition of fluid causes the ambient density profile, and hence the dynamics of the flow, to evolve with time. The flow of a plume into a confined region containing an initially homogeneous fluid was first analysed by Baines & Turner (1969). They determined the changes to the environmental density profile as progressively lighter plume fluid arrives at the roof of the container and spreads laterally to form a stratified layer of increasing thickness (figure 1.1d). These *plume filling box* models were developed for plumes from both point and line sources. Similar filling box models have since been applied to axisymmetric plumes in an initially stratified fluid (Cardoso & Woods 1993) (figure 1.1e) and to fountains in initially homogeneous surroundings (Baines *et al.* 1990) (figure 1.1f).

The *fountain filling box* models developed by Baines *et al.* (1990) describe the flow of a

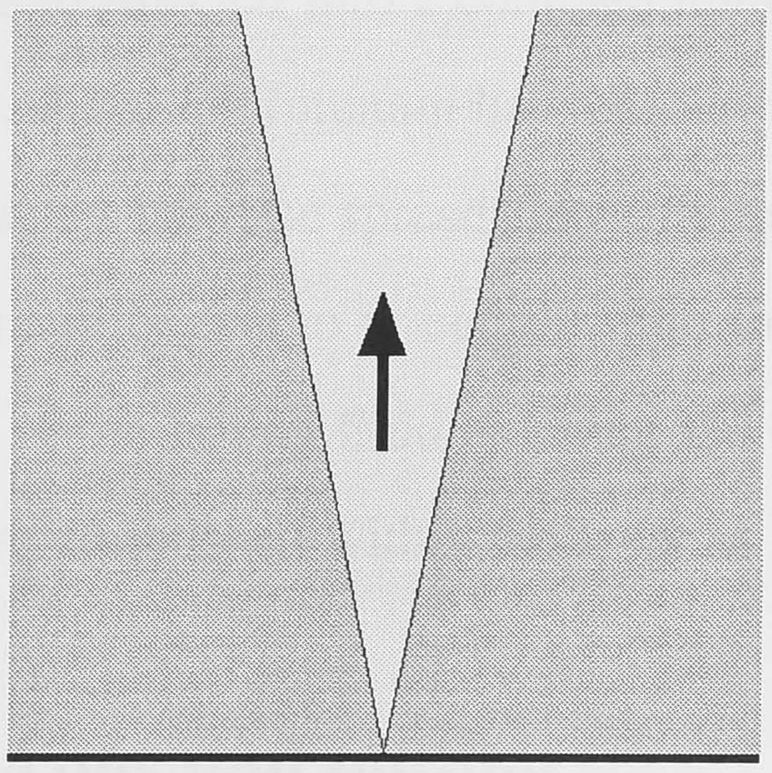

(a)

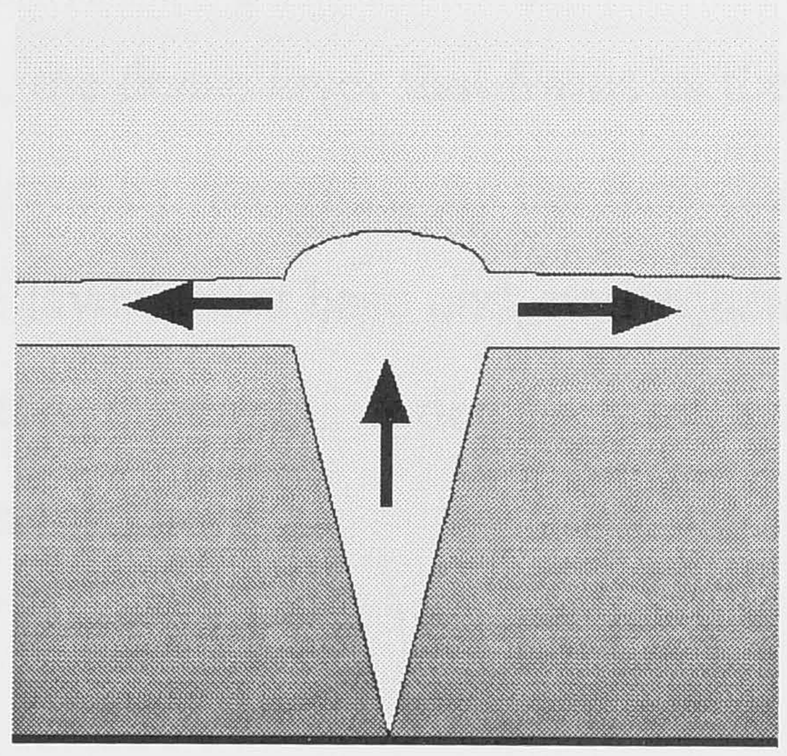

(b)

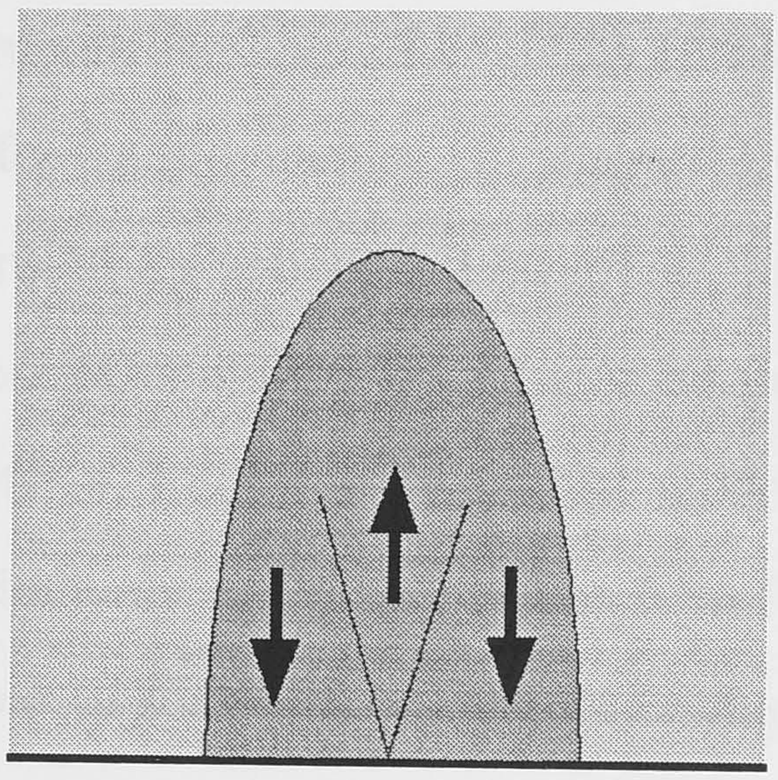

(c)

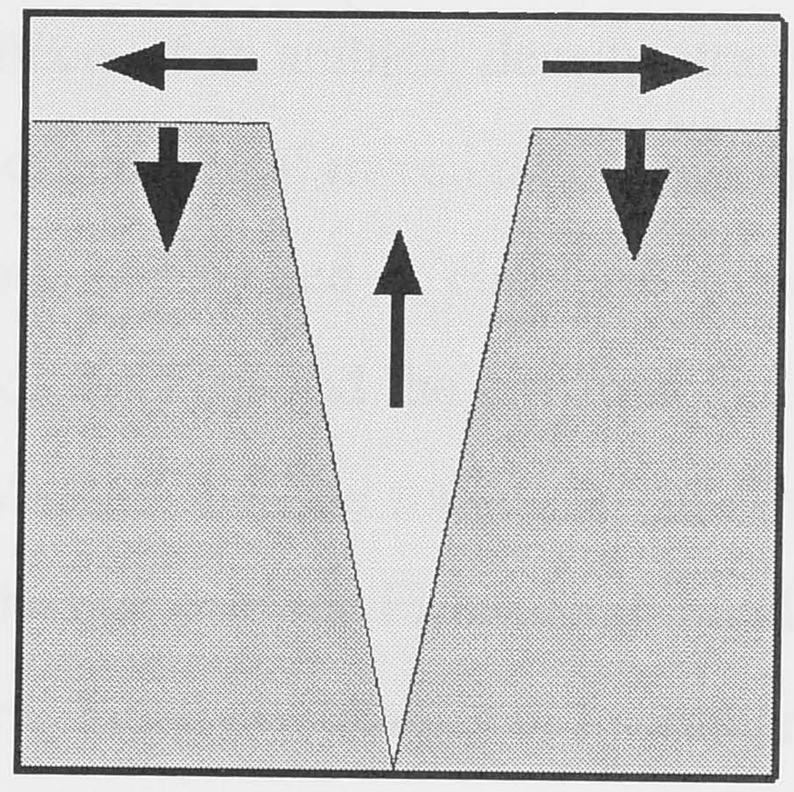

(d)

(e)

(f)

Figure 1.1: Illustrations of the turbulent plumes and fountains that have been investigated in the past: (a) plume in an unbounded homogeneous fluid (Morton *et al.* 1956), (b) plume in an unbounded stratified fluid (Morton *et al.* 1956), (c) fountain in an unbounded homogeneous fluid (Morton 1959a; Turner 1966), (d) plume in a confined homogeneous fluid (Baines & Turner 1969), (e) plume in a confined stratified fluid (Cardoso & Woods 1993) and (f) fountain in a confined homogeneous fluid (Baines *et al.* 1990).

dense fluid injected into a confined homogeneous region through both axisymmetric and line sources. After the fountain has reached a final height, the dense layer that forms as the downflow reaches the base spreads laterally until it is restricted by the walls. As the flow continues, the fountain begins to re-entrain fluid from the dense layer at the base and, consequently, the density of the falling fluid reaching the base continually increases. A density stratification is therefore established within the layer as it increases in thickness.

1.3 Aims and outline

The aim of this thesis is to explore the dynamics of turbulent fountains in homogeneous and stratified surroundings. I begin by focusing on the effects of an ambient density stratification on the fountain dynamics. In chapter 2, I present an experimental investigation into turbulent fountains in an unbounded stratified fluid. This work is extended in chapter 3 to consider the effect of confining boundaries on the evolution of the flow and the environment. Then, in chapter 4, I develop theoretical models of axisymmetric and line fountains. In chapter 5, I quantitatively apply this research to fountains of hot or cold air in buildings, and to the behaviour of fountains of magma in magma chambers. Finally in chapter 6, I summarize the work presented here and discuss some possible areas of future research.

Most of the research presented here has either been published or is under review. Chapter 2 constitutes Bloomfield & Kerr (1998), chapter 3 is reproduced from Bloomfield & Kerr (1999a) and the study in chapter 4 forms the basis for Bloomfield & Kerr (1999b).

Chapter 2

Turbulent Fountains in an Unbounded Stratified Fluid

"Observation and theory get on best when they are mixed together,
both helping one another in the pursuit of truth.
It is a good rule not to put overmuch confidence in a theory until
it has been confirmed by observation."

Sir Arthur Stanley Eddington (1882-1944)
English Astronomer and Physicist

In this chapter, I describe an experimental and theoretical study of turbulent fountains entering an unbounded stratified fluid through both point and line sources. A qualitative description of the flow of both axisymmetric and line fountains is presented in §2.1. In §2.2, I present the experimental and theoretical techniques, theoretical arguments and experimental results for axisymmetric fountains. A similar study of line fountains is then outlined in §2.3. The main results and conclusions of this study are summarised in §2.4.

2.1 Qualitative observations

Axisymmetric turbulent fountains are produced in the laboratory by injecting dense fluid upwards through a small nozzle into a tank containing a stably stratified fluid. The environmental fluid is entrained into the initial upflow, increasing the fountain radius (figure 2.1a), and decreasing the density of the fountain fluid. The momentum of the rising fluid is reduced by the opposing buoyancy force until the flow first comes to rest at an initial height above the source. The downflow which forms after this point continues to mix with the environment while also interacting turbulently with the upflow. This interaction restricts the rise of further fluid and therefore reduces the initial fountain height to a final value about which there are random fluctuations on the scale of 5 – 10% of the fountain height.

The final density of the downflow depends on the strength of the ambient stratification. In a homogeneous environment the falling fluid always remains denser than the ambient, so the flow must spread along the base of the tank (Turner 1966; Baines *et al.* 1990). However, when the density of the source fluid is the same as that at the base of a stable gradient, any entrainment of ambient fluid must reduce the density of the downflow to equal that in the environment at some intermediate height. At this point, the flow still has some downward momentum, so a small overshoot is observed before it intrudes into the environment (figure 2.1b). The thickness of the resulting outflow is comparable to the spreading height near the fountain axis but quickly becomes thinner with increasing radial distance (figure 2.1c). These two types of fountain behaviour — in a homogeneous fluid and in a stratified fluid with a zero buoyancy flux at the source — represent the two limiting cases in this study of fountains in a stratified fluid.

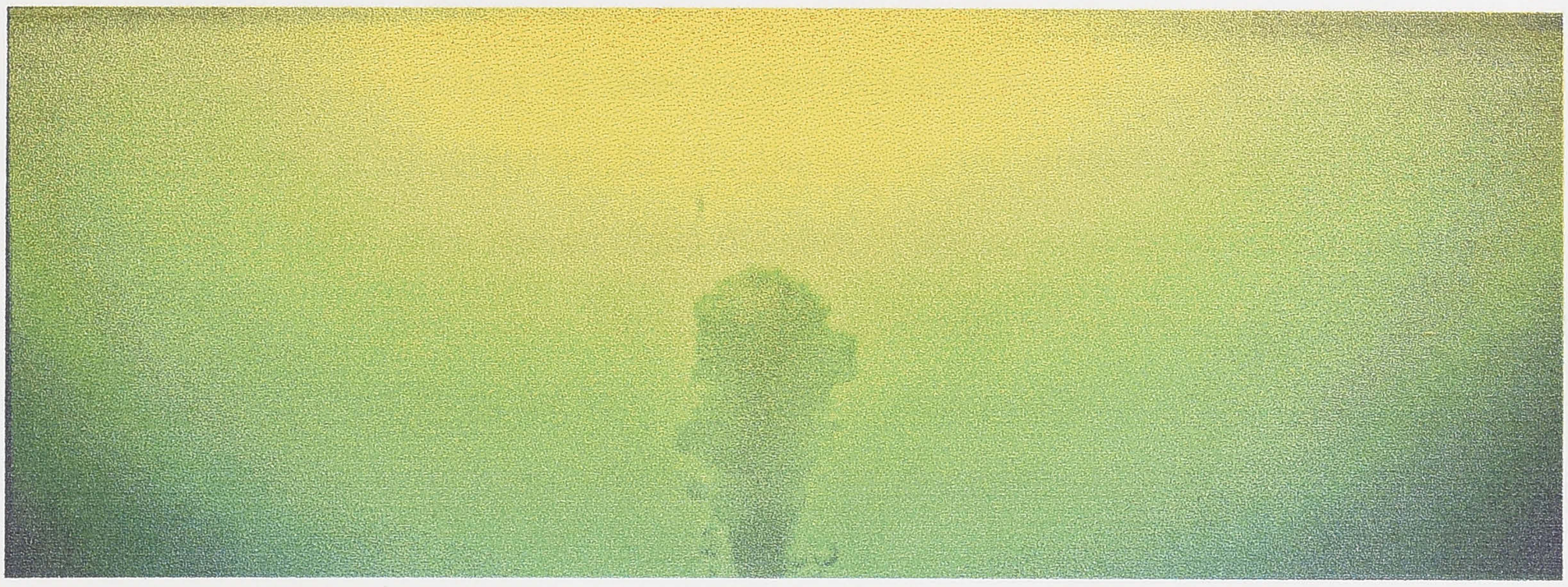

(a)

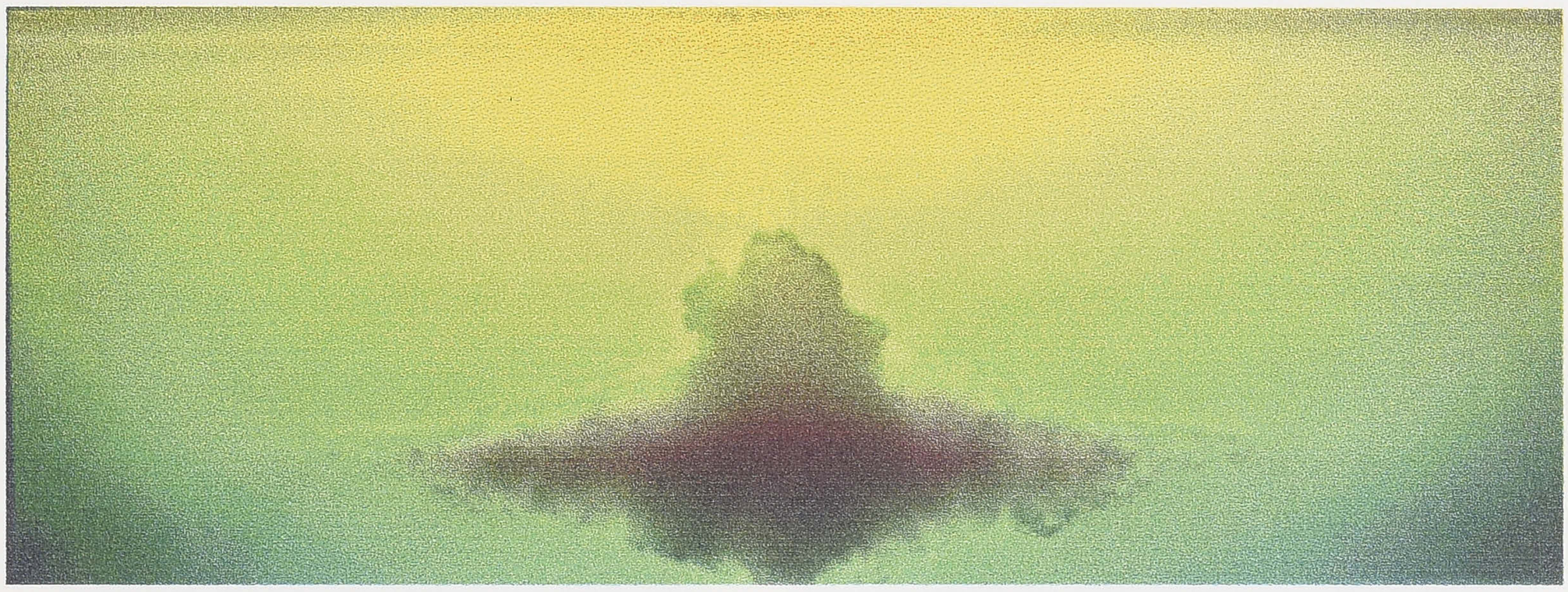

(b)

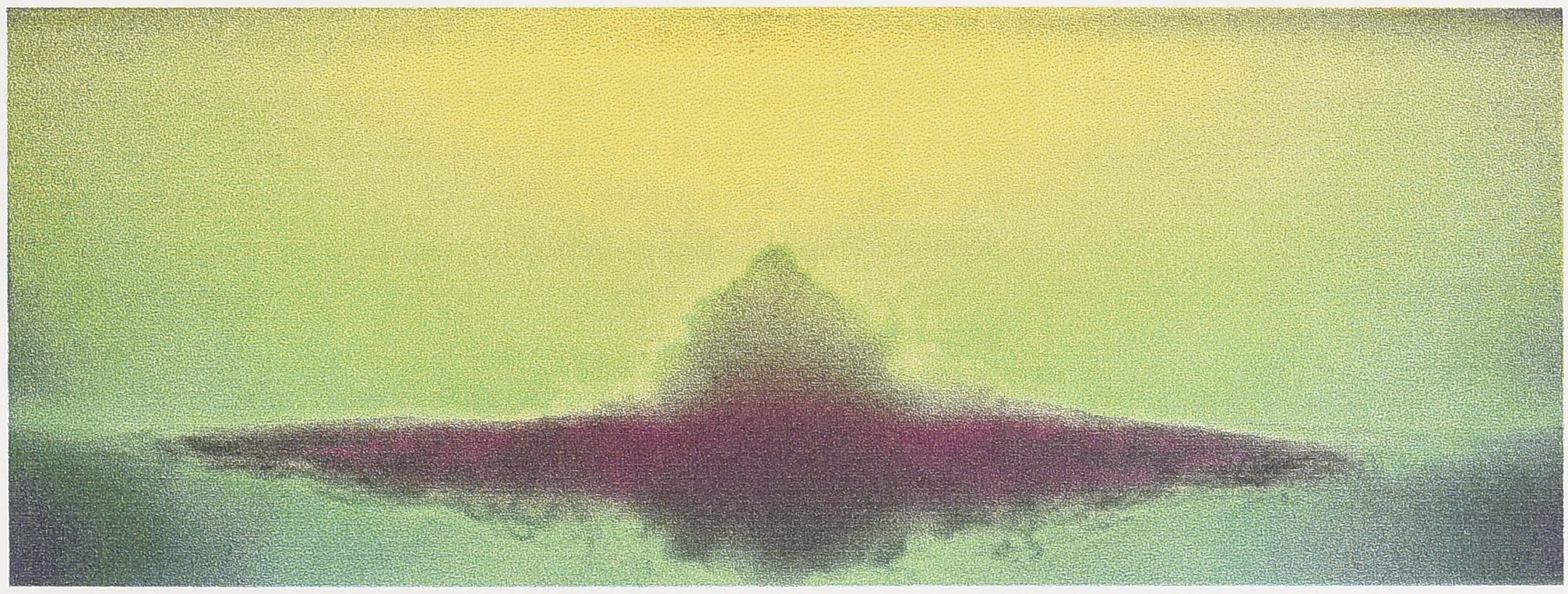

(c)

Figure 2.1: Photographs of an axisymmetric fountain where the density of the input fluid is equal to that at the base of the environment, the input volume flux is 4.5×10^{-5} m^3 s^{-1} and the density gradient is 0.3 kg m^{-4}. (a) The flow rises initially as a jet, entraining surrounding fluid ($t = 3$ s), until it reaches an initial height. (b) After reaching the initial height, the falling fluid intrudes into the environment ($t = 10$ s). (c) A layer forms as fluid continues to intrude at the same height ($t = 23$ s).

Qualitatively similar behaviour is observed when the dense fluid is injected through a slot, or line source. Just after starting the flow, the injected fluid rises through the environment until first coming to rest at an initial height. Depending on the strength of the stratification, the falling fluid may again either spread along the base or intrude into the environment at a height of neutral buoyancy (figure 2.2a). The thickness of this intruding layer once more decreases with increasing distance from the axis of the flow. The profile of a line fountain oscillates randomly between an asymmetric (figure 2.2a) and symmetric (figure 2.2b) profile. During the intervals in which the downflow is deflected to one side of the upflow, a corresponding decrease in the final fountain height is observed. These additional instabilities were also seen in a homogeneous environment (Baines *et al.* 1990), although the fluctuations appear to be reduced in the present case, resulting in a more stable fountain.

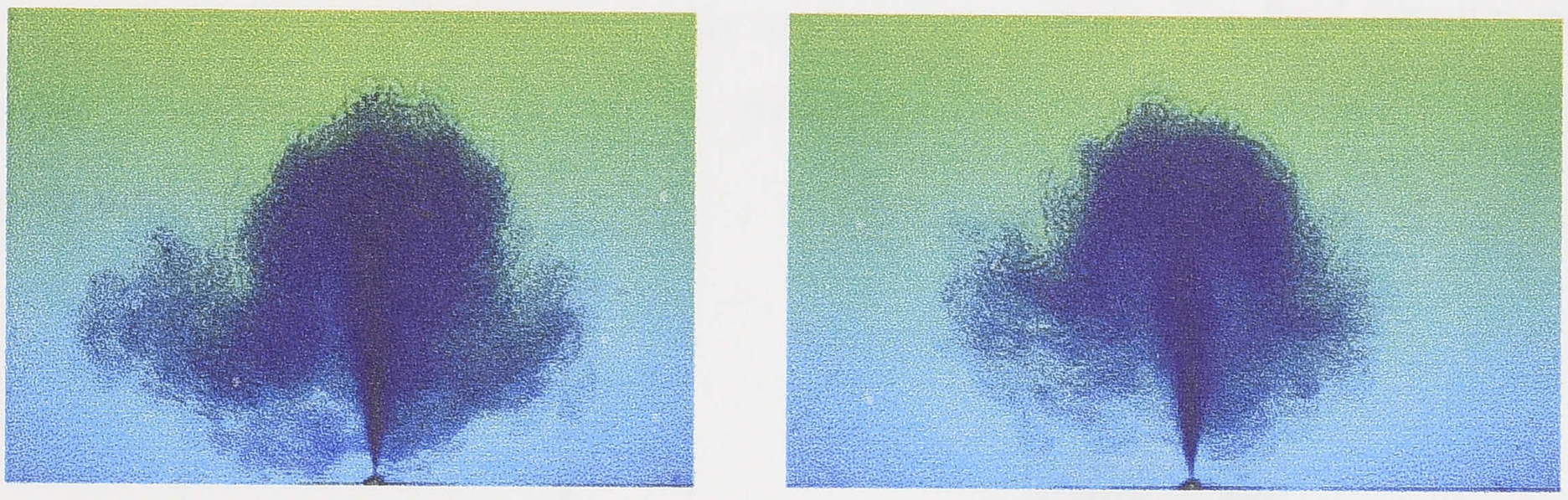

(a) (b)

Figure 2.2: Photographs of a line fountain where the density of the input fluid equals that at the base of the tank, the input volume flux per unit length is $8.8 \times 10^{-5}\ \mathrm{m^2\,s^{-1}}$ and the density gradient is $0.06\ \mathrm{kg\,m^{-4}}$. (a) After the fluid starts to intrude into the environment, the fountain profile may become asymmetric ($t = 30$ s). When this occurs, the fountain height decreases. (b) The fountain fluctuates randomly between an asymmetric and a symmetric profile ($t = 50$ s).

2.2 Axisymmetric fountains

In this section I present the analysis for axisymmetric fountains. In §2.2.1, I outline the experimental apparatus and techniques, before introducing the theoretical framework in §2.2.2. Experimental results are presented for three cases: a homogeneous fluid (§2.2.3), a stratified fluid in which the density of the source fluid equals that at the base of the stratification (§2.2.4), and the general case where the source fluid is denser than any fluid in the environment (§2.2.5).

2.2.1 Experimental techniques

The setup used in these experiments is illustrated in figure 2.3. The fountains were produced in an acrylic tank 38 cm $\times$ 38 cm in internal cross section and 80 cm deep, which was filled to a depth of approximately 25 cm. The ambient linear density gradient was established with NaCl solutions using the *double bucket* method (Oster 1965). The fluid densities were measured by refractometry to within 0.1%, giving a relative error in the density gradient of approximately 1%.

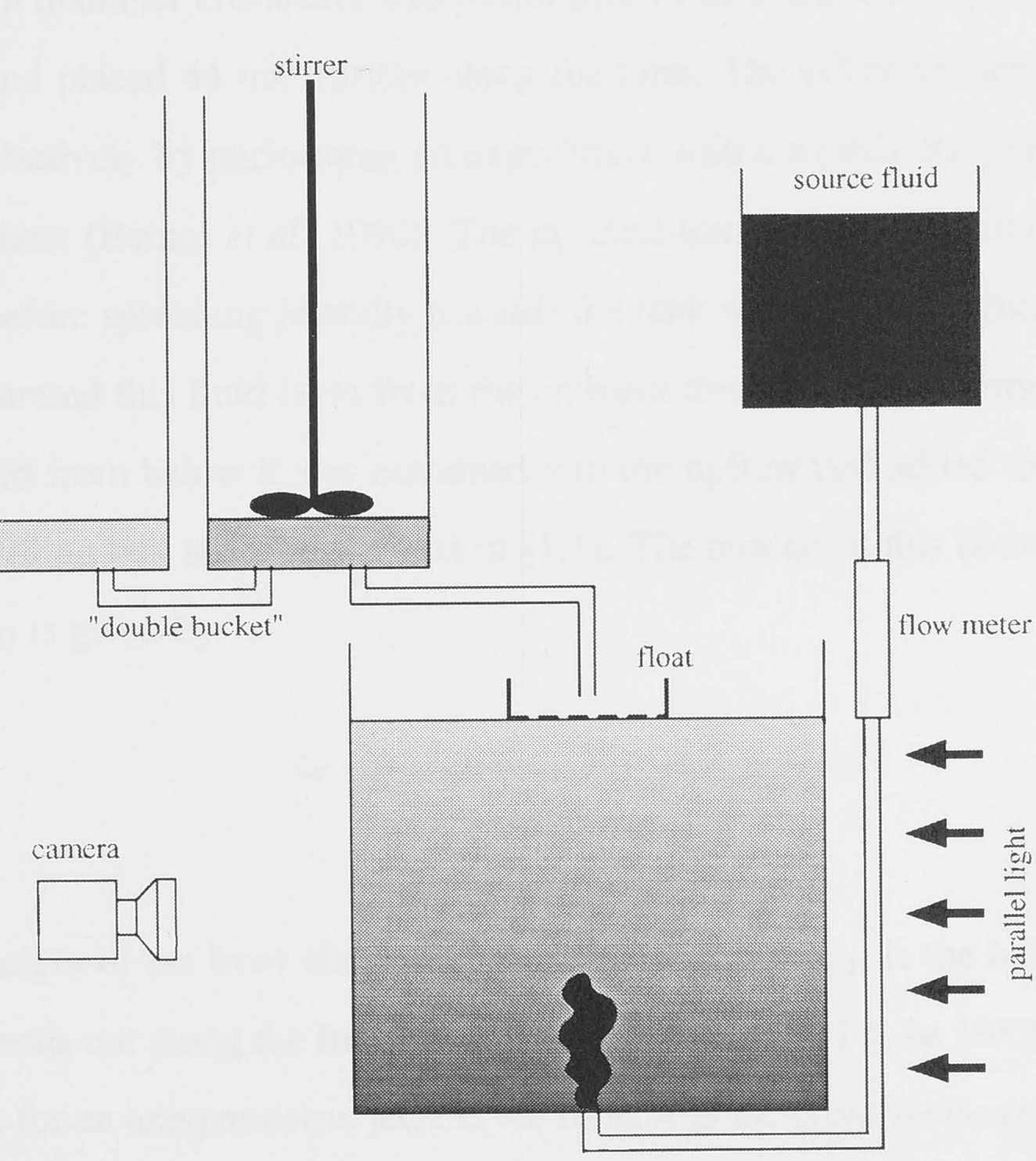

Figure 2.3: The experimental setup used in this investigation.

The source fluid was placed in a 20 l container which was raised 1.5 m higher than the main tank. The flow rate resulting from this gravitational head was adjusted with a valve and measured with a flow meter to an accuracy of 1 – 4%. The source fluid was injected upwards from the base of the tank through a tube with an 8.8 mm inner diameter.

The flows were observed using the *shadowgraph* method, in which parallel light incident on one side of the tank projects an image of the flow onto the opposite side. As the refractive index of the fluid is almost linearly dependent on its density, a non-zero third derivative of the density profile results in shadows being produced in the image (Merzkirch 1974). This method therefore makes the turbulence in the flow, and hence the fountain structure, clearly visible. The shadowgraph projections of the flows were recorded on video, allowing the fountain heights to be measured to within 0.5 cm (2 – 5% of the fountain height), and an average value of the fluctuating final height to be found over a period of time.

In preliminary experiments, the flow from the source was observed to be laminar for the first 2 – 3 cm, so thin wire crosshairs were introduced within the tube to induce turbulence. One set of 0.5 mm diameter crosshairs was positioned 3 mm from the tube outlet and the second set aligned and placed 44 mm further along the tube. The effect of these crosshairs was determined quantitatively by performing an experiment with a weakly buoyant jet in a homogeneous environment (Baines *et al.* 1990). The injected source fluid rose until it impinged on the free surface before spreading laterally towards the tank walls. The horizontal boundary, or *front* , which separated this fluid layer from the ambient then descended through the environment as more fluid from below it was entrained into the upflow and added to the layer above (as in the plume filling box model described in §1.1). The motion of this boundary (see §3.2.1 for the derivation) is given by

$$\begin{aligned} z_d &= z_H e^{-2\alpha(\pi M_o)^{1/2} t/A} \\ &= z_H e^{-2\alpha Q_o t/(A r_e)}, \end{aligned} \tag{2.1}$$

where z_d is the height of the front above the virtual point source, z_H is the height at which the fluid initially spreads out along the free surface, $\alpha = 0.076 \pm 0.004$ (List 1982a) is the entrainment co-efficient for an axisymmetric jet, t is the time, A is the cross sectional area of the tank and r_e is the effective source radius. The momentum flux at the source, $\rho_i M_o$ (where ρ_i is the

density of the source fluid) is related to the volume flux at the source, Q_o, by $M_o = Q_o^2/(\pi r_e^2)$. For fully turbulent flow, r_e is equal to the measured source radius, $r_o = 4.4$ mm, while in laminar flow, $r_e = \sqrt{3}r_o/2 = 3.8$ mm. Equation (2.1) quantifies the flow originating from a point source, while experimental flows arise from a real source with a finite radius. The position of the virtual source, z_v, is determined by noting that when the heights in (2.1) are measured above z_v, a plot of $\ln(z_d)$ against time should be linear. The location of z_v was therefore obtained by varying its assumed location until, when $z_v = 1.0 \pm 0.25$ cm, the plot of the measured values of $\ln(z_d)$ against time resulted in a straight line (figure 2.4). Then, from the slope of this line, the effective source radius was found to be $r_e = 4.16 \pm 0.23$ mm. The conclusion was therefore reached that the cross hairs have significantly increased the turbulence at the source.

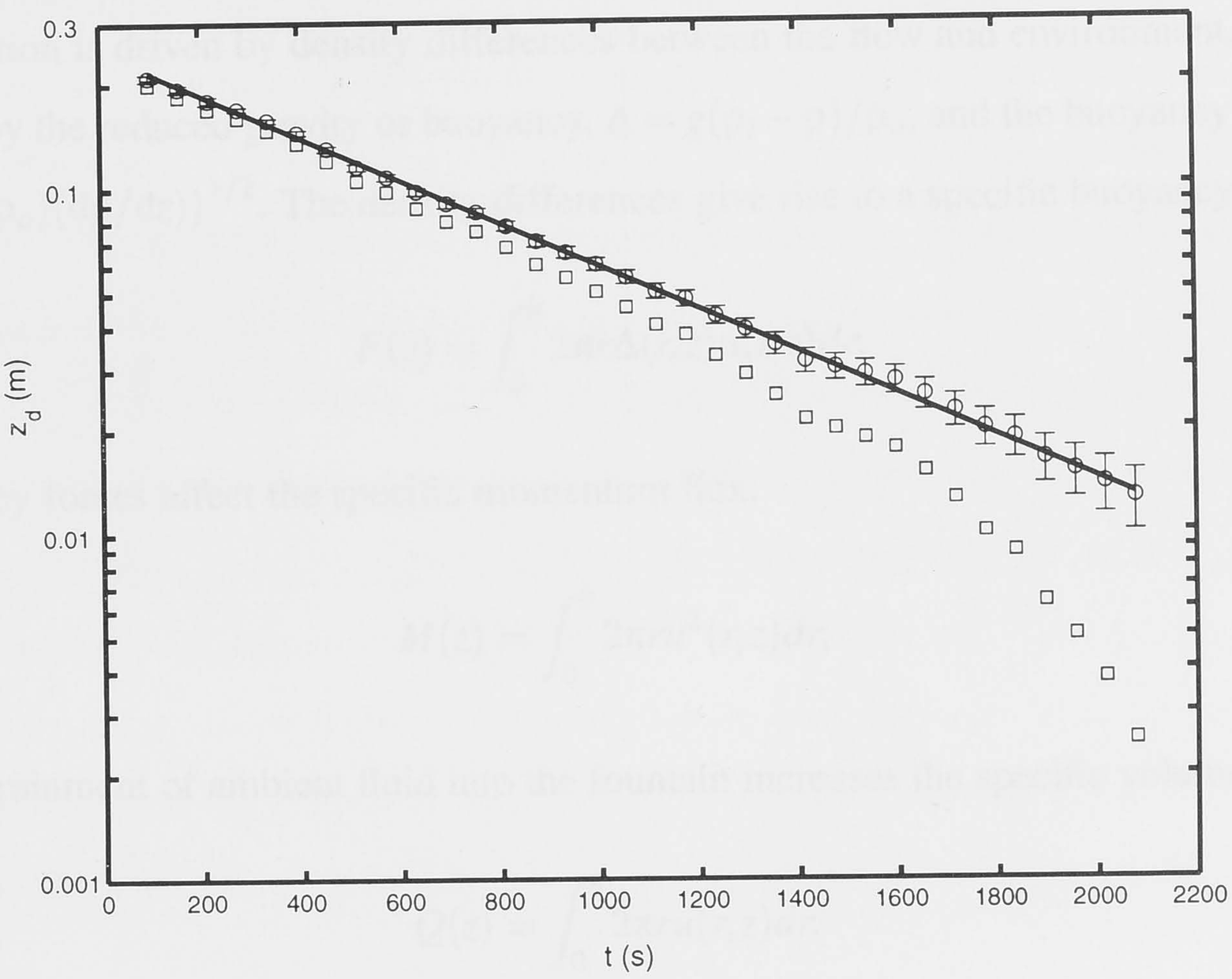

Figure 2.4: The position of the front formed by an axisymmetric jet in a homogeneous environment. The squares represent heights measured above the base of the tank, while the circles are the heights above the virtual point source which is located 1 cm below the base of the tank. From the slope of the line, the effective source radius was found to be $r_e = 4.16$ mm.

Morton (1959a) showed that the lower part of a fountain is not significantly different from that of a jet, even with a density difference between the source and environmental fluid. Hence, for these experiments in which the flow in the region between the virtual and actual sources remains jet-like, the values of r_e and z_v can be assumed to remain invariant.

2.2.2 Theoretical techniques

Dimensional analysis represents a powerful tool for solving mixing problems in fluid mechanics. The aim in using this approach is to find an appropriate group of variables to non-dimensionalise a property of the flow (e.g. length, velocity, buoyancy). The use of dimensionless variables then allows the same quantitative analysis to be applied to flows on different scales and in different media.

In a turbulent fountain, the only physical quantities of importance are the velocity of the fluid, u, the radius (or half width) of the flow, b, the density of the source fluid, ρ_i, the ambient density at the level of the source, ρ_o, the magnitude of the density gradient, $d\rho/dz$ (where ρ is the ambient density at a height z above the source) and the gravitational acceleration, g. The convection is driven by density differences between the flow and environment, which are quantified by the reduced gravity or buoyancy, $\Delta = g(\rho_i - \rho)/\rho_o$, and the buoyancy frequency, $N = ((-g/\rho_o)(d\rho/dz))^{1/2}$. The density differences give rise to a specific buoyancy flux:

$$F(z) = \int_0^b 2\pi r \Delta(r,z) u(r,z) dr, \tag{2.2}$$

the buoyancy forces affect the specific momentum flux:

$$M(z) = \int_0^b 2\pi r u^2(r,z) dr, \tag{2.3}$$

and the entrainment of ambient fluid into the fountain increases the specific volume flux:

$$Q(z) = \int_0^b 2\pi r u(r,z) dr. \tag{2.4}$$

In a stratified environment, the radial distributions of velocity and buoyancy ($u(r)$ and $\Delta(r)$) are replaced by average, *top hat* profiles, in which the quantity is constant throughout the flow and zero outside (Morton 1959b). The fluxes of buoyancy, momentum and volume are therefore $F = \pi b^2 u \Delta$, $M = \pi b^2 u^2$ and $Q = \pi b^2 u$, respectively.

The main feature of interest in an unbounded environment is the height of the fountain. Hence, a length scale is sought which is based on the buoyancy frequency, the specific momentum flux at the source, $M_o = \pi r_e^2 u_o^2$, and the specific buoyancy flux at the source,

$F_o = \pi r_e^2 u_o \Delta_o = \Delta_o Q_o$, where u_o is the flow velocity through the source, and $\Delta_o = g(\rho_i - \rho_o)/\rho_o$ is the buoyancy of the source fluid as it enters the tank.

2.2.3 Homogeneous fluid

In a homogeneous fluid ($N = 0$), the fountain properties depend on M_o and F_o. The fountain heights are therefore quantified in terms of the length scale $M_o^{3/4} F_o^{-1/2}$ (Turner 1966), so that

$$z = C M_o^{3/4} F_o^{-1/2}, \tag{2.5}$$

where the constant C is different for the initial and final heights (C_i and C_f, respectively). A number of investigators have measured C_i and C_f under a variety of conditions (table 2.1). The most extensive measurements of the fountain height were presented by Baines *et al.* (1990), who obtained a value of $C_f = 1.85 \pm 0.25$ (where I have estimated the error from their experimental data). This data set included some experiments made previously by Turner (1966), in which the ratio of the initial to final fountain height was found to be $C_i/C_f = 1.43$. Combining these two results gives an estimate of $C_i = 2.65 \pm 0.36$ for the initial fountain height. Some measurements of the final fountain height were made by Mizushina *et al.* (1982), who obtained a value of $C_f = 1.76 \pm 0.15$ (where I have once again estimated the error from their data set). Some other investigations (e.g. McDougall (1981), Lindberg (1994)) also give values of C_f, but these studies do not carefully document the source conditions such as the position of the virtual source and the effective source radius. The variation in the reported values of C_f, and the limited measurements of C_i motivated me to perform further experiments.

$\tilde{z}_i$	$\tilde{z}_f$	reference
2.65 ± 0.36	1.85 ± 0.25	Turner (1966), Baines *et al.* (1990)
	1.76 ± 0.15	Mizushina *et al.* (1982)
2.32 ± 0.08	1.70 ± 0.17	**this study**

Table 2.1: Dimensionless values of the initial and final fountain heights in a homogeneous fluid that were measured in several experimental investigations.

Nine experiments were performed to determine the values of C_i and C_f. In these experiments, Q_o was varied between $(9 - 36) \times 10^{-6}$ m^3 s^{-1} and Δ_o was in the range $0.08 - 0.42$ m s^{-2}.

The measured initial and final heights of the fountain above the virtual source are plotted against the length scale, $M_o^{3/4} F_o^{-1/2}$ in figure 2.5. Straight lines constrained to pass through the origin were fitted using a least sqaures method. The slopes of these lines give values, within two standard deviations, of $C_i = 2.32 \pm 0.08$ and $C_f = 1.70 \pm 0.17$.

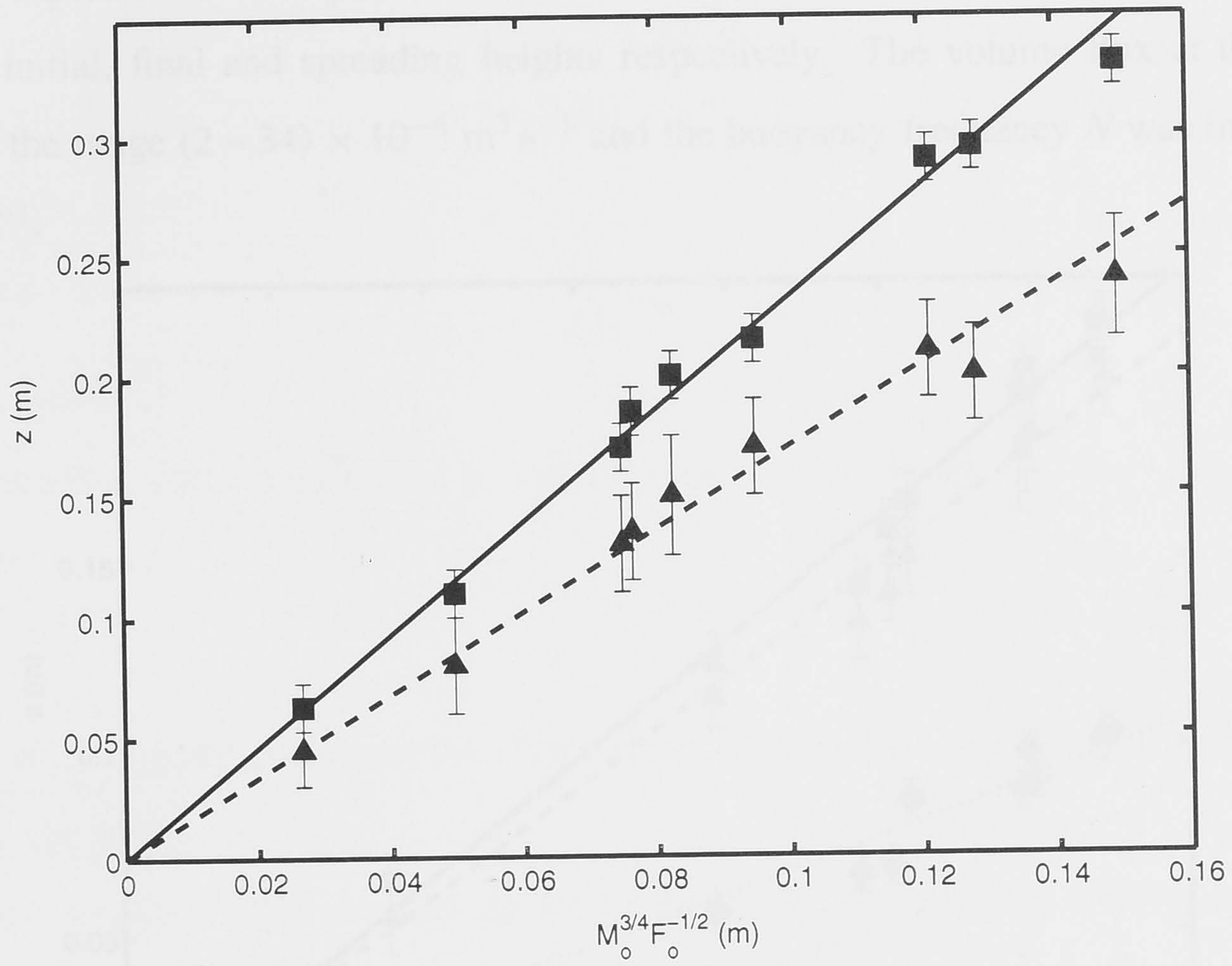

Figure 2.5: Experimental measurements of the initial (■) and final (▲) heights of an axisymmetric fountain in a homogeneous fluid, plotted against the length scale, $M_o^{3/4} F_o^{-1/2}$.

Both my measurements and those of Mizushina *et al.* (1982) are somewhat lower than the results of Baines *et al.* (1990), although they do lie within the range of experimental scatter. For the purposes of this study, average values of $C_i = 2.49 \pm 0.18$ and $C_f = 1.77 \pm 0.11$ are used.

2.2.4 Zero buoyancy flux at the source

In the limiting case when the density of the source fluid is equal to the density of the ambient fluid at the base of the tank ($F_o = 0$), the flow depends only on the momentum flux at the source and the buoyancy frequency. Dimensional arguments indicate that the only length scale that can be obtained from a combination of these parameters is $M_o^{1/4} N^{-1/2}$ (Fischer *et al.* 1979). The initial fountain height, z_i, the final height, z_f, and the spreading height, z_s, must all

therefore take the form

$$z = CM_o^{1/4} N^{-1/2}, \tag{2.6}$$

where C is an unknown constant.

Eleven experiments were performed to determine the values of the constants C_i, C_f and C_s for the initial, final and spreading heights respectively. The volume flux at the source, Q_o, was in the range $(2-34) \times 10^{-6}$ m^3 s^{-1} and the buoyancy frequency N was in the range $0.9 - 1.8$ s^{-1}.

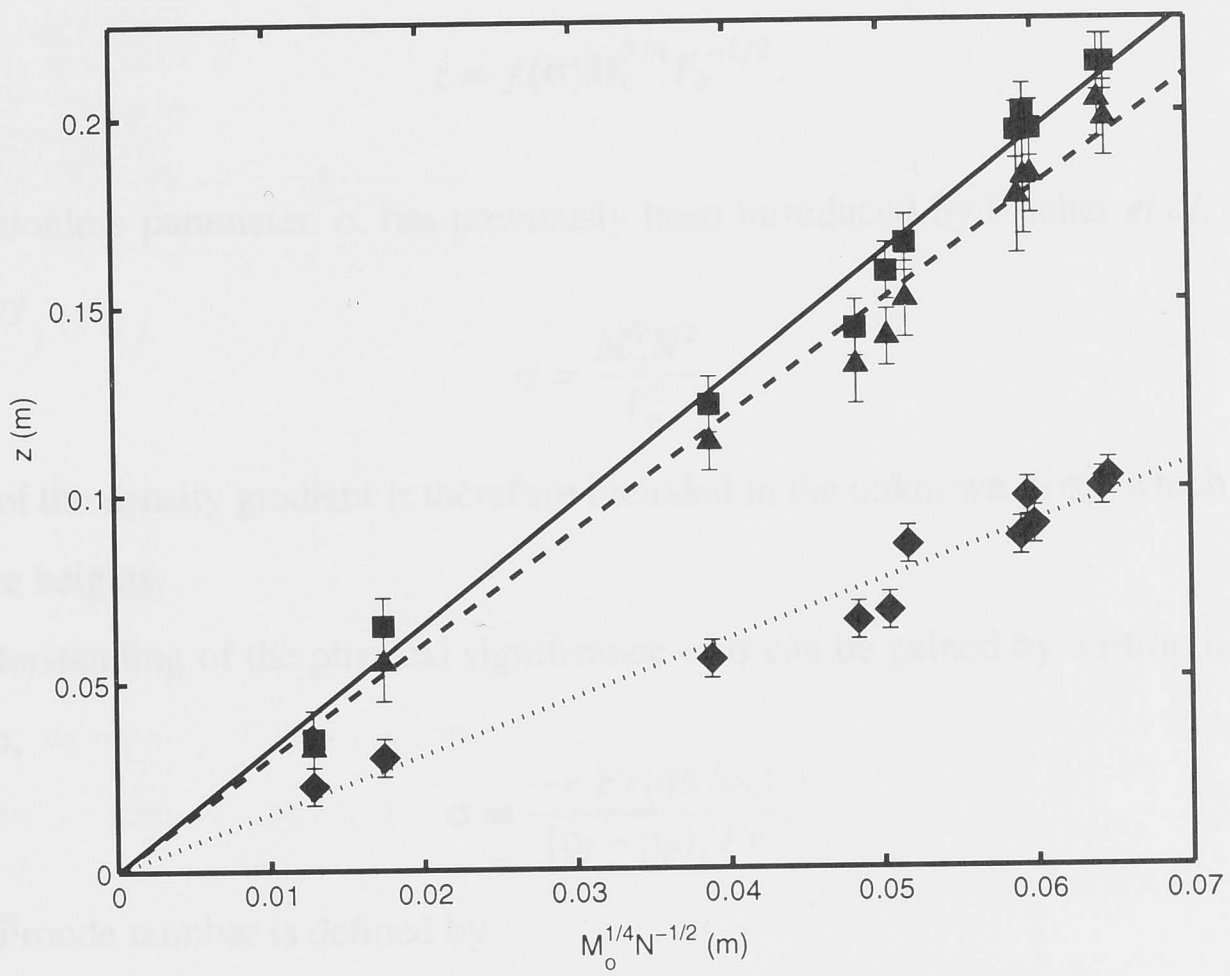

Figure 2.6: The initial (■), final (▲) and spreading (♦) heights of an axisymmetric fountain in a stratified fluid with a zero buoyancy flux at the source, plotted against the length scale $M_o^{1/4} N^{-1/2}$.

The experimental results for the three heights are plotted against $M_o^{1/4} N^{-1/2}$ in figure 2.6. Straight lines constrained to pass through the origin were fitted by a least squares method through the data points, confirming the linear relationship in (2.6). The slopes of these lines give constants, within two standard deviations, of $C_i = 3.25 \pm 0.17$, $C_f = 3.00 \pm 0.23$ and $C_s = 1.53 \pm 0.10$. The ratio of the initial to final fountain height is on average 1.08; a value much lower than the ratio of 1.36 (§2.2.3) observed in a homogeneous environment. The ratio decreases for intermediate intrusion because the downflow has a smaller velocity and so has less influence on the momentum of the upflow (see chapter 4), and the interaction between the

up and down flows takes place over a shorter distance, leading to less reduction of the initial height.

2.2.5 Non-zero buoyancy flux at the source

The fountain behaviour in this general case depends on M_o, F_o and N. As there is no unique length scale, an expression for the three heights is written in terms of the length scale for a homogeneous environment:

$$z = f(\sigma) M_o^{3/4} F_o^{-1/2}. \tag{2.7}$$

The dimensionless parameter, σ, has previously been introduced by Fischer *et al.* (1979) and is defined by

$$\sigma = \frac{M_o^2 N^2}{F_o^2}. \tag{2.8}$$

The effect of the density gradient is therefore included in the unknown $f(\sigma)$, which is different for the three heights.

An understanding of the physical significance of σ can be gained by writing it in an alternative form,

$$\sigma = \frac{-r_e Fr(\mathrm{d}\rho/\mathrm{d}z)}{(\rho_i - \rho_o)/Fr}, \tag{2.9}$$

where the Froude number is defined by

$$Fr = u_o/(r_e \Delta_o)^{1/2}. \tag{2.10}$$

In a homogeneous environment, both a dimensionless fountain height, z_f/r_e, and the volume of environmental fluid entrained into the fountain depend linearly on Fr (Baines *et al.* 1990). Hence, the numerator in (2.9) is a measure of the ambient density variation over the fountain height, while the denominator is a measure of the final density difference between the fountain and ambient fluids. The parameter σ therefore quantifies the relative magnitudes of the two buoyancy effects that control the behaviour of the fountain.

To determine the form of $f(\sigma)$ for the three heights, twenty-four experiments were performed using values of Q_o between $(11 - 45) \times 10^{-6}$ m^3 s^{-1}, Δ_o between $0.01 - 0.53$ m s^{-2}

and N in the range $0.3 - 1.8\ s^{-1}$. In figures 2.7(a) and 2.7(b), respectively, the measured dimensionless initial and final heights, $M_o^{-3/4} F_o^{1/2} z$, are plotted against σ. Included are the known asymptotic limits of $f(\sigma)$:

$$f_i(\sigma) = \begin{cases} 2.49 & \sigma = 0 \quad (\S 2.2.3) \\ 3.25\sigma^{-1/4} & \sigma \to \infty \quad (\S 2.2.4) \end{cases} \tag{2.11}$$

and

$$f_f(\sigma) = \begin{cases} 1.77 & \sigma = 0 \quad (\S 2.2.3) \\ 3.00\sigma^{-1/4} & \sigma \to \infty \quad (\S 2.2.4). \end{cases} \tag{2.12}$$

The experimental data approaches to within 5% of the large σ limit at $\sigma \approx 20 - 40$. The difference between the experimental data and the known homogeneous limit falls to 5% at $\sigma \approx 0.1 - 0.5$. Figures 2.7(a) and 2.7(b) also include the simple analytical functions,

$$f_i(\sigma) = \left(2.49^{-4} + 3.25^{-4}\sigma\right)^{-1/4} \tag{2.13}$$

$$f_f(\sigma) = \left(1.77^{-4} + 3.00^{-4}\sigma\right)^{-1/4}, \tag{2.14}$$

which coincide exactly with the known asymptotic limits, and can be seen to agree well with experimental measurements for all values of σ.

As previously discussed for the case of a zero buoyancy flux at the source, the ratio of the initial to the final fountain height is less than that observed in a homogeneous fluid. Figure 2.8 shows explicitly how this ratio decreases as the dimensionless spreading height, $M_o^{-3/4} F_o^{1/2} z_s$, increases. This effect is due to the lower velocity of the downflow and the smaller distance over which the up and down flows interact, as discussed in §2.2.4.

The effect of the changing ambient density gradient on the dimensionless spreading height is shown in figure 2.9. In a homogeneous environment the intrusion occurs along the base of the tank, and in a stratified environment the spreading height must again approach zero as $\sigma \to \infty$. Hence there is a value of the density gradient at $\sigma_m \approx 40 - 60$ which gives a maximum in the dimensionless spreading height. In figures 2.7(a) and 2.7(b), this value of σ is seen to be close to the point at which the asymptotic limit for large σ becomes valid.

To determine the value of σ_c, the critical point at which the spreading height first rises from

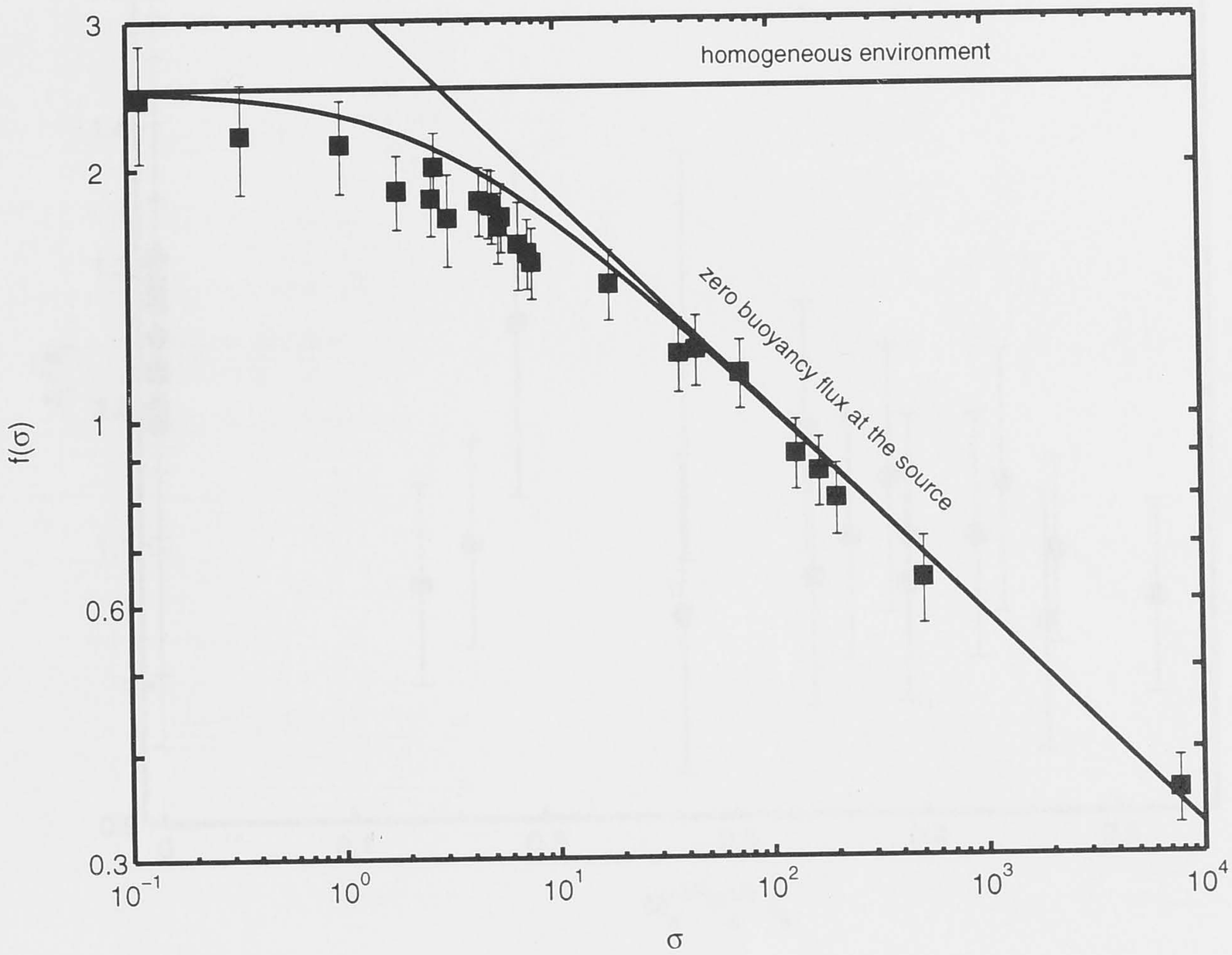

(a)

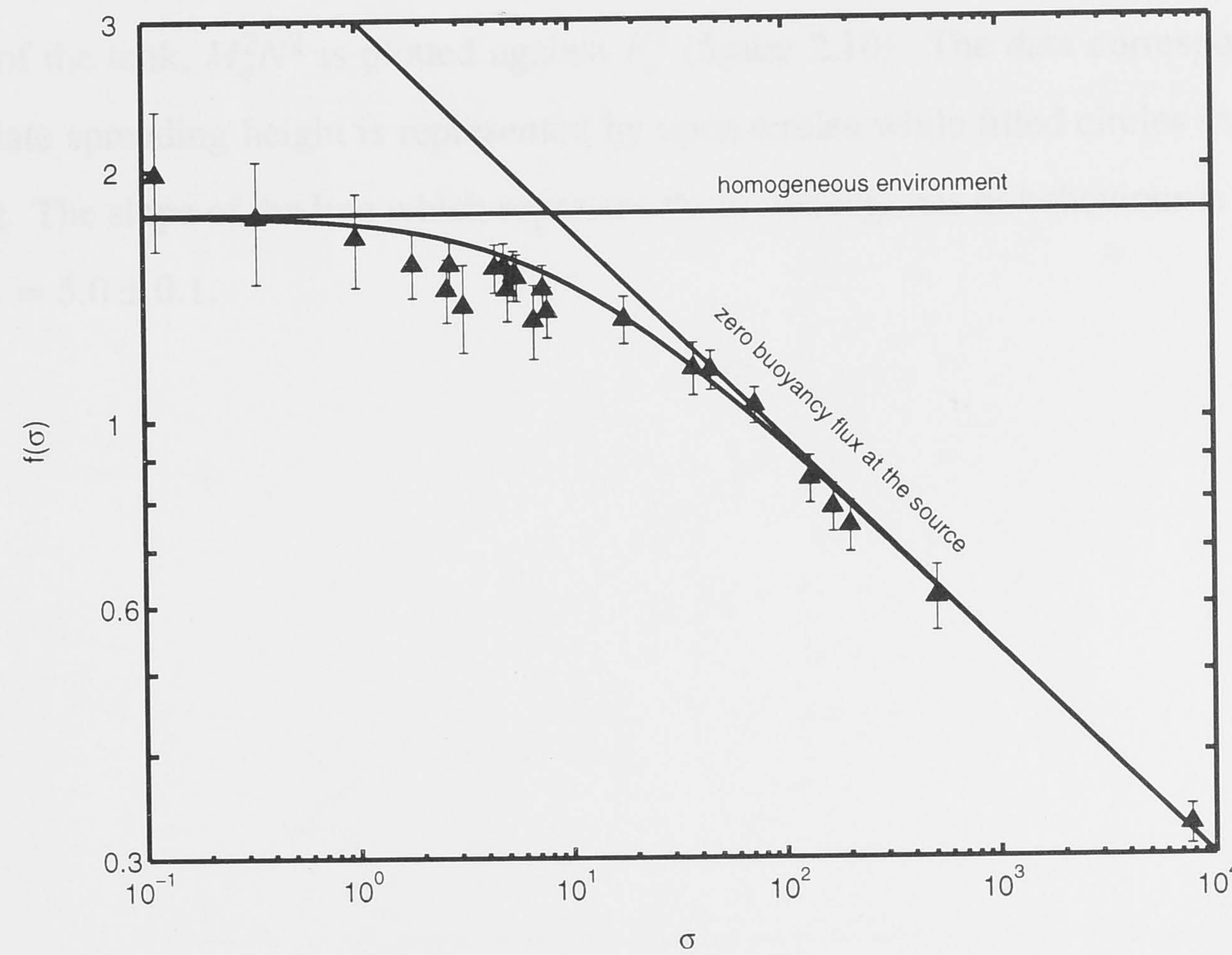

(b)

Figure 2.7: Dimensionless heights of an axisymmetric fountain showing the asymptotic results along with the simple analytical functions given in (2.13) and (2.14). (a) Initial height: as $\sigma \to 0$, $f(\sigma) = 2.49$ (§2.2.3), and as $\sigma \to \infty$, $f(\sigma) = 3.25\sigma^{-1/4}$ (§2.2.4). (b) Final height: as $\sigma \to 0$, $f(\sigma) = 1.77$ (§2.2.3), and as $\sigma \to \infty$, $f(\sigma) = 3.00\sigma^{-1/4}$ (§2.2.4).

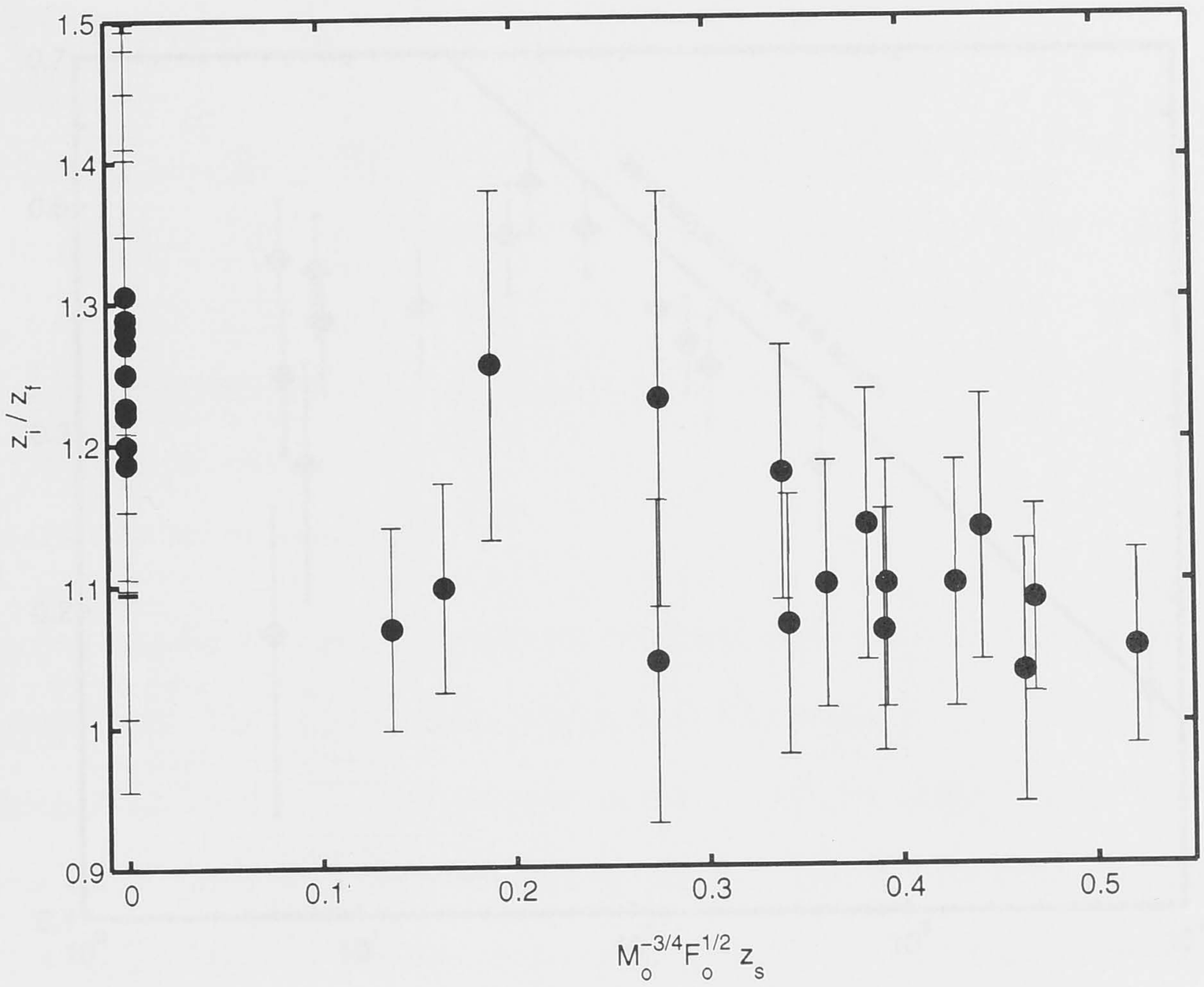

Figure 2.8: Ratio of the initial to final height of an axisymmetric fountain showing the decrease in the ratio as the spreading height increases.

the base of the tank, $M_o^2 N^2$ is plotted against F_o^2 (figure 2.10). The data corresponding to an intermediate spreading height is represented by open circles while filled circles indicate basal spreading. The slope of the line which separates these two regimes of behaviour is equal to σ_c, giving $\sigma_c = 5.0 \pm 0.1$.

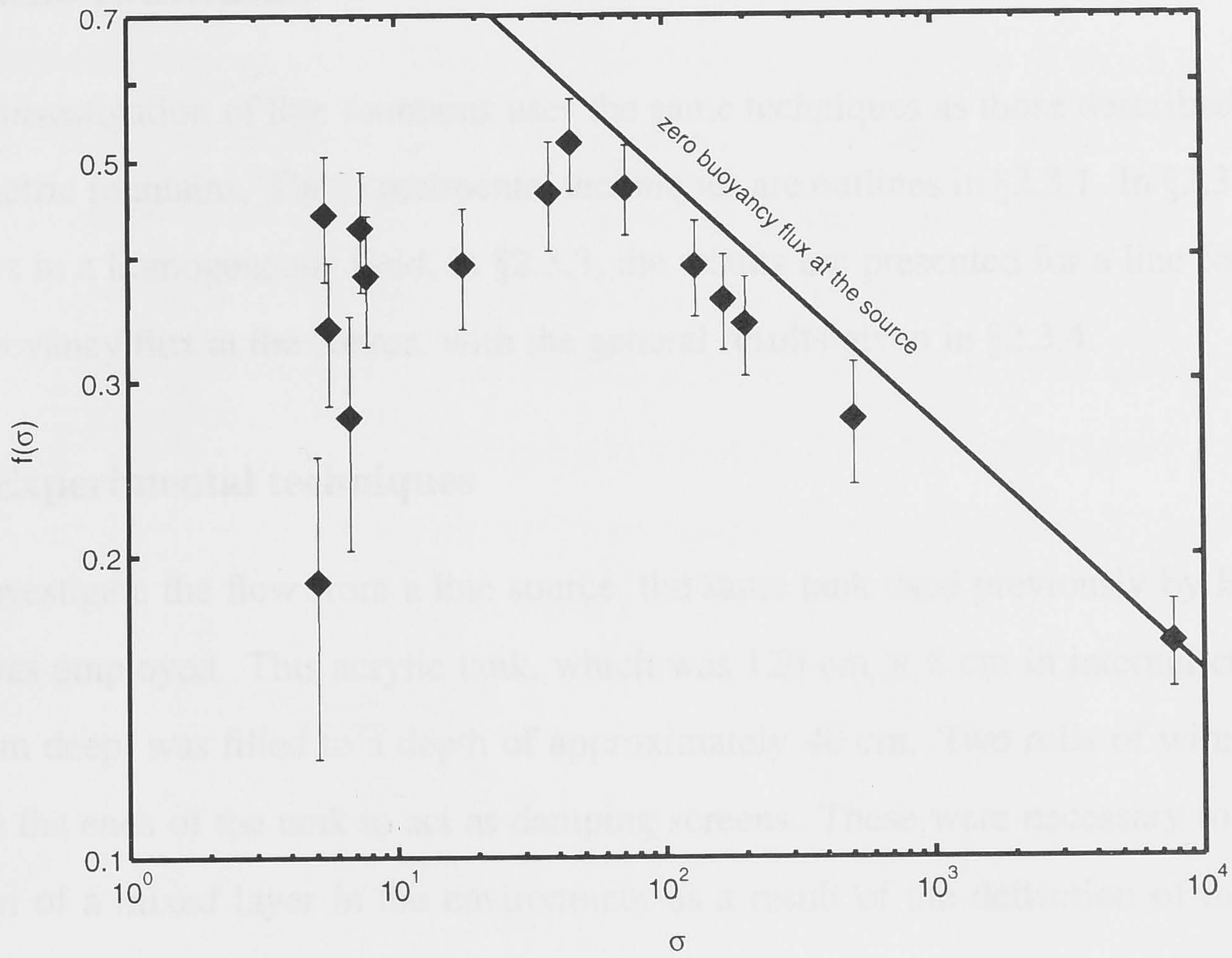

Figure 2.9: Dimensionless spreading height of an axisymmetric fountain as a function of σ showing the transition to the asymptotic behaviour for large σ, where $f(\sigma) = 1.53\sigma^{-1/4}$ (§2.2.4).

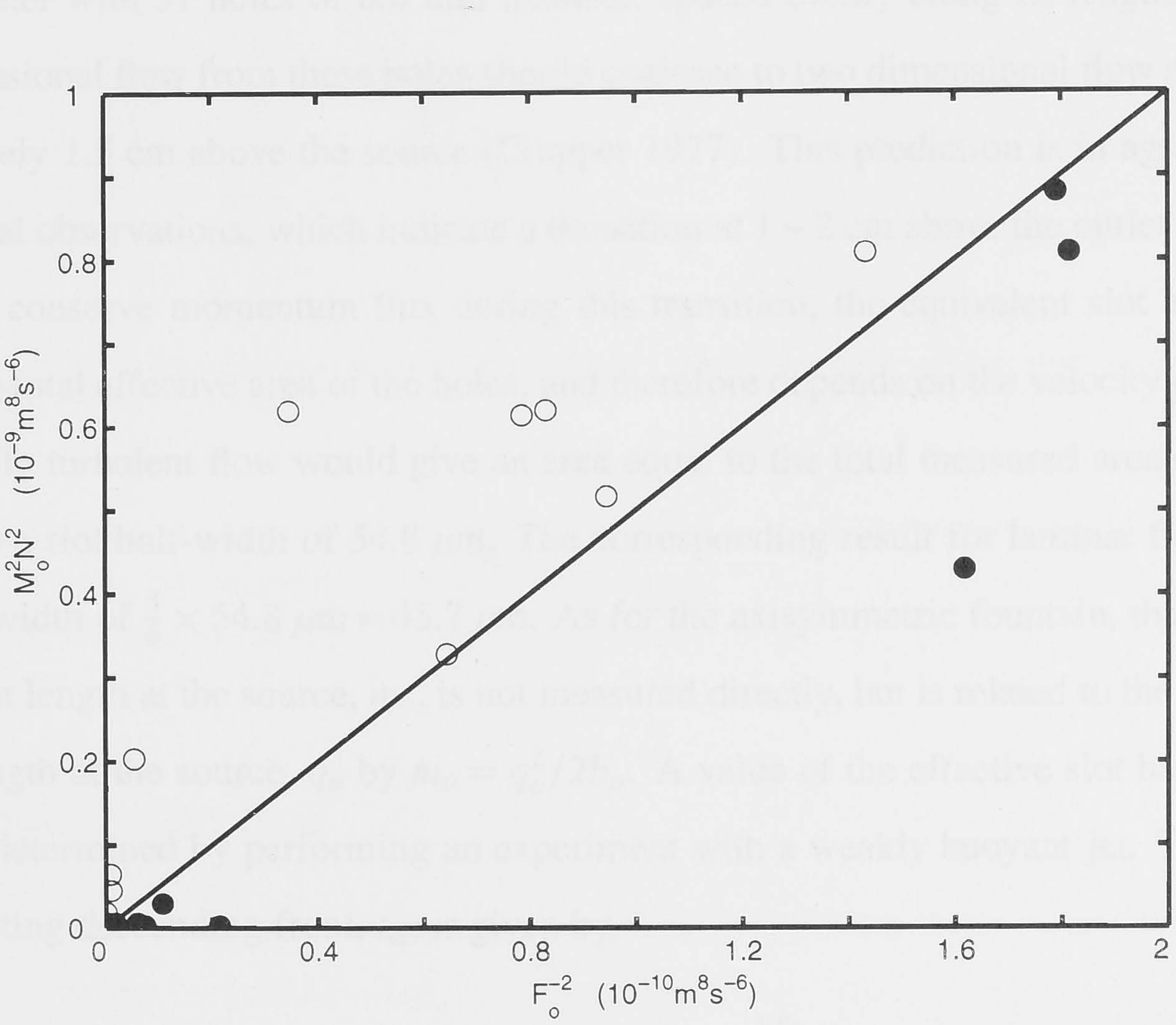

Figure 2.10: The conditions for experiments with an intermediate spreading height (○) and those in which spreading occurs along the base (●) are separated by the plotted line which has a slope of 5.0.

2.3 Line fountains

This investigation of line fountains uses the same techniques as those described in §2.2 for axisymmetric fountains. The experimental techniques are outlines in §2.3.1. In §2.3.2, I outline the results in a homogeneous fluid, in §2.3.3, the results are presented for a line fountain with a zero buoyancy flux at the source, with the general results given in §2.3.4.

2.3.1 Experimental techniques

To investigate the flow from a line source, the same tank used previously by Baines *et al.* (1990) was employed. This acrylic tank, which was 120 cm $\times$ 8 cm in internal cross section and 60 cm deep, was filled to a depth of approximately 40 cm. Two rolls of wire mesh were placed in the ends of the tank to act as damping screens. These were necessary to prevent the formation of a mixed layer in the environment as a result of the deflection of the spreading layer as it reached the tank walls (Baines *et al.* 1990). The source, which was located centrally on the base of the tank and perpendicular to its length, consisted of a circular pipe of 4 mm inner diameter with 31 holes of 0.6 mm diameter spaced evenly along its length. The initial three dimensional flow from these holes should coalesce to two dimensional flow at a height of approximately 1.5 cm above the source (Crapper 1977). This prediction is in agreement with experimental observations, which indicate a transition at 1 – 2 cm above the outlet of the holes. In order to conserve momentum flux during this transition, the equivalent slot area must be equal to the total effective area of the holes, and therefore depends on the velocity profile at the source. Fully turbulent flow would give an area equal to the total measured area of the holes, resulting in a slot half-width of 54.8 μm. The corresponding result for laminar flow indicates a slot half-width of $\frac{5}{6} \times 54.8\ \mu\text{m} = 45.7\ \mu\text{m}$. As for the axisymmetric fountain, the momentum flux per unit length at the source, m_o, is not measured directly, but is related to the volume flux per unit length at the source, q_o by $m_o = q_o^2/2b_o$. A value of the effective slot half-width, b_o, was again determined by performing an experiment with a weakly buoyant jet. The elevation of the resulting descending front, z_d, is given by

$$z_d^{1/2} = z_H^{1/2} - \left(\frac{q_o^2 \alpha}{2 b_o L^2}\right)^{1/2} t, \tag{2.15}$$

where $\alpha = 0.074 \pm 0.004$ (List 1982a) is the two dimensional jet entrainment coefficient and L is the length of the tank (see §3.3.1 for the derivation of (2.15)). The square root of the measured elevation of the descending front is plotted against time in figure 2.11, showing the transition from the three dimensional flow at small heights to the linear relationship in the two dimensional regime. From the slope of the line, the effective half-width of the slot is determined to be $b_o = 46.5 \pm 2.2$ μm. This value indicates that the flow is virtually laminar at the source. The virtual source was found to coincide with the top of the nozzle, so that all heights in this and subsequent experiments were measured above the outlet of the holes, which were located a distance of $z_e = 1.4$ cm above the base of the tank.

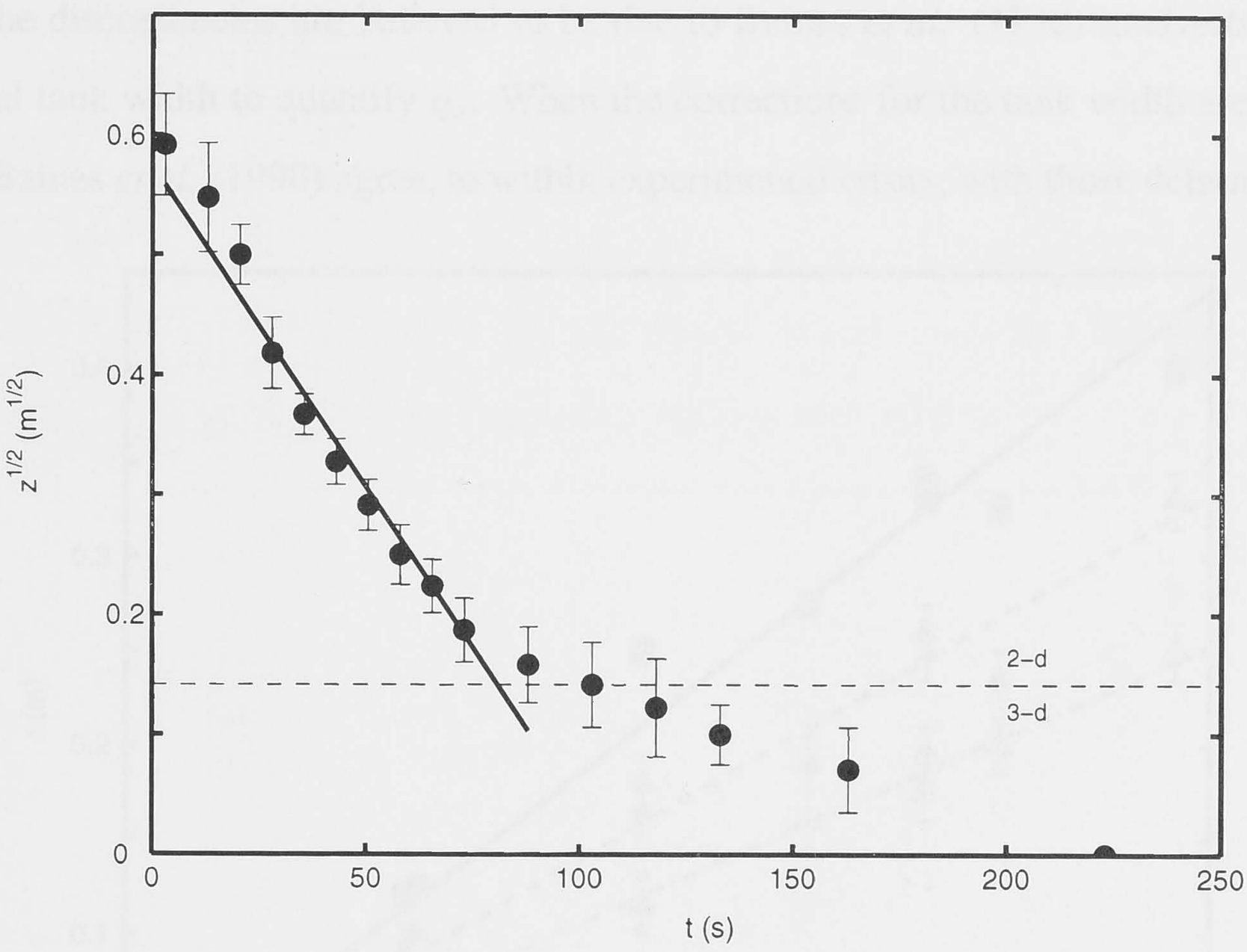

Figure 2.11: The position of the front formed by a line jet in a homogeneous environment, showing the transition from three dimensional flow to two dimensional flow at a height of 2 cm above the source. From the slope of the solid line, the effective half-width of the slot was found to be $b_o = 46.5 \pm 2.2$ μm.

2.3.2 Homogeneous fluid

In a homogeneous fluid, a dimensional argument leads to the expression

$$z = c m_o f_o^{-2/3} \tag{2.16}$$

for the fountain heights, where $f_o = \Delta_o q_o$ is the specific buoyancy flux per unit length at the source. Initial experiments that were performed in order to verify the results of Baines *et al.* (1990) showed significant deviation from the previously measured constants, c. Consequently, I performed 12 experiments in a homogeneous fluid, with the volume flux in the range $(5-22)\times 10^{-5}\ \mathrm{m^2\,s^{-1}}$ and the buoyancy between $0.06-1.0\ \mathrm{m\,s^{-2}}$. From the results shown in figure 2.12, the constants, c, were found within an error of two standard deviations to be $c_i = 1.26\pm0.14$ (for the initial height), $c_{fs} = 0.95\pm0.15$ (for the final symmetric height) and $c_{fa} = 0.72\pm0.05$ (for the final asymmetric height). These constants differ significantly from the values of $c_i = 1.69$, $c_{fs} = 1.3$ and $c_{fa} = 1.04$ which were determined by Baines *et al.* (1990). The discrepancies are believed to be due to Baines *et al.* (1990) inadvertantly using the external tank width to quantify q_o. When the corrections for the tank width are made, the results of Baines *et al.* (1990) agree, to within experimental errors, with those determined here.

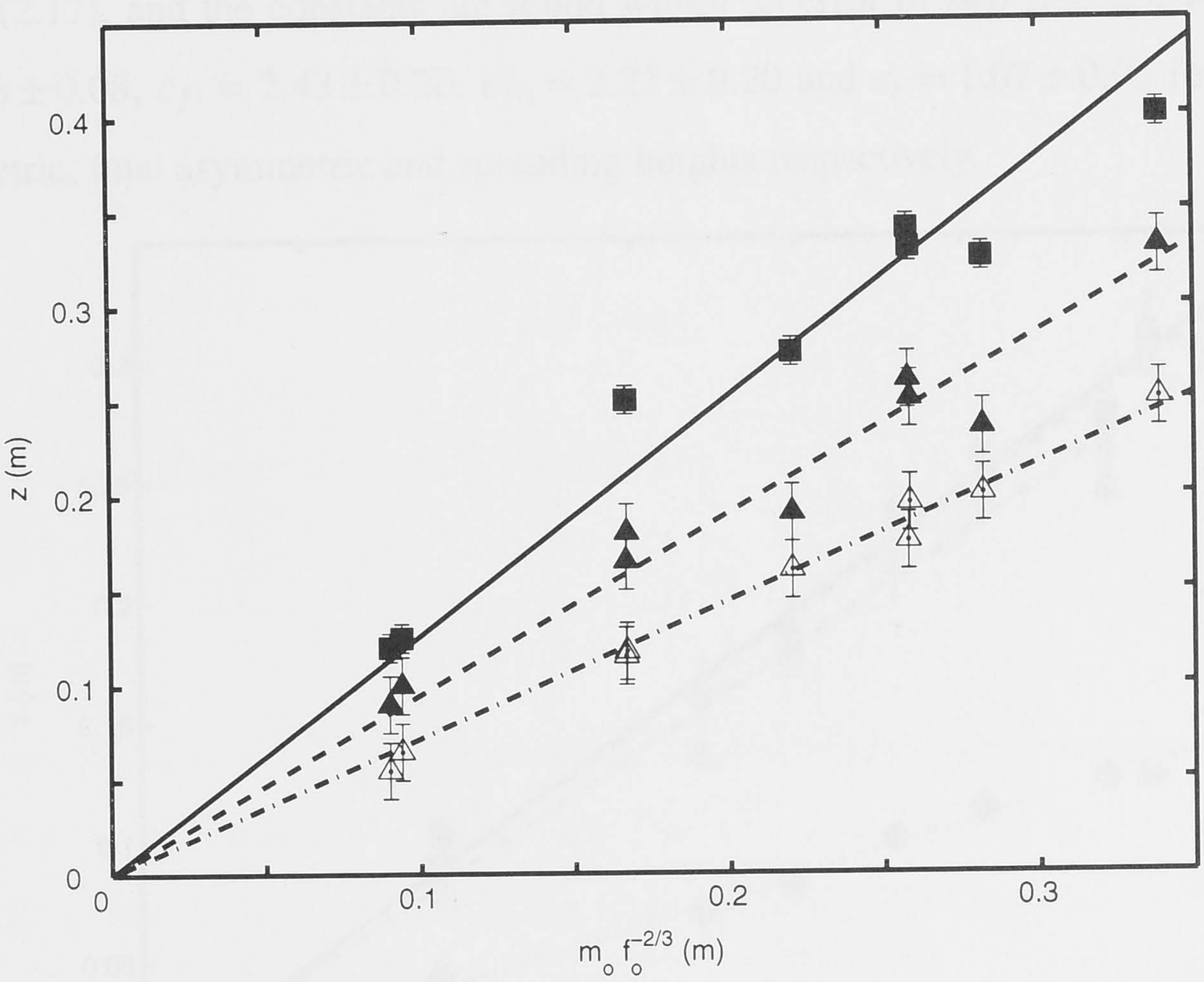

Figure 2.12: Experimental measurements of the initial (■), final symmetric (▲) and final asymmetric (△) heights of a line fountain in a homogeneous fluid, plotted against the length scale $m_o f_o^{-2/3}$.

2.3.3 Zero buoyancy flux at the source

In the special case of a zero buoyancy flux at the source, the initial, final and spreading heights of a line fountain take the form

$$z = c\, m_o^{1/3} N^{-2/3}, \tag{2.17}$$

where c is an unknown constant.

Eight experiments were performed with q_o in the range $(3.2 - 10.1) \times 10^{-5}$ m^2 s^{-1} and N in the range $0.4 - 1.4$ s^{-1}. Figure 2.13 shows the experimental measurements of the initial, final and spreading heights as a function of $m_o^{1/3} N^{-2/3}$. Two values of the final fountain height are plotted; those measured during the periods when the fountain profile was symmetric, z_{fs}, and asymmetric, z_{fa}. The straight lines fitted through the data points confirm the linear relationship in (2.17), and the constants are found within an error of two standard deviations to be $c_i = 2.46 \pm 0.08$, $c_{fs} = 2.43 \pm 0.20$, $c_{fa} = 2.27 \pm 0.20$ and $c_s = 1.07 \pm 0.05$ for the initial, final symmetric, final asymmetric and spreading heights respectively.

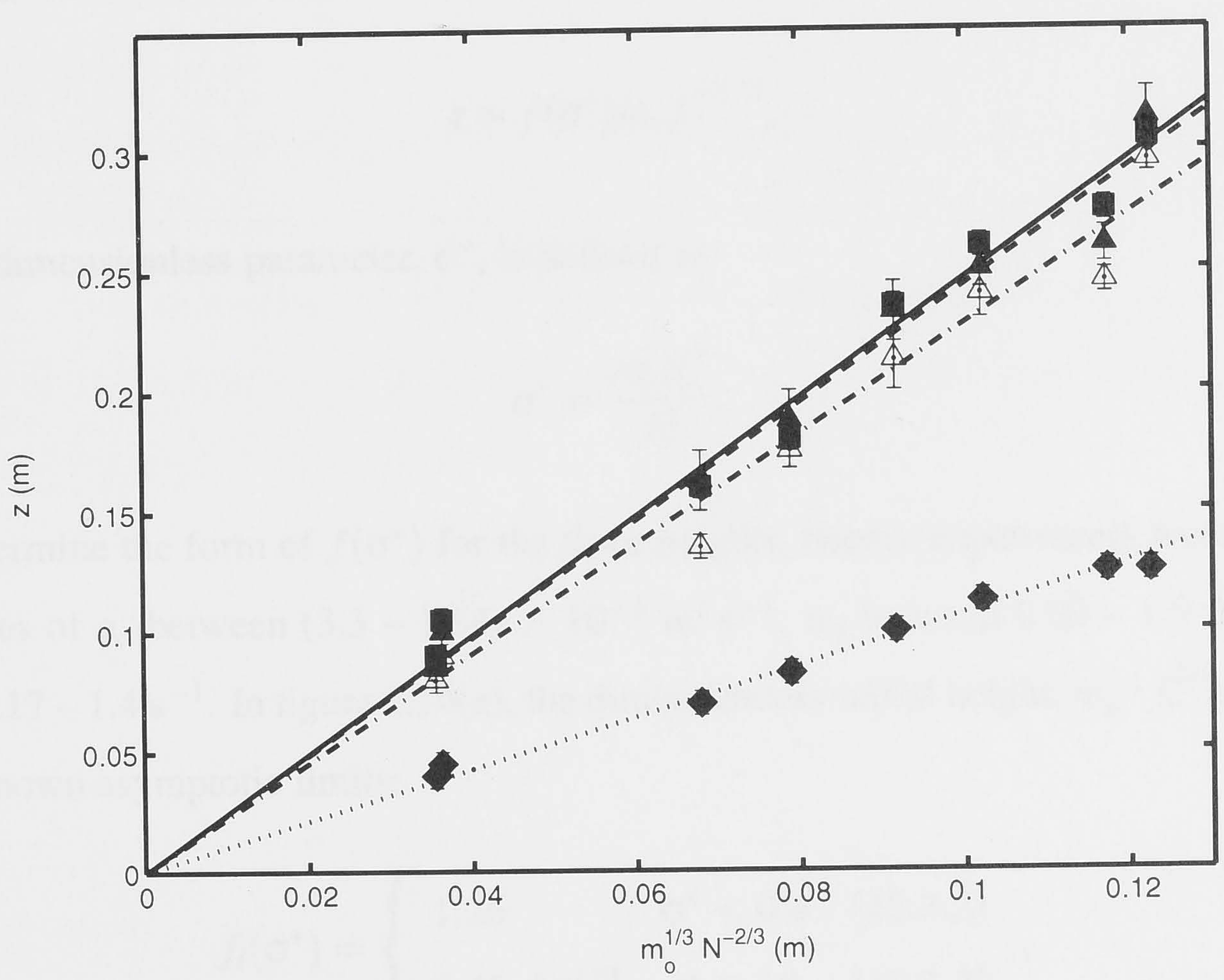

Figure 2.13: Experimental measurements of the initial (■), final symmetric (▲), final asymmetric (△) and spreading (♦) heights of a line fountain in a stratified fluid with a zero buoyancy flux at the source, plotted against the length scale $m_o^{1/3} N^{-2/3}$.

In some experiments, the large fluctuations in the final symmetric height resulted in an average value that was greater than the initial height of the fountain. Hence, while most individual measurements indicate that the initial height is reduced by a small amount to the final value, the difference between c_i and c_{fs} is not statistically significant. A similar result is found for the final fountain heights, where the large fluctuations in the symmetric and asymmetric heights result in values of c_{fs} and c_{fa} that do not differ significantly. These results contrast the measurements made in a homogeneous environment (§2.3.2), where c_{fs} is 25% less than c_i, and c_{fa} is a further 25% lower than c_{fs}. The small differences between the initial, symmetric final and asymmetric final heights measured in a stratified fluid occur for the same reason as was discussed in §2.2.4 for axisymmetric fountains, where the effect of intermediate intrusion reduces the distance over which the up and down flows interact and the smaller downflow velocity has less effect on the upflow.

2.3.4 Non-zero buoyancy flux at the source

In this general case, the fountain heights take the form

$$z = f(\sigma^*) m_o f_o^{-2/3}, \tag{2.18}$$

where the dimensionless parameter, σ^*, is defined by

$$\sigma^* = \frac{m_o^2 N^2}{f_o^2}. \tag{2.19}$$

To determine the form of $f(\sigma^*)$ for the three heights, twenty experiments were performed using values of q_o between $(3.3 - 10.4) \times 10^{-5}$ m^2 s^{-1}, Δ_o between $0.02 - 1.9$ m s^{-2} and N between $0.17 - 1.4$ s^{-1}. In figure 2.14(a), the dimensionless initial height, $m_o^{-1} f_o^{2/3} z_i$, is plotted with the known asymptotic limits:

$$f_i(\sigma^*) = \begin{cases} 1.26 & \sigma^* < 0.4 \quad (\S 2.3.2) \\ 2.46\sigma^{*-1/3} & \sigma^* > 30 \quad (\S 2.3.3) \end{cases}, \tag{2.20}$$

as well as the simple analytical function

$$f_i(\sigma^*) = \left(1.26^{-3} + 2.46^{-3}\sigma^*\right)^{-1/3}. \tag{2.21}$$

Figure 2.14(b) shows the dimensionless final heights measured when the fountain profile was both symmetric and asymmetric, along with the asymptotic limits for the symmetric final height:

$$f_f(\sigma^*) = \begin{cases} 0.95 & \sigma^* < 0.4 \quad (\S 2.3.2) \\ 2.43\sigma^{*-1/3} & \sigma^* > 100 \quad (\S 2.3.3) \end{cases}, \tag{2.22}$$

and the analytical function for the symmetric final height,

$$f_f(\sigma^*) = \left(0.95^{-3} + 2.43^{-3}\sigma^*\right)^{-1/3}. \tag{2.23}$$

The experimental results approach to within 5% of the limit for large values of σ^* at $\sigma^* \approx 30$ for the initial height and at $\sigma^* \approx 100$ for the final symmetric height. For both heights, the deviation between the experimental results and the predicted homogeneous limit only falls to 5% at $\sigma^* \approx 0.4$.

The dimensionless spreading height is plotted in figure 2.15(c), showing a rapid transition from a zero spreading height to a maximum in $f(\sigma^*)$ at $\sigma^*_m \approx 10-20$. Unlike the axisymmetric fountain, σ^*_m does not correspond to the value of σ^* at which the asymptotic limit for a zero buoyancy flux at the source becomes valid. A value of σ^*_c is found from the graph of $m_o^2 N^2$ against f_o^2 to be $\sigma^*_c = 6.0 \pm 0.1$ (figure 2.15).

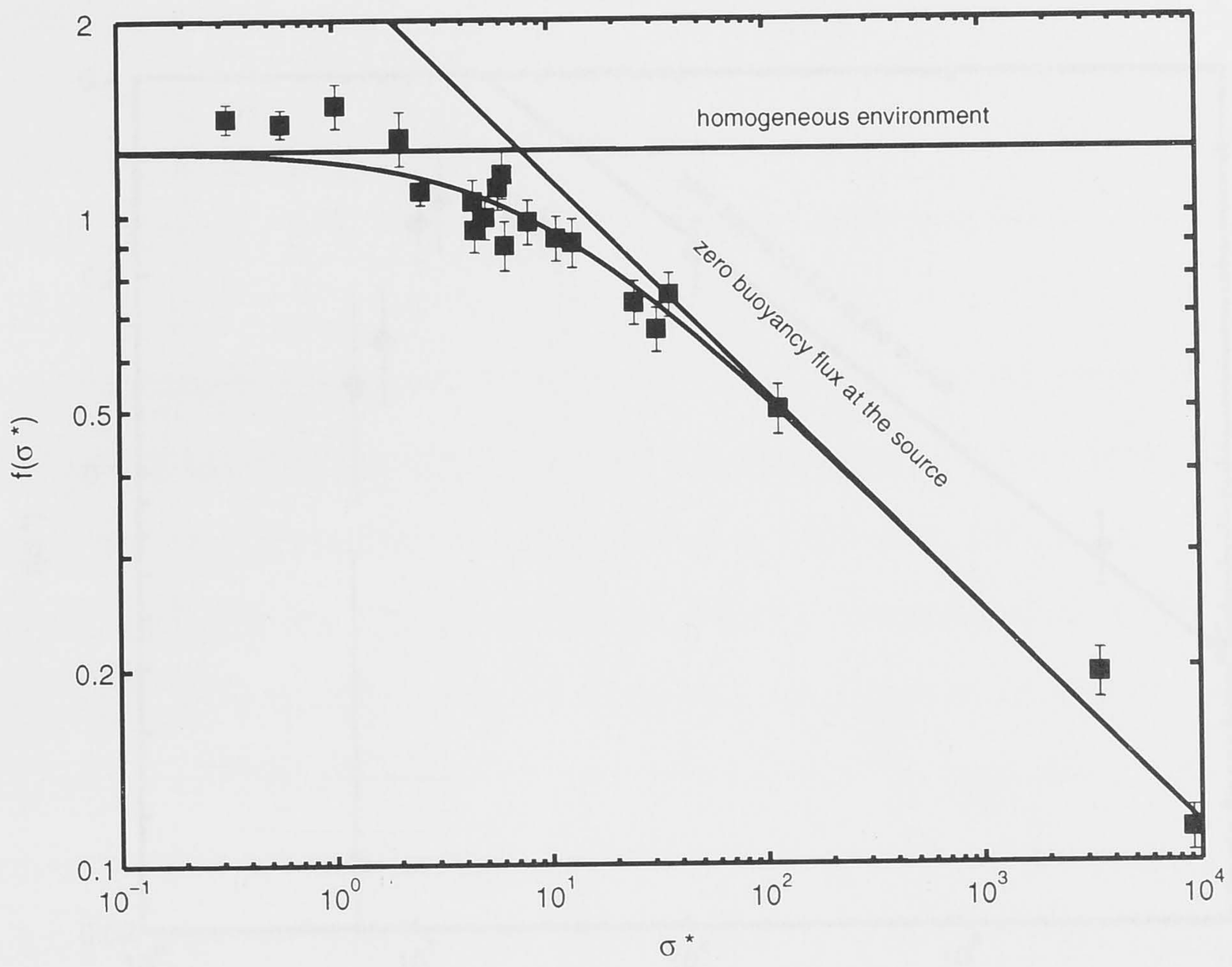

(a)

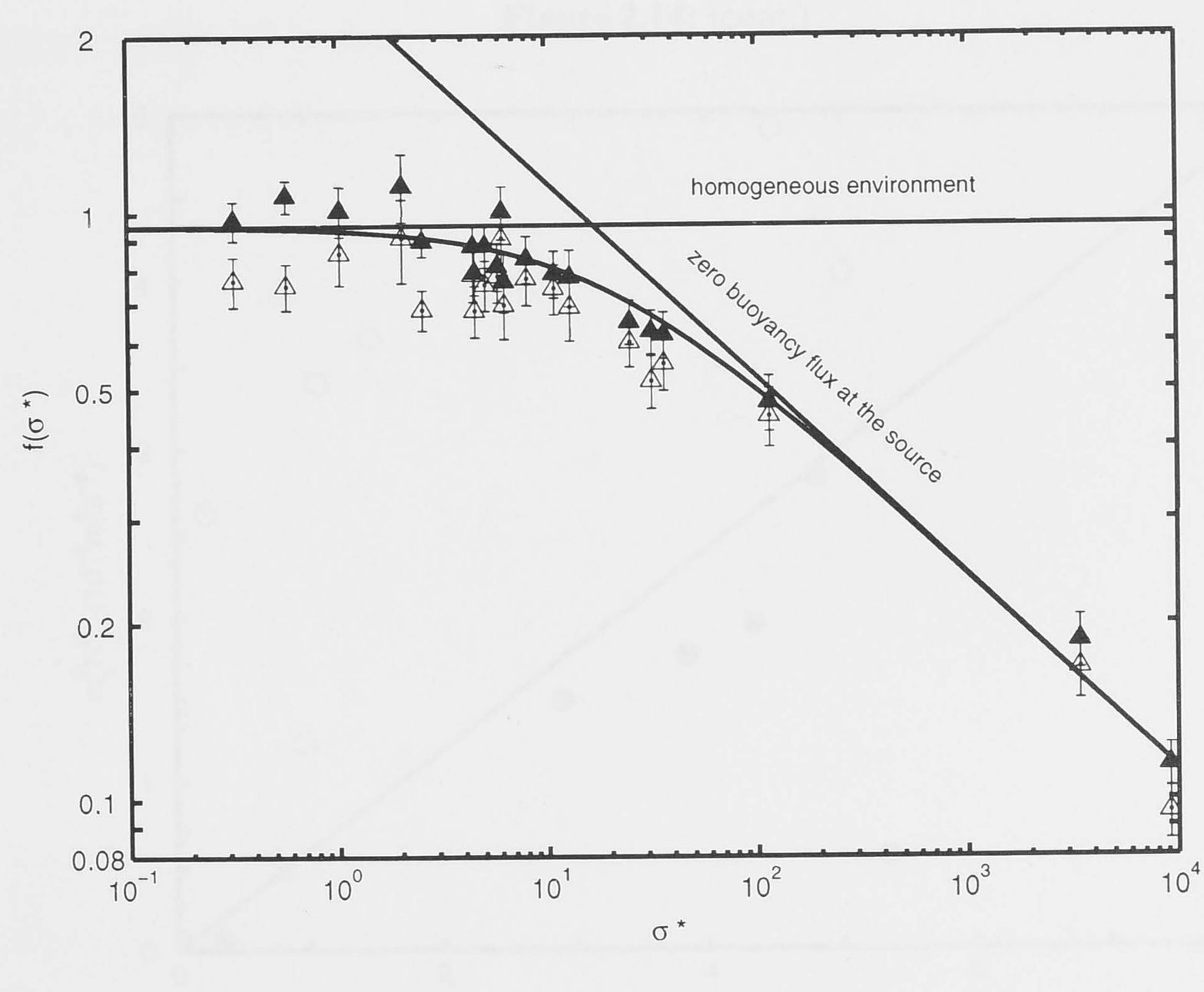

(b)

Figure 2.14: Dimensionless heights of a line fountain showing the asymptotic results along with the simple analytical functions for the initial and final heights given in (2.21) and (2.23). (a) Initial height: as $\sigma^* \to 0$, $f(\sigma^*) = 1.26$ (§2.3.2) and as $\sigma^* \to \infty$, $f(\sigma^*) = 2.46\sigma^{*-1/3}$ (§2.3.3). (b) Symmetric (▲) and asymmetric (△) final height with the asymptotic results for the symmetric height: as $\sigma^* \to 0$, $f(\sigma^*) = 0.95$ (§2.3.2) and as $\sigma^* \to \infty$, $f(\sigma^*) = 2.43\sigma^{*-1/3}$ (§2.3.3). (c) Spreading height: as $\sigma^* \to \infty$, $f(\sigma^*) = 1.07\sigma^{*-1/3}$ (§2.3.3).

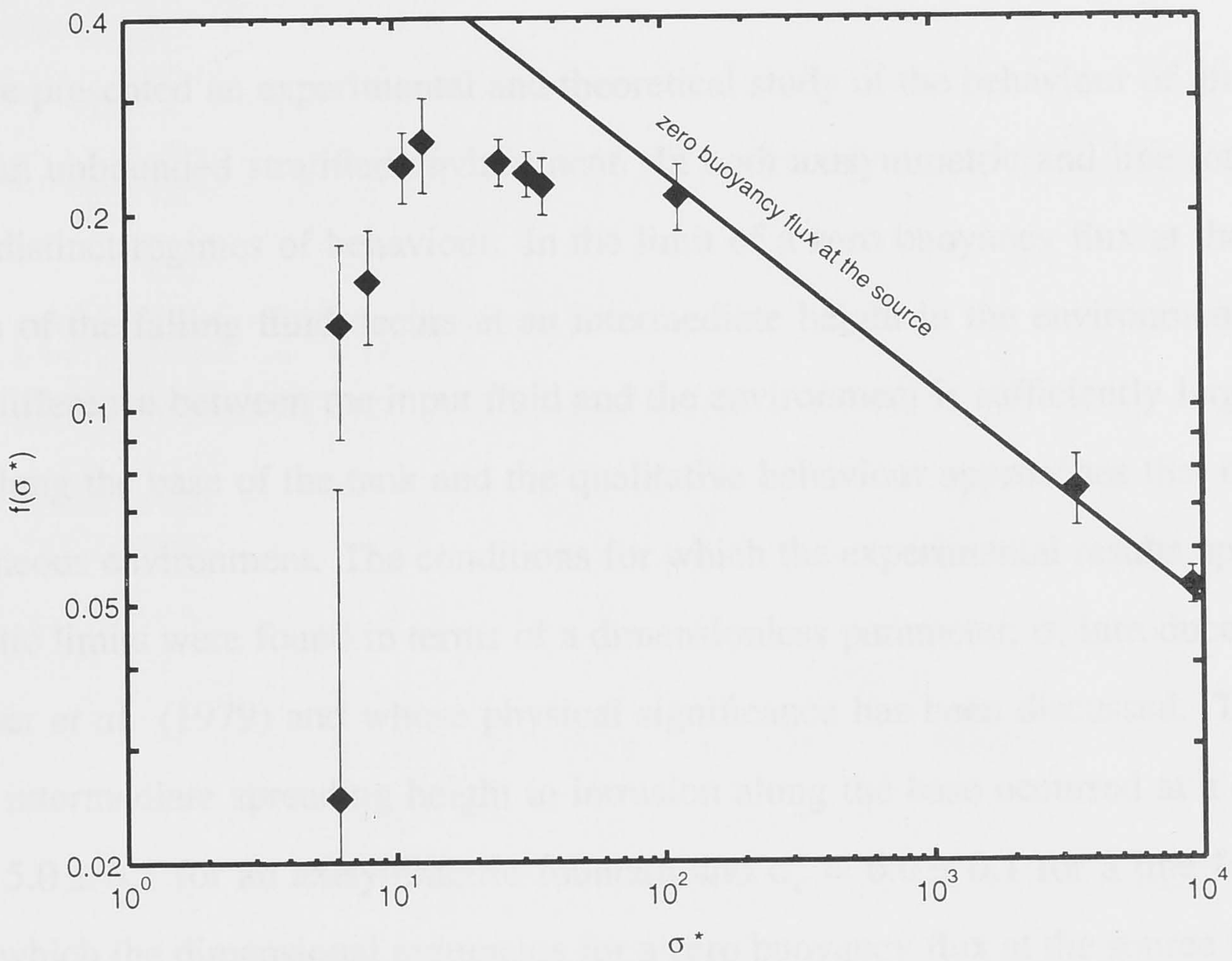

(c)

Figure 2.14: (cont.)

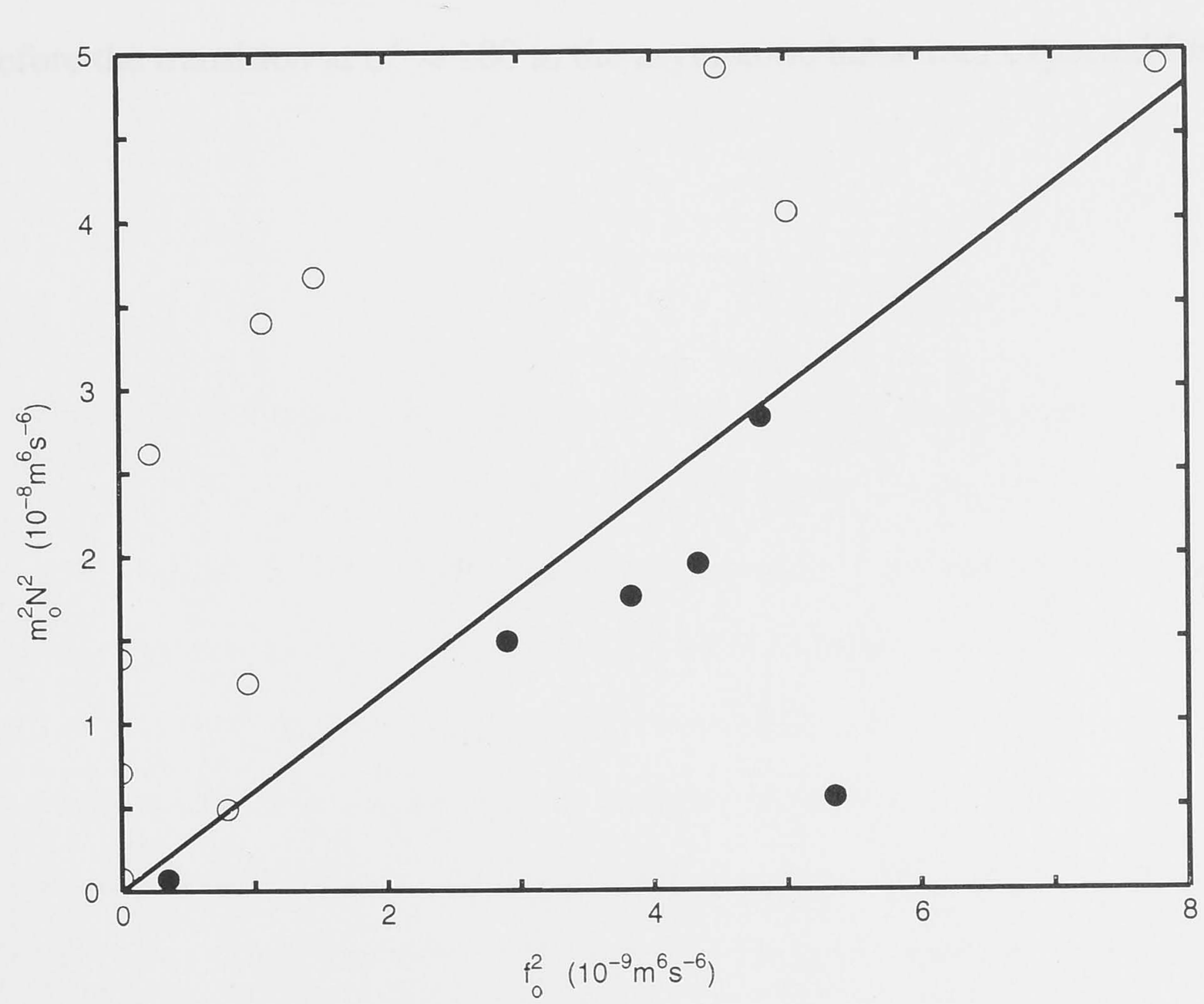

Figure 2.15: The conditions for experiments with an intermediate spreading height (○) and in which spreading occurs along the base (●) are separated by the plotted line which has a slope of 6.0.

2.4 Conclusions

I have presented an experimental and theoretical study of the behaviour of turbulent fountains in an unbounded stratified environment. In both axisymmetric and line fountains there are two distinct regimes of behaviour. In the limit of a zero buoyancy flux at the source, the intrusion of the falling fluid occurs at an intermediate height in the environment. When the density difference between the input fluid and the environment is sufficiently large, spreading occurs along the base of the tank and the qualitative behaviour approaches that observed in a homogeneous environment. The conditions for which the experimental results approach these asymptotic limits were found in terms of a dimensionless parameter, σ, introduced previously by Fischer *et al.* (1979) and whose physical significance has been discussed. The transition from an intermediate spreading height to intrusion along the base occurred at a critical value of $\sigma_c = 5.0 \pm 0.1$ for an axisymmetric fountain and $\sigma_c^* = 6.0 \pm 0.1$ for a line fountain. The point at which the dimensional arguments for a zero buoyancy flux at the source become valid coincided approximately with a maximum in the spreading height at $\sigma_m \approx 40 - 60$ for the axisymmetric fountain. In line fountains, the maximum in the spreading height at $\sigma_m^* \approx 10$ occurred before the transition at $\sigma^* \approx 100$ to the asymptotic behaviour expected for large σ^*.

Chapter 3

Turbulent Fountains in a Confined Stratified Fluid

"The scientist is a practical man and his are practical aims.
He does not seek the ultimate but the proximate.
He does not speak of the last analysis but rather of the next approximation."

G. N. Lewis (1875 - 1946)
American Physical Chemist

When turbulent fountains arise in the world around us, the continuation of the flow into a region of finite extent eventually results in the accumulation of source fluid in the environment. In this chapter, I develop a stratified fountain filling box model to quantify the time evolution of both the fountain and the ambient density profile. I begin in §3.1 by qualitatively describing the evolution of both axisymmetric and line fountains. In §3.2, the theoretical analysis is presented and compared with experimental measurements of axisymmetric fountains. A similar study is then outlined for line fountains in §3.3. The results and conclusions are summarized in §3.4.

3.1 Qualitative observations

The behaviour and evolution of a fountain in a confined environment depend critically on whether intermediate or basal spreading occurs, and hence varies as σ increases from $\sigma = 0$ (homogeneous fluid) to $\sigma \to \infty$ (zero buoyancy flux at the base of a stratified fluid). In a homogeneous environment, the falling fluid reaches the base of the tank where it spreads as a thin layer until restricted by the walls (Baines *et al.* 1990). The density discontinuity at the top of the layer, the *ascending front* , rises as ambient fluid from above it is entrained into the downflow. As the layer increases in thickness, the dense fluid that has accumulated below the front is re-entrained back into the downflow of the fountain. Consequently, all subsequent fluid arrives at the base of the tank even denser, and a weak, stable density gradient is established in the environment below the front. The presence of the dense layer reduces the density difference between the source fluid and its immediate environment, and thus causes the fountain height to rise. However, the ascending front rises faster than the fountain height, so that, eventually, it overtakes the top of the fountain. After this point, the fountain interacts only with the stratified layer, and the rise of the front is controlled only by the rate at which source fluid is added.

In a weakly stratified environment with a sufficiently large buoyancy flux at the source, the downflow still spreads along the base and the subsequent behaviour is qualitatively similar to that observed in a homogeneous environment. However, as the stratification increases and the buoyancy flux at the source decreases, the spreading height rises from the base of the tank (figure 3.1a). In this situation, the qualitative behaviour of the fountain height and the ascending front remain unchanged from that observed in a homogeneous fluid (figure 3.1b,c). However, an additional *descending front* at the bottom of the spreading layer moves towards the base of the tank (figure 3.1b) as fluid from below it is entrained into the upflow of the fountain. The formation of a second front in a stratified fluid is analogous to the plume filling box models in which one front is observed in a homogeneous environment (Baines & Turner 1969) while two form in a stratified fluid (Cardoso & Woods 1993).

When intermediate intrusion occurs, the changes to the ambient density profile differs from those observed in an initially homogeneous fluid. The initial density of the intruding layer is equal to that in the environment at the spreading height, so that the environmental density profile is not significantly altered by the first, thin outflow. Subsequent fluid which re-entrains

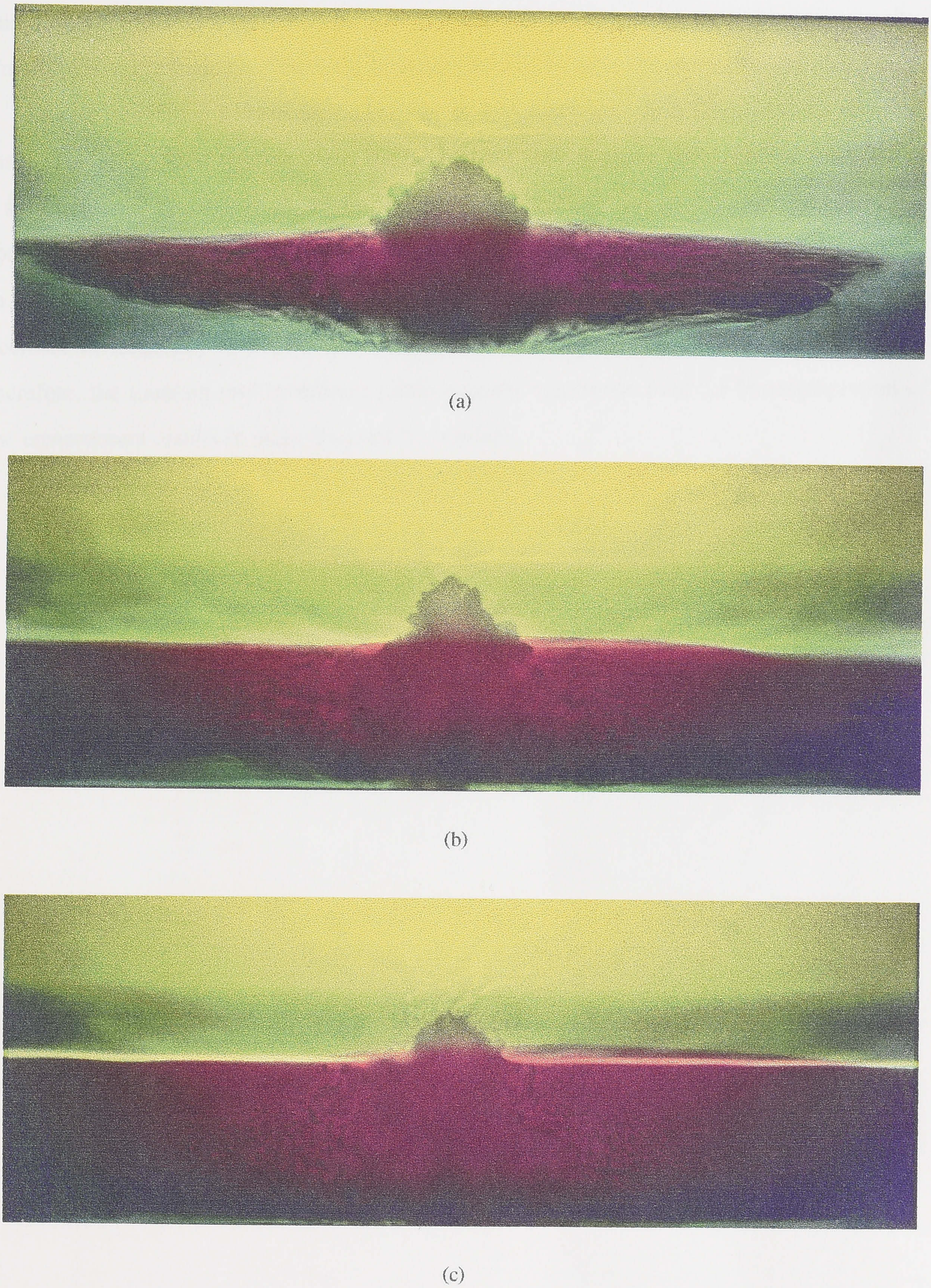

(a)

(b)

(c)

Figure 3.1: Photographs of an axisymmetric fountain with $Q_o = 4.5 \times 10^{-5}$ m^3 s^{-1}, $N = 1.7$ s^{-1} and $\Delta_o = 0$. (a) When intermediate intrusion occurs, both ascending and descending fronts are observed ($t = 50$ s). As the flow continues, (b) the descending front reaches the base of the tank ($t = 2$ min), while (c) the ascending front approaches the top of the fountain ($t = 3$ min 30 s).

this new layer therefore arrives at the spreading height with approximately the same density. Consequently, the fountain effectively homogenizes the initially stratified ambient fluid.

Similar qualitative behaviour is observed in line fountains. In a homogeneous environment, the falling fluid spreads along the base of the tank forming an ascending front above a stratified layer (Baines *et al.* 1990). As the initial ambient density gradient increases, the spreading height rises from the base and both ascending and descending fronts are observed to bound a nearly homogeneous layer (figure 3.2a,b). The fluctuations in the fountain profile decrease in frequency as the ambient stratification increases. In an initially stratified fluid, therefore, the fountain profile remains predominantly symmetric until the homogenization of the environment results in more frequent fluctuations.

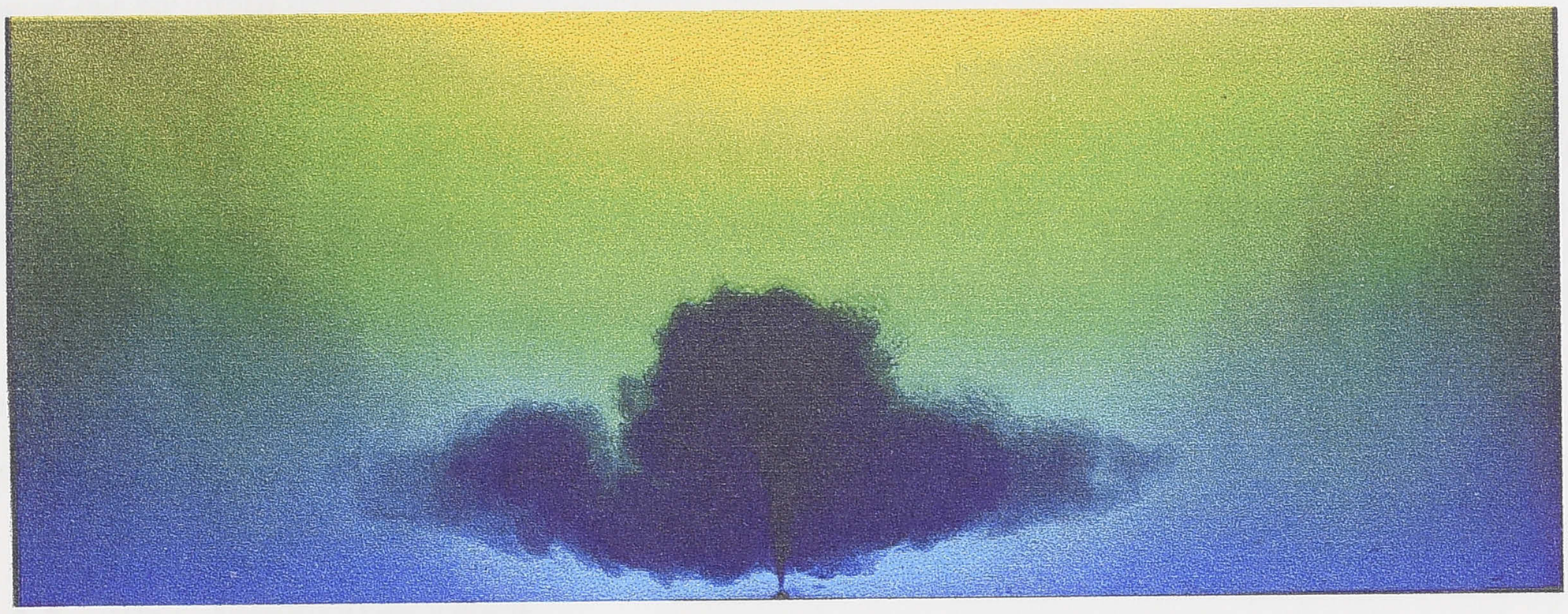

(a)

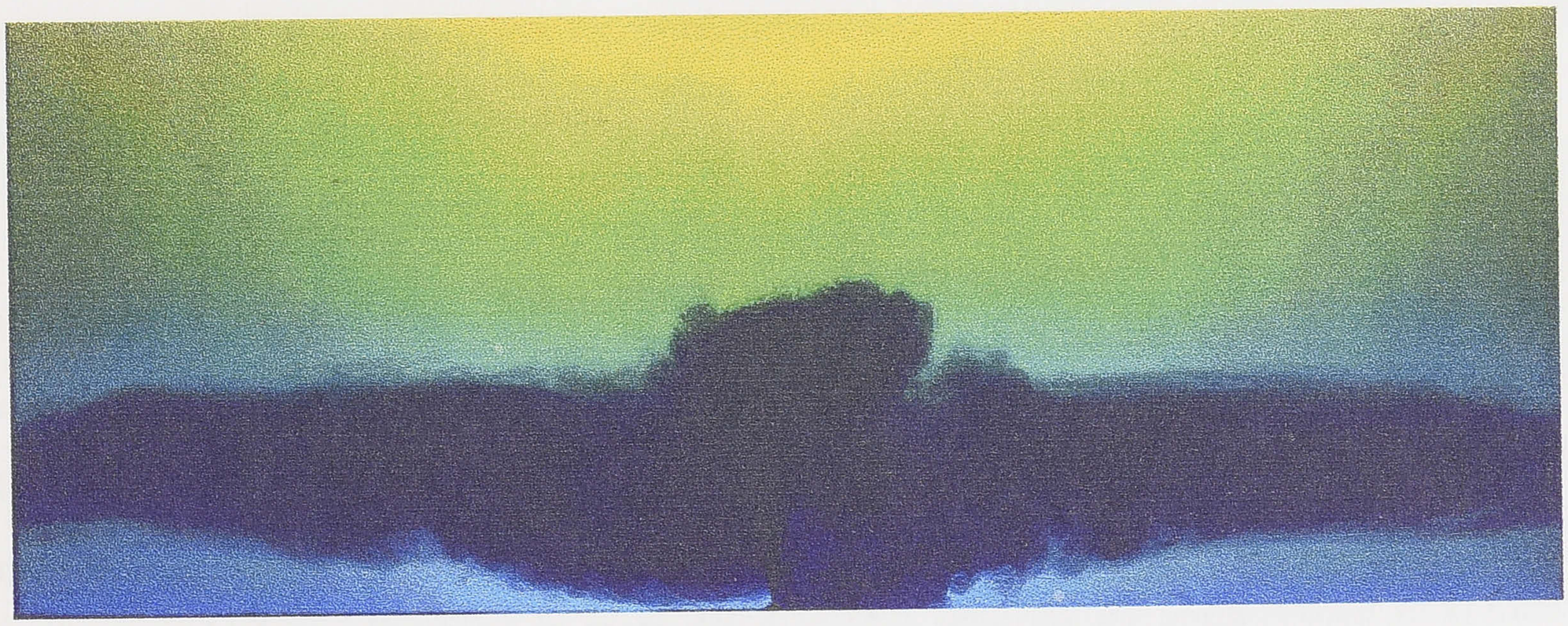

(b)

Figure 3.2: Photographs of a line fountain in which $q_o = 8.8 \times 10^{-5}$ m^2 s^{-1}, $N = 0.75$ s^{-1} and $\Delta_o = 0$. (a) Intermediate intrusion again leads to the formation of two fronts ($t = 21$ s). (b) As the thickness of the spreading layer increases, the fountain continues to oscillate between a symmetric and asymmetric profile ($t = 47$ s).

3.2 Axisymmetric fountains

In this section I develop a fountain filling box model for axisymmetric fountains. In §3.2.1 and §3.2.2, I examine the motion of the descending and ascending fronts, respectively. The rise of the fountain height, which affects the motion of the ascending front, and which depends on the ambient density profile, is quantified in §3.2.3. In this filling box model, it is assumed that the intrusion of fluid into the environment forms a thin layer and occurs on a significantly smaller timescale than that taken for the descending front to fall to a small fraction of its initial level. These assumptions are discussed in detail in §3.2.4. Then, the theoretical results are compared with experimental measurements in §3.2.5. In §3.2.6 I present a theoretical model of the evolution of the ambient density profile.

3.2.1 The descending front

The motion of the descending front can be found using the equation for the conservation of volume flux in the region below the front. If the cross-sectional area of the tank, A, is much greater than that of the fountain, then

$$A\frac{\mathrm{d}z_d}{\mathrm{d}t} = -Q_d, \tag{3.1}$$

where $z_d(t)$ is the height of the front above the virtual point source and Q_d is the volume flux of fluid entrained into the fountain from below z_d. An expression for the total volume flux in the upflow of the fountain, $Q(z)$, can be found from a solution of the entrainment equations. These equations, which are discussed in more detail in §4.2, describe the conservation of volume, b^2u, momentum, b^2u^2, and buoyancy, $b^2u\Delta$, in the flow (Morton *et al.* 1956; Turner 1973):

$$\frac{\mathrm{d}}{\mathrm{d}z}(b^2u) = 2\alpha bu, \quad \frac{\mathrm{d}}{\mathrm{d}z}(b^2u^2) = b^2\Delta, \quad \frac{\mathrm{d}}{\mathrm{d}z}(b^2u\Delta) = -b^2uN^2. \tag{3.2}$$

Equations (3.2) were integrated numerically for the flow through the actual source ($Q_o \neq 0$) with Q_o, Δ_o and N^2 varied over the range of experimental values. The solutions for the volume flux were then compared with the corresponding analytical result for a jet ($F_o = 0$, $N^2 = 0$) showing, in all cases, a difference of less than 1% at the respective spreading heights (see figure 3.3 for the $\sigma \to \infty$ comparison). As the $\sigma \to \infty$ case represents the conditions furthest from

a pure jet, the volume flux in the upflow of the fountain for all values of σ can be approximated by the corresponding result for a jet.

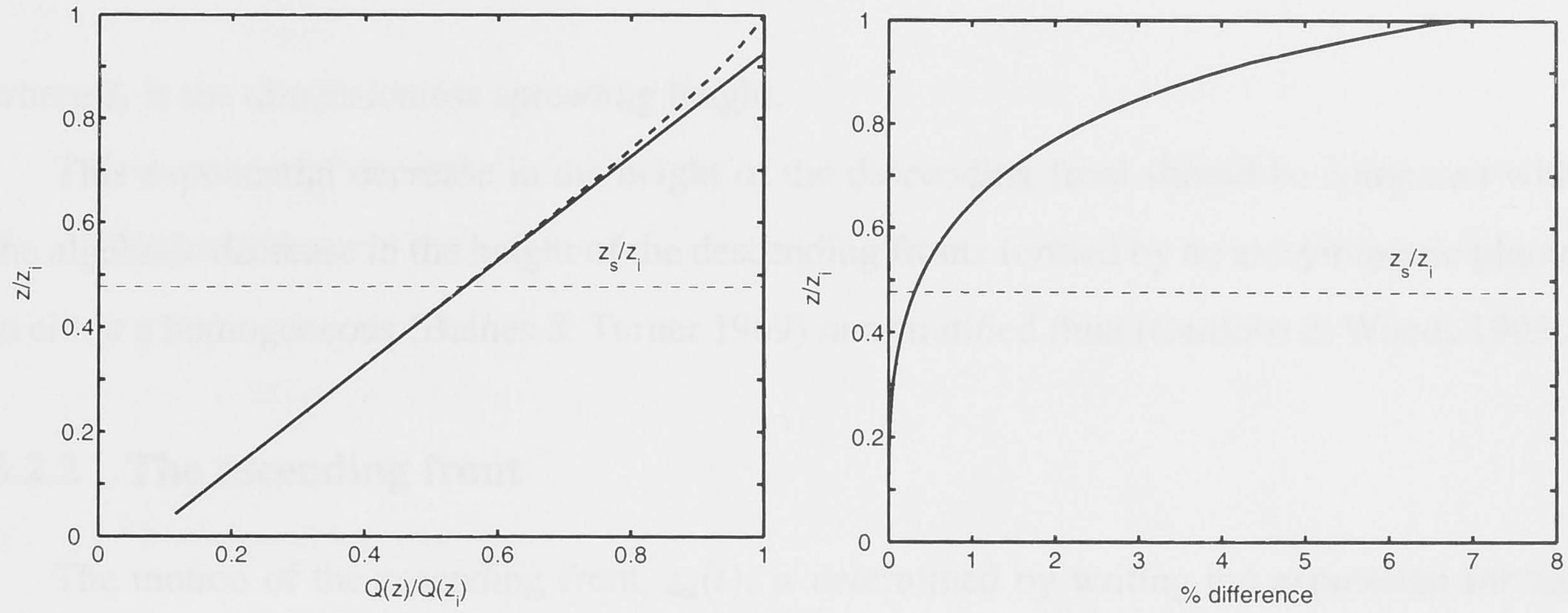

Figure 3.3: (a) Comparison between the volume flux in a fountain with $\sigma \to \infty$ (broken line) and a jet in homogeneous surroundings (solid line), with (b) showing the small difference in regions below the spreading height (indicated by the horizontal line).

An analytical solution of (3.2) for a jet, which satisfies the boundary conditions at the actual source (which is a height z_v above the virtual source) gives:

$$Q(z) = 2\alpha Q_o \frac{z - z_v}{r_e} + Q_o, \tag{3.3}$$

where $\alpha = 0.076 \pm 0.004$ (List 1982a). Whenever intermediate intrusion occurs, therefore, the entrained volume flux between z_v and z_d is

$$Q_d = 2\alpha Q_o \frac{z_d - z_v}{r_e}. \tag{3.4}$$

To simplify this and subsequent expressions, the dimensionless heights, $\tilde{z}$, and times, $\tilde{t}$, defined by

$$\tilde{z} = \frac{z}{r_e} \text{ and } \tilde{t} = \frac{Q_o t}{A r_e}, \tag{3.5}$$

are introduced. With the use of (3.4) and (3.5), (3.1) is integrated to give a solution for the

height of the descending front above the base of the tank:

$$(\tilde{z}_d - \tilde{z}_v) = (\tilde{z}_s - \tilde{z}_v)e^{-2\alpha\tilde{t}}, \tag{3.6}$$

where $\tilde{z}_s$ is the dimensionless spreading height.

This exponential decrease in the height of the descending front should be compared with the algebraic decrease in the height of the descending fronts formed by an axisymmetric plume in either a homogeneous (Baines & Turner 1969) or a stratified fluid (Cardoso & Woods 1993).

3.2.2 The ascending front

The motion of the ascending front, $z_a(t)$, is determined by writing the expression for the conservation of volume flux at the level of the front. Thus

$$A\frac{\mathrm{d}z_a}{\mathrm{d}t} = Q_o + Q_a, \tag{3.7}$$

where Q_a is the volume flux of ambient fluid entrained into the downflow from above the front. Baines *et al.* (1990) described some experimental measurements made by T.J. Reedman which indicated that, in a homogeneous fluid, the entrained volume flux per unit height into the downflow of the fountain is constant and is given by

$$\frac{\mathrm{d}Q_a}{\mathrm{d}z} = B\frac{Q_o}{r_e}, \tag{3.8}$$

where B was found experimentally to be $B = 0.25 \pm 0.03$. Baines *et al.* (1990) also explained that the observation of constant entrainment per unit height can be understood by viewing the downflow as a line plume which encircles the upflow. In a linearly stratified environment, the behaviour of a plume is little different to that in a uniform fluid until close to the spreading height (Cardoso & Woods 1993). As a result, (3.8) is expected to accurately predict the entrainment into the downflow of a fountain in a stratified fluid. The total volume flux entrained between z_a and z_f is therefore

$$Q_a = \frac{BQ_o}{r_e}(z_f - z_a). \tag{3.9}$$

Using (3.5), and introducing (3.9) into (3.7), leads to the general result that

$$\frac{\mathrm{d}\tilde{z}_a}{\mathrm{d}\tilde{t}} = 1 + B(\tilde{z}_f - \tilde{z}_a). \tag{3.10}$$

This result is independent of the environmental conditions and so it applies for all values of σ.

After the ascending front has reached the top of the fountain at a time t^*, the position of the front increases at the same rate as which the free surface rises due to the addition of fluid to the tank, so that $\mathrm{d}\tilde{z}_a/\mathrm{d}\tilde{t} = 1$. To integrate (3.10) for times $t < t^*$, an expression for the increase in the fountain height with time is needed.

3.2.3 The fountain height

In developing an expression for the fountain height, two separate effects must be considered. As discussed in §3.1 and shown quantitatively in figure 3.4, the fountain effectively homogenizes the initially stratified environment, while the addition of dense source fluid increases the average ambient density. The environment of the fountain quickly becomes mixed so that at small times (figure 3.4b), the decrease in the average ambient density gradient over the height of the fountain is a more significant effect than the increase in the average density. At large times, when the environment is nearly homogeneous (figure 3.4c,d), the opposite is true. To determine the contribution from each of these effects, two expressions for the fountain height are derived: $z_{fs}(t)$, which gives the rise due to the decreasing stratification, and $z_{fh}(t)$, which is based on the results of Baines *et al.* (1990) for a fountain in a homogeneous fluid of increasing density.

To quantify $z_{fs}(t)$, the average ambient density gradient over the height of the fountain is approximated by

$$\frac{\mathrm{d}\rho}{\mathrm{d}z}(t) = \frac{\rho_{z_f}(t) - \rho_o}{z_{fs} - z_v}, \tag{3.11}$$

where $\rho_{z_f}(t)$ is the ambient density at the level of the top of the fountain, which is at a height $(z_{fs} - z_v)$ above the base of the tank. At small times, a good approximation for ρ_{z_f} is obtained by assuming that all ambient density levels above the ascending front rise at the same rate as the free surface (figure 3.4). The position of a thin layer which is initially at an arbitrary height, z_o, is therefore given by $z(t) = z_o + Q_o t/A$. When this layer reaches z_{fs}, $\rho_{z_f} = \rho_o +$

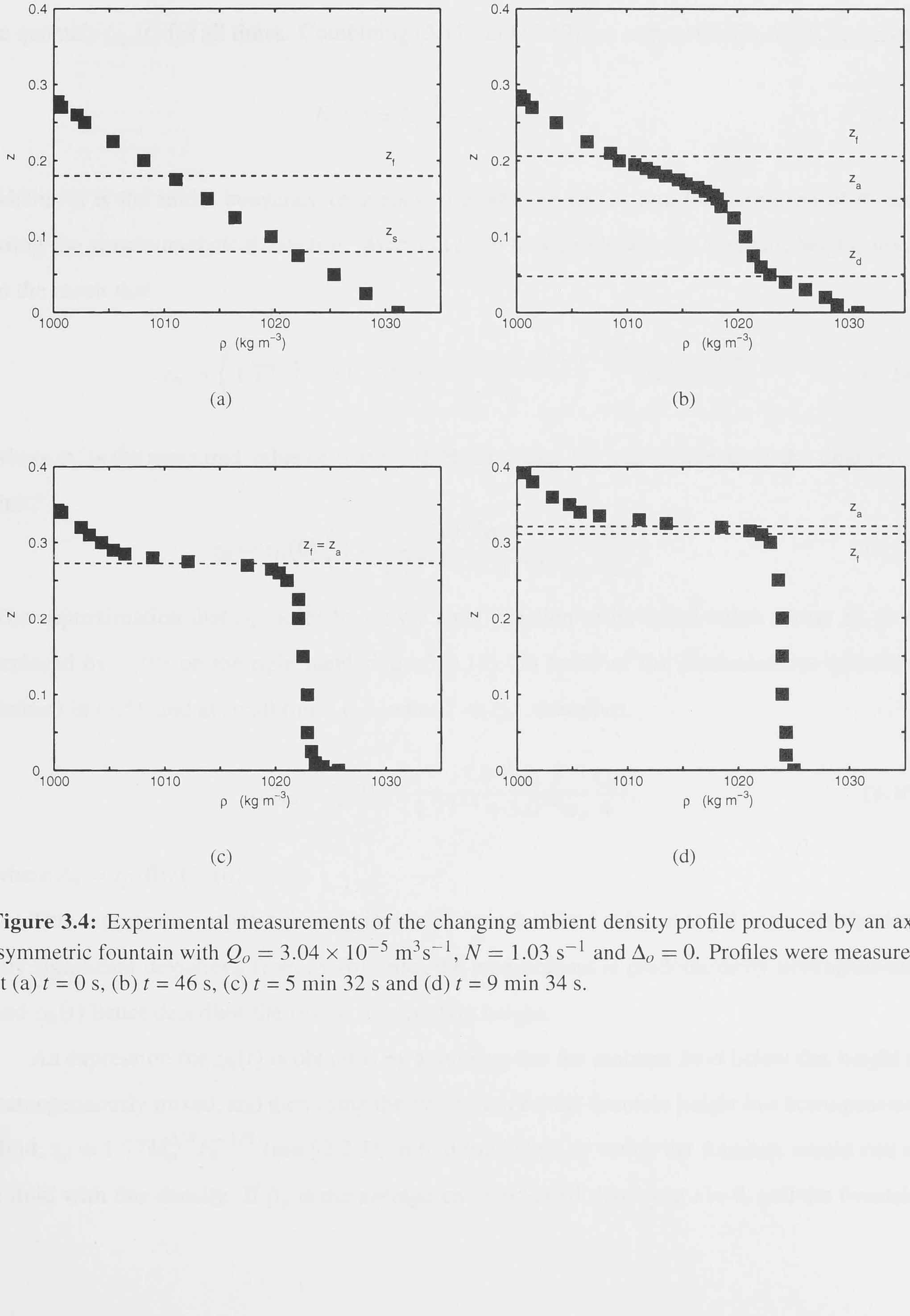

Figure 3.4: Experimental measurements of the changing ambient density profile produced by an axisymmetric fountain with $Q_o = 3.04 \times 10^{-5}$ m^{3}s^{-1}, $N = 1.03$ s^{-1} and $\Delta_o = 0$. Profiles were measured at (a) $t = 0$ s, (b) $t = 46$ s, (c) $t = 5$ min 32 s and (d) $t = 9$ min 34 s.

$(\mathrm{d}\rho/\mathrm{d}z)|_o\,(z_o - z_v)$, giving

$$\rho_{z_f} = \rho_o + \left.\frac{\mathrm{d}\rho}{\mathrm{d}z}\right|_o \left(z_{fs} - z_v - \frac{Q_o t}{A}\right), \tag{3.12}$$

where $(\mathrm{d}\rho/\mathrm{d}z)|_o$ is the initial density gradient. As a first approximation for z_{fs}, (3.12) is used to quantify $\rho_{z_f}(t)$ for all times. Combining (3.11) and (3.12), an expression for $N^2(t)$ becomes:

$$N^2(t) = N_o^2 \frac{z_{fs} - z_v - Q_o t/A}{z_{fs} - z_v}, \tag{3.13}$$

where N_o is the initial buoyancy frequency. Introducing (3.13) into the definition of σ, and using the simple analytical function given in (2.14) to approximate the fountain height, leads to the result that

$$z_{fs} = \left(1.77^{-4} + 3.0^{-4}\sigma_o \frac{z_{fs} - z_v - Q_o t/A}{z_{fs} - z_v}\right)^{-1/4} M_o^{3/4} F_o^{-1/2}, \tag{3.14}$$

where σ_o is the measured value of σ at $t = 0$. Rearranging this expression gives the final result that

$$z_{fs} = z_{fs}(0)\left(1 - \frac{3.0^{-4}\sigma_o}{1.77^{-4} + 3.0^{-4}\sigma_o} \frac{Q_o t/A}{z_{fs} - z_v}\right)^{-1/4}. \tag{3.15}$$

The approximation that z_{fs} varies by only a small fraction of its initial value allows z_{fs} to be replaced by $z_{fs}(0)$ on the right hand side of (3.15). In terms of the dimensionless quantities defined in (3.5), and at small times (i.e. when $\tilde{t} \ll \tilde{z}_{fs}$), therefore,

$$\tilde{z}_{fs} \approx \tilde{z}_{fs}(0) + \frac{3.0^{-4}\sigma_o}{1.77^{-4} + 3.0^{-4}\sigma_o} \frac{\tilde{z}_{rs}}{4}\tilde{t}, \tag{3.16}$$

where $\tilde{z}_{rs} = \tilde{z}_{fs}(0)/(\tilde{z}_{fs}(0) - \tilde{z}_v)$.

This expression quantifies how $\tilde{z}_{fs}$ increases from its initial value at small times. By the time any significant deviations from (3.16) arise, the environment is predominantly homogeneous, and $z_{fh}(t)$ better describes the rise of the fountain height.

An expression for $z_{fh}(t)$ is obtained by assuming that the ambient fluid below this height is homogeneously mixed, and then using the expression for the fountain height in a homogeneous fluid, $z_f = 1.77 M_o^{3/4} F_o^{-1/2}$ (see §2.2.3), to find the height to which the fountain would rise in a fluid with this density. If $\bar{\rho}_o$ is the average environmental density at $t = 0$, and the fountain

reaches a height $z_{fh}(0)$ in this homogeneous fluid, then

$$\bar{\rho}_o = \rho_o + \left.\frac{d\rho}{dz}\right|_o \frac{(z_{fh}(0) - z_v)}{2}. \tag{3.17}$$

The initial buoyant acceleration of the source fluid is found using the definition of Baines *et al.* (1990) to be

$$\bar{\Delta}_o = \frac{g(\rho_i - \bar{\rho}_o)}{\bar{\rho}_o} = \frac{\Delta_o + N_o^2(z_{fh}(0) - z_v)/2}{1 - N_o^2(z_{fh}(0) - z_v)/(2g)}. \tag{3.18}$$

Using this definition of $\bar{\Delta}_o$ in the expression for the fountain height, an equation is obtained, which can be solved numerically for $z_{fh}(0)$:

$$z_{fh}(0) = 1.77 M_o^{3/4} Q_o^{-1/2} \left(\frac{1 - N_o^2(z_{fh}(0) - z_v)/(2g)}{\Delta_o + N_o^2(z_{fh}(0) - z_v)/2} \right)^{1/2}. \tag{3.19}$$

In a homogeneous fluid, Baines *et al.* (1990) have shown both experimentally and theoretically that the fountain height rises at close to half the rate at which the free surface rises due to the inflow. If the same theoretical arguments are applied to estimate z_{fh}, then the equivalent result is

$$\tilde{z}_{fh} = \tilde{z}_{fh}(0) + \frac{1}{2}\tilde{z}_{rh}\tilde{t}, \tag{3.20}$$

where $\tilde{z}_{rh} = \tilde{z}_{fh}(0)/(\tilde{z}_{fh}(0) - \tilde{z}_v)$.

To quantify the fountain height at all times, (3.16) and (3.20) are combined into a single expression which characterizes the transition from $\tilde{z}_{fs}$ at small times to $\tilde{z}_{fh}$ as $\tilde{t} \to \tilde{t}^*$. A suitable expression for $\tilde{z}_f(\tilde{t})$ is therefore

$$\tilde{z}_f(\tilde{t}) = (1 - w(\tilde{t}))\tilde{z}_{fs} + w(\tilde{t})\tilde{z}_{fh}, \tag{3.21}$$

where $w(\tilde{t})$ is a function which is equal to 0 at $\tilde{t} = 0$ and becomes equal to 1 at $\tilde{t} = \tilde{t}^*$. A simple weighting function which quantifies the fraction of fluid below $\tilde{z}_f$ which is homogeneous, and therefore satisfies the required limits, is given by

$$w = \frac{\tilde{z}_a - \tilde{z}_d}{\tilde{z}_f - \tilde{z}_v}. \tag{3.22}$$

Introducing (3.22) into (3.21) and solving for $\tilde{z}_f$ gives a final expression for the fountain height:

$$\tilde{z}_f = \frac{1}{2}\left(\tilde{z}_{fs} + \tilde{z}_v\right) + \left(\frac{1}{4}\left(\tilde{z}_{fs} + \tilde{z}_v\right)^2 + \left(\tilde{z}_a - \tilde{z}_d\right)\left(\tilde{z}_{fh} - \tilde{z}_{fs}\right) - \tilde{z}_v\tilde{z}_{fs}\right)^{1/2}. \tag{3.23}$$

This expression can then be used in the numerical integration of (3.10) to give a solution for the ascending front. Finally, from this result for $\tilde{z}_a$, the position of the fountain height is calculated from (3.23).

3.2.4 Outflow dynamics — the assumption of instantaneous spreading

The expressions derived for the ascending and descending fronts relied on the assumption that the spreading layer intrudes almost instantaneously as a thin layer. The observation is made that, as the radial distance increases, the thickness of the outflow quickly becomes small compared to the spreading height. The validity of assuming instantaneous spreading is now determined by analysing the effect of the tank size and source conditions on the timescales for intrusion and for vertical advection. The following analysis applies to the situations in which intrusion occurs at an intermediate height in the environment.

Following the analysis presented by Cardoso & Woods (1993) for a plume in a stratified fluid, several simplifying assumptions are used to determine expressions for the dynamics of the intruding fluid. As the downflow reaches the spreading height, the flow into the intruding layer is still turbulent. However, it is assumed that the ambient stratification quickly damps this turbulence, so that little mixing occurs between the spreading layer and the environment. The dynamics of the intruding layer may then simply be described by an outflow Froude number,

$$Fr = \frac{v}{Nd}, \tag{3.24}$$

where v is the horizontal velocity of the fluid in the layer and d is its thickness (figure 3.5). It was shown by Manins (1979) that the Froude number of a lateral outflow into a stratified fluid is approximately constant with a lower bound of $2^{-1/2}$.

The velocity of the descending front is then assumed to be horizontally constant and equal to U_s. From the conservation of volume, the horizontal volume flux at a distance r from the

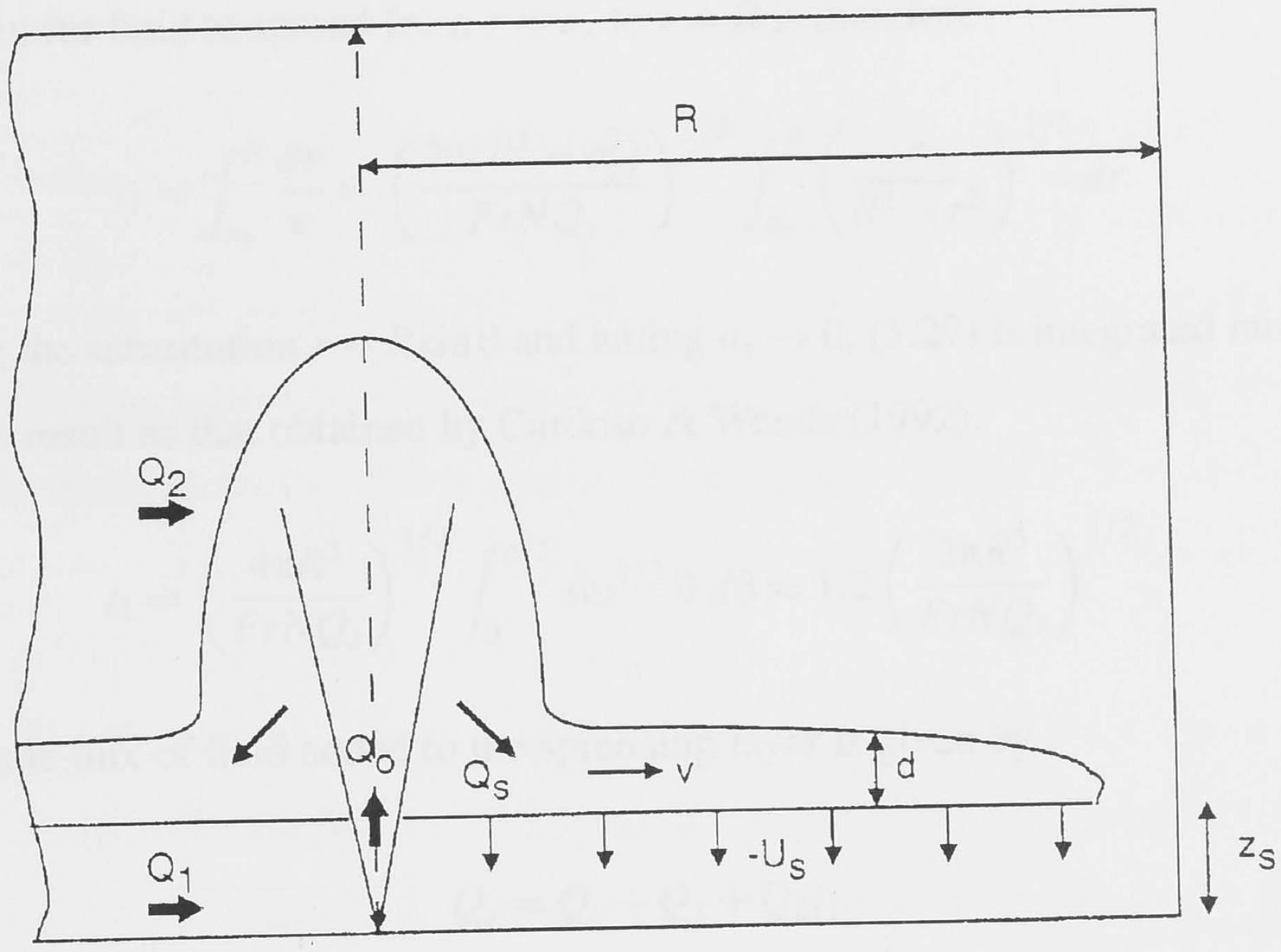

Figure 3.5: Geometry illustrating the outflow of fluid into the spreading layer.

fountain axis is written as

$$Q(r) = 2\pi r v d = Q_s - U_s \pi (r^2 - a_s^2), \tag{3.25}$$

where a_s is the fountain radius at the spreading height and Q_s is the volume flux into the intruding layer at $r = a_s$. To simplify the analysis, a tank of circular cross section with radius R is considered, so that the area, πR^2, is equal to the area, A, of the actual tank. As there can be no flow through the walls of the tank, $Q(R) = 0$. This result is used to eliminate U_s from (3.25) giving

$$Q(r) = 2\pi r dv = Q_s \left(\frac{R^2 - r^2}{R^2 - a_s^2} \right). \tag{3.26}$$

Introducing (3.24) in (3.26), the radial dependence of d and v is found to be:

$$d = \left(\frac{Q_s}{2\pi r Fr N} \left(\frac{R^2 - r^2}{R^2 - a_s^2} \right) \right)^{1/2} \tag{3.27}$$

$$v = \left(\frac{Fr N Q_s}{2\pi r} \left(\frac{R^2 - r^2}{R^2 - a_s^2} \right) \right)^{1/2}. \tag{3.28}$$

The time taken for fluid to spread from $r = a_s$ to $r = R$ is therefore

$$t_1 = \int_{a_s}^{R} \frac{dr}{v} = \left(\frac{2\pi(R^2 - a_s^2)}{FrNQ_s}\right)^{1/2} \int_{a_s}^{R} \left(\frac{r}{R^2 - r^2}\right)^{1/2} dr. \tag{3.29}$$

After making the substitution $r = R\sin\theta$ and letting $a_s \to 0$, (3.29) is integrated numerically to give the same result as that obtained by Cardoso & Woods (1992):

$$t_1 = \left(\frac{4\pi R^3}{FrNQ_s}\right)^{1/2} \int_0^{\pi/2} \sin^{1/2}\theta \, d\theta \approx 1.2 \left(\frac{2\pi R^3}{FrNQ_s}\right)^{1/2}. \tag{3.30}$$

The volume flux of fluid added to the spreading layer is given by

$$Q_s = Q_o + Q_1 + Q_2, \tag{3.31}$$

where $Q_1 = 2\alpha Q_o(z_s - z_v)/r_e$ is the volume flux entrained into the jet-like flow below the spreading height (§3.2.1) and $Q_2 = BQ_o(z_f - z_s)/r_e$ is the volume flux entrained into the down-flow of the fountain (§3.2.2). The first term in (3.31) is negligible in these experiments, so that:

$$Q_s \approx \frac{Q_o}{r_e}\left(2\alpha(z_s - z_v) + B(z_f - z_s)\right). \tag{3.32}$$

The timescale for vertical advection in the tank, t_2, is chosen to be the time taken for the position of the descending front to fall from its initial height above the base, $z_s - z_v$, to a height of $e^{-2}(z_s - z_v) \approx 0.1(z_s - z_v)$:

$$t_2 = \frac{Ar_e}{\alpha Q_o}. \tag{3.33}$$

Using (3.32) and a value of $Fr = 2^{-1/2}$, the ratio of (3.30) to (3.33) becomes

$$\frac{t_1}{t_2} = 0.09\left(\frac{Q_o}{Nr_eR}\right)^{1/2} \left(2\alpha(z_s - z_v) + B(z_f - z_s)\right)^{-1/2}. \tag{3.34}$$

This ratio is valid while the fluid intrudes at an intermediate height, that is for σ in the range $\sigma_c < \sigma < \infty$. For the source parameters in the experiments performed, values of $t_1/t_2 \approx 0.08$ are obtained. This small value indicates that the assumption of instantaneous spreading is valid in these experiments.

3.2.5 Experimental results

The basic experimental setup was unchanged from that described in §2.2.1, except that a larger tank (70 cm × 70 cm in cross section and 40 cm deep) was used in some experiments. In addition to the shadowgraph technique, dye was also introduced into the source fluid to clearly mark the extent of the spreading layer. The density profile was measured during the experiment by stopping the flow and withdrawing samples from a range of depths. The densities of these samples were then measured by refractometry. It was observed that stopping and starting the flow did not disturb the position of the fronts.

The positions of the fountain height and the fronts were measured in a series of experiments performed for a range of values of σ. The data from three of these experiments are shown in figure 3.6 along with the result of integrating (3.10) for the ascending front, the predicted position of the fountain height (3.23) and, where applicable, the expression for the descending front (3.6). The fountain height at $\tilde{t} = 0$ was determined from (2.7) and (2.14). The value of z_s was estimated from the experimental results for the spreading height (figure 2.9). In general, the good agreement between theory and experiment for the fountain height and ascending front indicates that the assumptions made, and the simple weighting function used, describe the actual fountain behaviour well. The experimental results indicate that the descending front falls slightly faster than predicted by (3.6). This faster descent is almost certainly due to the effect of the additional entrainment into the overshooting fluid below the front, which is not included in the model.

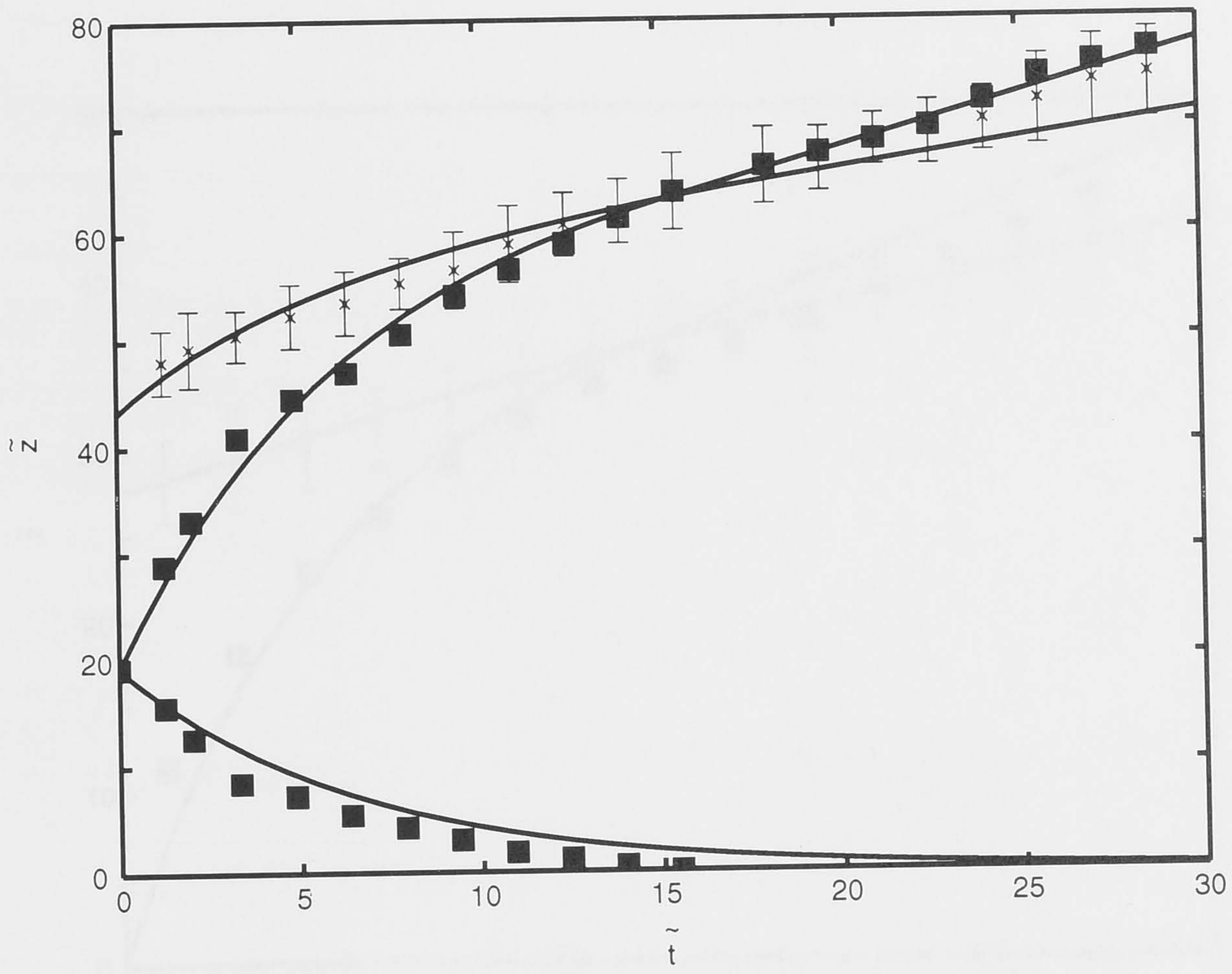

(a)

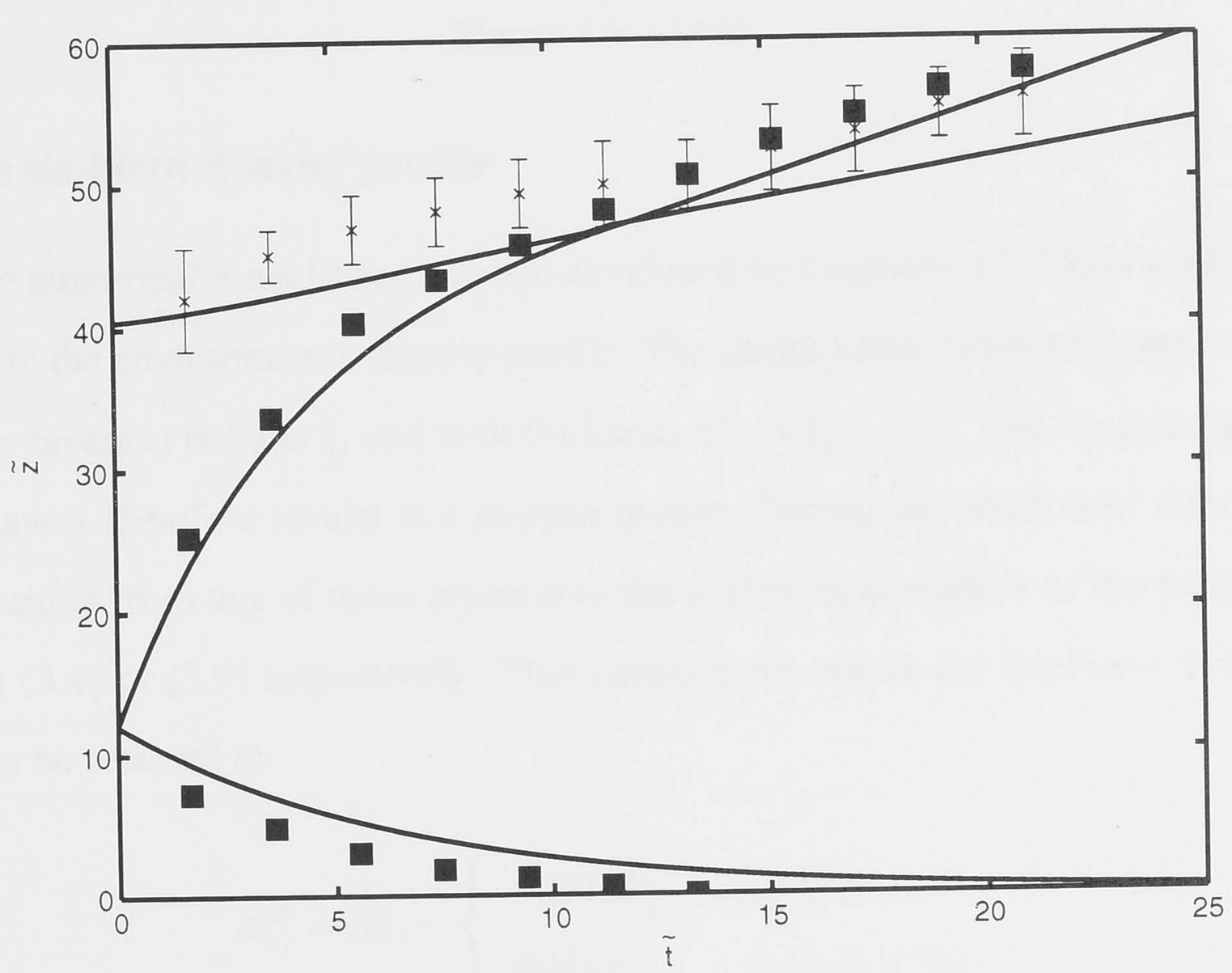

(b)

Figure 3.6: The non-dimensional height of the axisymmetric fountain (×) and the positions of the fronts (■), as a function of time, together with the theoretical predictions (solid lines) for the fountain height (3.23), the ascending front (3.10) and, where applicable, the descending front (3.6). The experimental parameters were (a) $Q_o = 3.04 \times 10^{-5}\,\mathrm{m^3\,s^{-1}}$, $N = 1.03\,\mathrm{s^{-1}}$; $\sigma \to \infty$, (b) $Q_o = 3.87 \times 10^{-5}\,\mathrm{m^3\,s^{-1}}$, $N = 1.22\,\mathrm{s^{-1}}$, $\Delta_o = 0.23\,\mathrm{m\,s^{-2}}$; $\sigma = 14$, and (c) $Q_o = 3.25 \times 10^{-5}\,\mathrm{m^3\,s^{-1}}$, $N = 1.28\,\mathrm{s^{-1}}$, $\Delta_o = 0.37\,\mathrm{m\,s^{-2}}$; $\sigma = 4$.

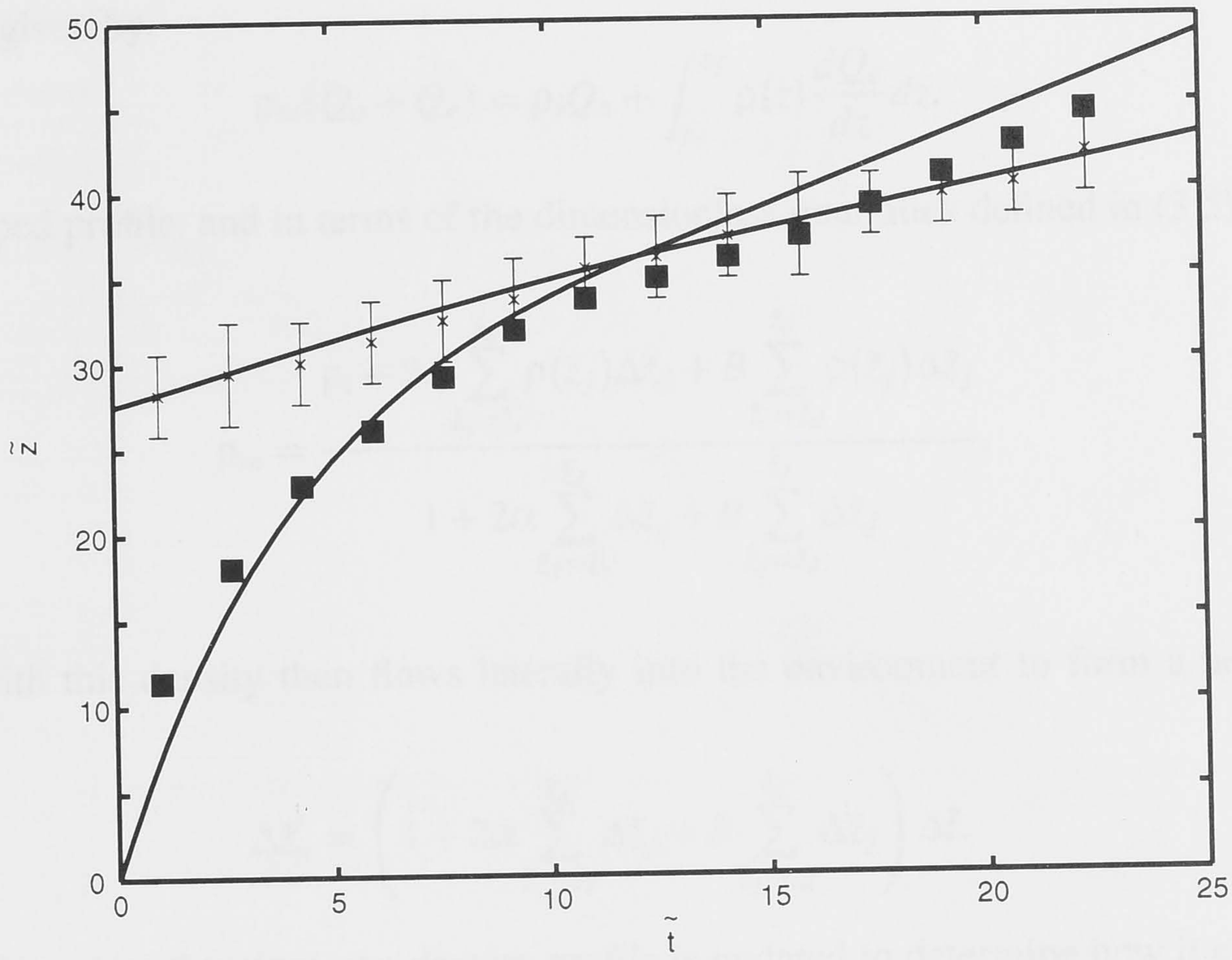

(c)

Figure 3.6: (cont.)

3.2.6 The ambient density profile

A simple numerical model based on that developed by Germeles (1975) is used to quantify the changes to the environmental density profile. The initial linear gradient is approximated by thin, discrete layers at heights $\tilde{z}_j$ and with thickness $\Delta\tilde{z}_j = \tilde{z}_{j+1} - \tilde{z}_j$. The decreasing density in successive layers therefore results in a stepped profile. During any small time interval, $\Delta\tilde{t}$, the volume entrained from any of these layers into the upflow or downflow of the fountain can be found using (3.4) or (3.9) respectively. This entrainment causes the thickness of the steps in the profile to be reduced to

$$\Delta\tilde{z}'_j = \Delta\tilde{z}_j - \begin{cases} 2\alpha\Delta\tilde{t}\Delta\tilde{z}_j & \tilde{z}_j < \tilde{z}_d \\ B\Delta\tilde{t}\Delta\tilde{z}_j & \tilde{z}_d < \tilde{z}_j < \tilde{z}_f, \end{cases} \tag{3.35}$$

while the density at each step is unchanged. The positions of $\tilde{z}_d$ and $\tilde{z}_f$ in this stepped profile are determined from (3.6) and (3.23), respectively.

The ambient fluid entrained into the fountain in the interval $\Delta\tilde{t}$ mixes with the injected

source fluid, so that when the downflow reaches the point of intrusion, the fountain fluid has a density, ρ_m, given by

$$\rho_m(Q_o + Q_e) = \rho_i Q_o + \int_{z_v}^{z_f} \rho(z) \frac{dQ_e}{dz} dz. \tag{3.36}$$

For the stepped profile, and in terms of the dimensionless quantities defined in (3.5),

$$\rho_m = \frac{\rho_i + 2\alpha \sum_{\tilde{z}_j=\tilde{z}_v}^{\tilde{z}_d} \rho(\tilde{z}_j)\Delta\tilde{z}_j + B \sum_{\tilde{z}_j=\tilde{z}_d}^{\tilde{z}_f} \rho(\tilde{z}_j)\Delta\tilde{z}_j}{1 + 2\alpha \sum_{\tilde{z}_j=\tilde{z}_v}^{\tilde{z}_d} \Delta\tilde{z}_j + B \sum_{\tilde{z}_j=\tilde{z}_d}^{\tilde{z}_f} \Delta\tilde{z}_j}. \tag{3.37}$$

The fluid with this density then flows laterally into the environment to form a new layer of thickness

$$\Delta\tilde{z}_n' = \left(1 + 2\alpha \sum_{\tilde{z}_j=\tilde{z}_v}^{\tilde{z}_d} \Delta\tilde{z}_j + B \sum_{\tilde{z}_j=\tilde{z}_d}^{\tilde{z}_f} \Delta\tilde{z}_j\right) \Delta\tilde{t}. \tag{3.38}$$

With each time step, therefore, the density profile is updated to determine how it evolves with time by reducing the thickness of the layers below $\tilde{z}_f$ and adding the new layer at the correct step in the profile.

An example of the result of this procedure is compared to the experimental data in figure 3.7. The initial step sizes were chosen to be $\Delta z = 1$ mm, while Δt was decreased until $\Delta t = 1$ s, after which further decreases did not change the final result. At small times, the numerical results predict a much more homogeneous spreading layer than that observed experimentally. The additional variation in the densities in the spreading layer most probably arise from a combination of two effects - additional mixing below the descending front, and the fact that the downflow has a range of densities which leads to a range of intrusion heights. At later times, the agreement between the numerical and experimental results is much better, with the numerical results only slightly underestimating the density within the spreading layer.

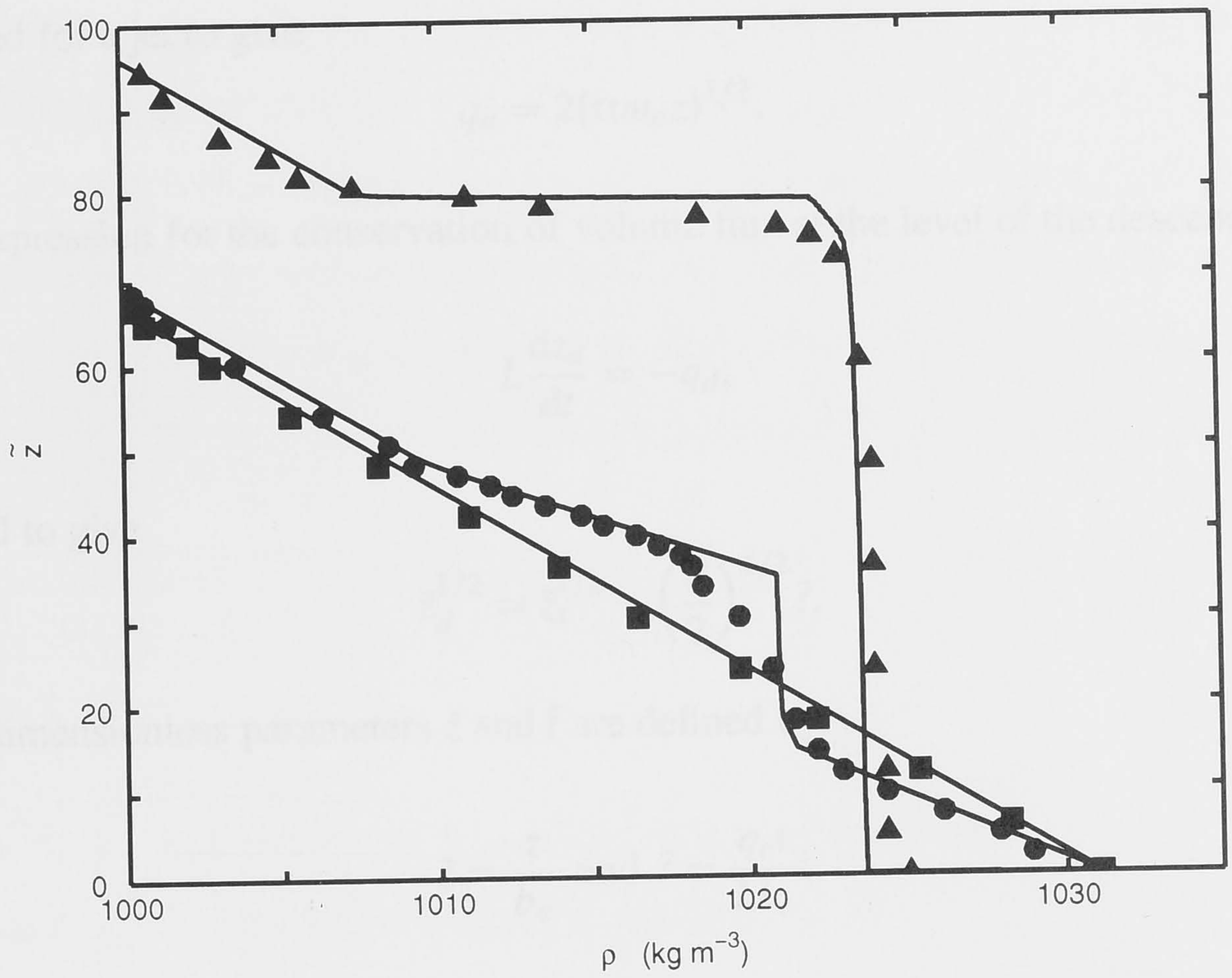

Figure 3.7: Ambient density profiles produced by an axisymmetric fountain, with $Q_o = 3.04 \times 10^{-5}$ m^3 s^{-1}, $N = 1.03$ s^{-1} and $\Delta_o = 0$. The measured profiles at $t = 0$ (■), $t = 46$ s (•) and $t = 9$ min 34 s (▲) are shown in comparison with the numerical predictions (solid line).

3.3 Line fountains

The analysis of line fountains follows the same procedure outlined in §3.2 for axisymmetric fountains. In §3.3.1, §3.3.2 and §3.3.3, I develop expressions for the motion of the descending front, ascending front and fountain height, respectively. The assumption of instantaneous spreading is then examined in §3.3.4. The theoretical predictions for the motion of the fronts and the fountain height are then compared with experimental measurements in §3.3.5. A model of the evolution of the ambient density profile is then outlined in §3.3.6.

3.3.1 The descending front

Using the arguments presented in §3.3.1, it is once more assumed that in a stratified fluid, the upflow remains jet-like for a significant distance above the source. The two dimensional entrainment equations, which are given by:

$$\frac{\mathrm{d}}{\mathrm{d}z}(2bu) = 2\alpha u, \quad \frac{\mathrm{d}}{\mathrm{d}z}(2bu^2) = 2b\Delta, \quad \frac{\mathrm{d}}{\mathrm{d}z}(2bu\Delta) = 0, \tag{3.39}$$

can be solved for a jet to give

$$q_d = 2(\alpha m_o z)^{1/2}. \tag{3.40}$$

Then, the expression for the conservation of volume flux at the level of the descending front,

$$L\frac{\mathrm{d}z_d}{\mathrm{d}t} = -q_d, \tag{3.41}$$

is integrated to give

$$\tilde{z}_d^{1/2} = \tilde{z}_s^{1/2} - \left(\frac{\alpha}{2}\right)^{1/2}\tilde{t}, \tag{3.42}$$

where the dimensionless parameters $\tilde{z}$ and $\tilde{t}$ are defined by

$$\tilde{z} = \frac{z}{b_o} \text{ and } \tilde{t} = \frac{q_o t}{L b_o}. \tag{3.43}$$

The descending front formed by a line fountain therefore reaches the level of the source after a time $\tilde{t}_d = (2\tilde{z}_s/\alpha)^{1/2}$. This result clearly differs from that for both axisymmetric fountains and plumes in stratified fluids, where the descending front only asymptotically approaches the level of the source.

3.3.2 The ascending front

The motion of the ascending front is again determined by the conservation of volume flux at the level of the front. Thus

$$L\frac{\mathrm{d}z_a}{\mathrm{d}t} = q_o + q_a, \tag{3.44}$$

where q_a is the total volume flux per unit length entrained into the downflow between the ascending front and the fountain height.

As a result of the fluctuations in the fountain profile, Baines *et al.* (1990) reported difficulties in finding a satisfactory expression for the entrained volume flux into the downflow. They hence made the assumption that q_a has the same dependence on height as the jet-like upflow (Baines *et al.* (1990), equation 43). This leads to the result that

$$\frac{\mathrm{d}q_a}{\mathrm{d}z} = \frac{Bq_o}{2b_o^{1/2}z^{1/2}}, \tag{3.45}$$

where B was determined experimentally to range between 0.5 and 1.0, with an average value of $B \approx 0.75$ (Baines *et al.* 1990).

In order to remain consistent with the results of Baines *et al.* (1990), the same result is used here for the flow in an ambient density gradient. The expression for the entrained volume flux above the ascending front is therefore $q_a = Bq_o(z_f^{1/2} - z_a^{1/2})/b_o^{1/2}$. Introducing this result into (3.44), along with the dimensionless quantities defined in (3.43), leads to the result that

$$\frac{\mathrm{d}\tilde{z}_a}{\mathrm{d}\tilde{t}} = 1 + B(\tilde{z}_f^{1/2} - \tilde{z}_a^{1/2}). \tag{3.46}$$

3.3.3 The fountain height

The rise of the fountain height is predicted using the same assumptions and method that were presented in §3.2.3 for an axisymmetric fountain.

First, the rise of the fountain height at small times due to the decrease in the average buoyancy frequency of the environment, z_{fs}, is quantified. The change in $N^2(t)$ is again given by (3.13), without the virtual source correction. Combining (3.13) with (2.18) and (2.23), and using the dimensionless forms of z and t, leads to the result that

$$\tilde{z}_{fs} = \tilde{z}_{fs}(0)\left(1 - \frac{2.43^{-3}\sigma_o^*}{0.96^{-3} + 2.43^{-3}\sigma_o^*}\frac{\tilde{t}}{\tilde{z}_{fs}}\right)^{-1/3}. \tag{3.47}$$

At small times, this implies that

$$\tilde{z}_{fs} = \tilde{z}_{fs}(0) + \frac{2.43^{-3}\sigma_o^*}{0.96^{-3} + 2.43^{-3}\sigma_o^*}\frac{\tilde{t}}{3}, \tag{3.48}$$

where $\tilde{z}_{fs}(0)$ is taken to be the dimensionless symmetric height, since the profile is predominantly symmetric at small times.

Second, to obtain an expression for the rise of the fountain due to the increasing average ambient density, $z_{fh}(t)$ and $z_{fh}(0)$ must be determined. The initial buoyant acceleration of the source fluid is again given by (3.18) with $z_v = 0$, so that an implicit expression for $z_{fh}(0)$ is found from a combination of (2.18) and (2.22) to be

$$z_{fh}(0) = \frac{\frac{1}{2}(0.96 + 0.77)m_o^{2/3}}{2^{1/3}b_o^{1/3}}\left(\frac{1 - N_o^2 z_{fh}(0)/(2g)}{\Delta_o + N_o^2 z_{fh}(0)/2}\right)^{2/3}. \tag{3.49}$$

In this expression, the average of the symmetric and asymmetric heights has been used, since the fountain in a homogeneous fluid continually fluctuates between a symmetric and an asymmetric profile. To quantify the fountain height at later times, the result for a homogeneous fluid is used, so that the dimensionless fountain height rises at a rate given by

$$\tilde{z}_{fh} = \tilde{z}_{fh}(0) + \frac{2}{3}\tilde{z}_r\tilde{t}. \tag{3.50}$$

where $\tilde{z}_r = \tilde{z}_{fh}(0)/(\tilde{z}_{fh}(0) + \tilde{z}_e)$ (Baines *et al.* 1990).

Finally, the weighting function which quantifies the transition between (3.48) and (3.50), is again given by (3.22), with $\tilde{z}_v = 0$. It therefore follows that the final expression for the fountain height is also given by (3.23), with $\tilde{z}_{fs}$ and $\tilde{z}_{fh}$ defined by (3.48) and (3.50) respectively. This expression for $\tilde{z}_f$ can then be used in the numerical integration of (3.46) to find the position of the ascending front.

3.3.4 Outflow dynamics

A similar analysis to that presented in §3.2.4 is used to determine the timescale of lateral intrusion for a line fountain. Conservation of horizontal volume flux in the spreading layer on one side of the upflow at a distance x from the fountain axis gives

$$q(x) = dv = \frac{q_s}{2} - U_s(x - a_s), \tag{3.51}$$

where q_s is the total volume flux in the outflow at the spreading height. Expressions for the thickness and velocity within the spreading layer are obtained by combining (3.24) with (3.51) under the condition that $q = 0$ at $x = L/2 = l$:

$$d = \left(\frac{q_s}{2NFr}\left(\frac{l-x}{l-a_s}\right)\right)^{1/2} \tag{3.52}$$

$$v = \left(\frac{NFrq_s}{2}\left(\frac{l-x}{l-a_s}\right)\right)^{1/2}. \tag{3.53}$$

The time taken for the fluid to spread from $x = a_s$ to $x = l$ is

$$t_1 = \int_{a_s}^{l} \frac{dx}{v} = \left(\frac{2(l-a_s)}{NFrq_s}\right)^{1/2} \int_{a_s}^{l} \frac{dx}{(l-x)^{1/2}}. \tag{3.54}$$

In the limit as $a_s \to 0$, this is integrated to give

$$t_1 = \left(\frac{8l^2}{NFrq_s}\right)^{1/2}. \tag{3.55}$$

The volume flux of fluid into the spreading layer is again given by $q_s = q_o + q_1 + q_2$ with $q_1 = (2\alpha q_o^2 z_s/b_o)^{1/2}$ (§3.3.1) and $q_2 = Bq_o(z_f^{1/2} - z_s^{1/2})/b_o^{1/2}$ (§3.3.2), so that

$$\begin{aligned} q_s &= q_o\left(1 + (2\alpha z_s/b_o)^{1/2} + B(z_f^{1/2} - z_s^{1/2})/b_o^{1/2}\right) \\ &\approx q_o\left((2\alpha z_s)^{1/2} + B(z_f^{1/2} - z_s^{1/2})\right)/b_o^{1/2}. \end{aligned} \tag{3.56}$$

A typical timescale for the vertical motion in the ambient fluid is the time taken for the descending front to reach the base of the tank:

$$t_2 = \left(\frac{8l^2 b_o z_s}{\alpha q_o^2}\right)^{1/2}. \tag{3.57}$$

Using (3.56) and a value of $Fr = 2^{-1/2}$, the ratio of (3.55) to (3.57) becomes

$$\frac{t_1}{t_2} = 0.32\left(\frac{q_o}{Nb_o^{1/2} z_s((2\alpha z_s)^{1/2} + B(z_f^{1/2} - z_s^{1/2}))}\right)^{1/2}. \tag{3.58}$$

Using typical experimental parameters gives the result that $t_1/t_2 \approx 0.4 - 0.5$. The assumption of instantaneous spreading may therefore introduce some deviation between the theory and experiments. In particular, at small times, the variation in the thickness of the outflow makes it difficult to accurately measure the position of the fronts. This effect was reduced, but not eliminated, by measuring the height of the fronts close to the axis of the fountain.

3.3.5 Experimental results

The position of the fountain height, the ascending front and the descending front were measured in three experiments in which σ^* was varied. These results are shown in figure 3.8,

along with the predicted position of the top of the fountain, the ascending front and, where applicable, the descending front. The fountain height at $t = 0$ is found from a combination of (2.18) and (2.23), while the spreading height was taken from the experimental measurements. In figures 3.8(a) and 3.9(b), the position of the descending front is well described by (3.42) until it approaches to within approximately 2 cm ($\tilde{z} \approx 430$) of the source. After this point, the environmental fluid is entrained into the initial axisymmetric flow from the holes, and consequently, the exponential decay predicted for axisymmetric flow can be observed. In figure 3.8(a), the position of the fountain height is slightly overestimated by the theoretical prediction. In contrast, in figures 3.9(b) and 3.9(c), in which the profile fluctuates significantly, (3.23) represents a good average of the measured heights. Using the average value of $B = 0.75$ in all experiments provides good predictions of the motion of the ascending front, and enables accurate estimates of the time t^* when the front reaches the height of the fountain.

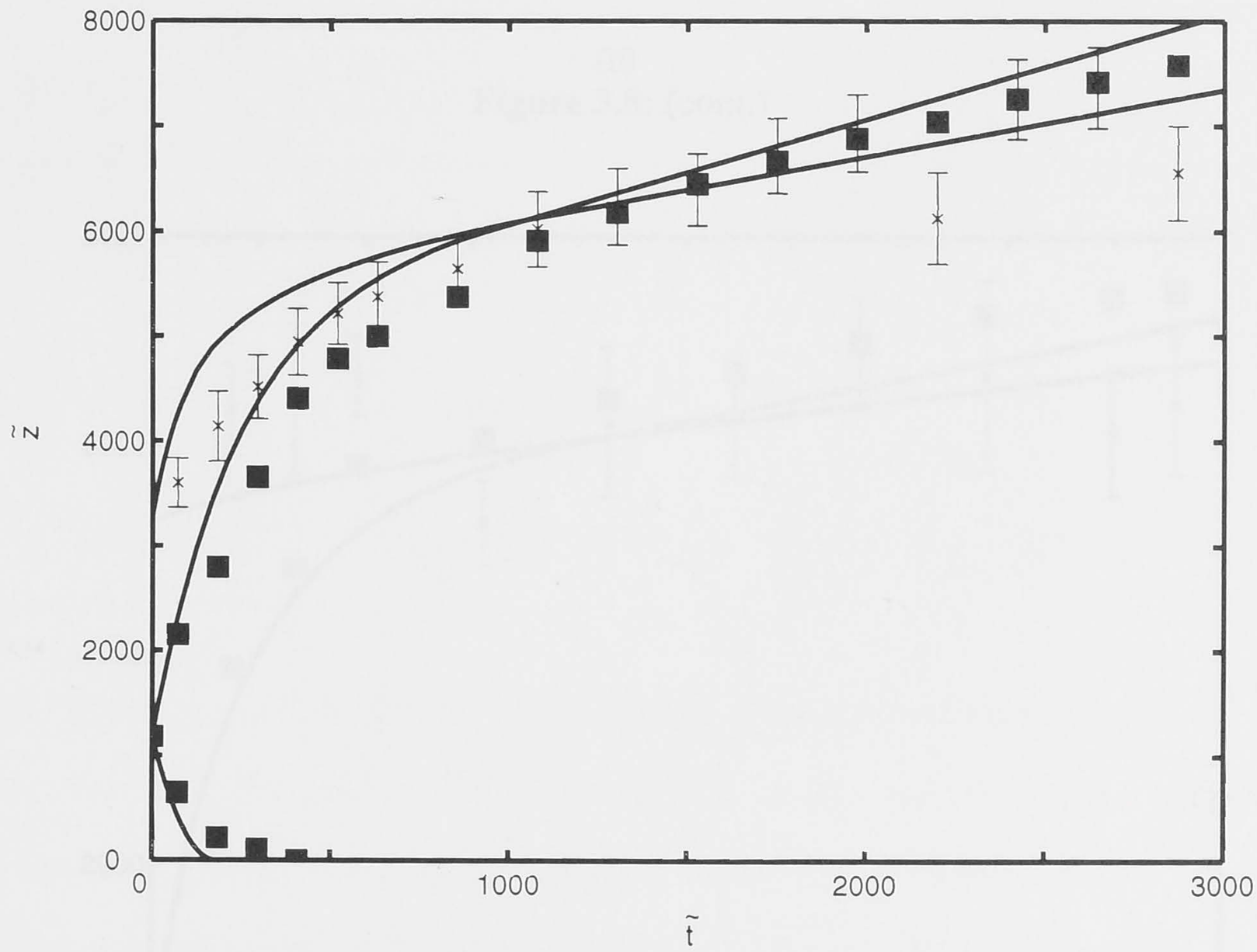

(a)

Figure 3.8: The non-dimensional height of a line fountain (×) and the positions of the fronts (■), as a function of time, together with the theoretical predictions (solid lines) for the fountain height (3.23), the ascending front (3.46) and, where applicable, the descending front (3.42). The experimental parameters were (a) $q_o = 2.19 \times 10^{-4}\ \mathrm{m^2\,s^{-1}}$, $N = 1.38\ \mathrm{s^{-1}}$; $\sigma^* = \infty$; (b) $q_o = 2.19 \times 10^{-4}\ \mathrm{m^2\,s^{-1}}$, $N = 0.71\ \mathrm{s^{-1}}$, $\Delta_o = 0.34\ \mathrm{m\,s^{-2}}$; $\sigma^* = 21$; (c) $q_o = 2.19 \times 10^{-4}\ \mathrm{m^2\,s^{-1}}$, $N = 0.32\ \mathrm{s^{-1}}$, $\Delta_o = 0.31\ \mathrm{m\,s^{-2}}$; $\sigma^* = 5.2$.

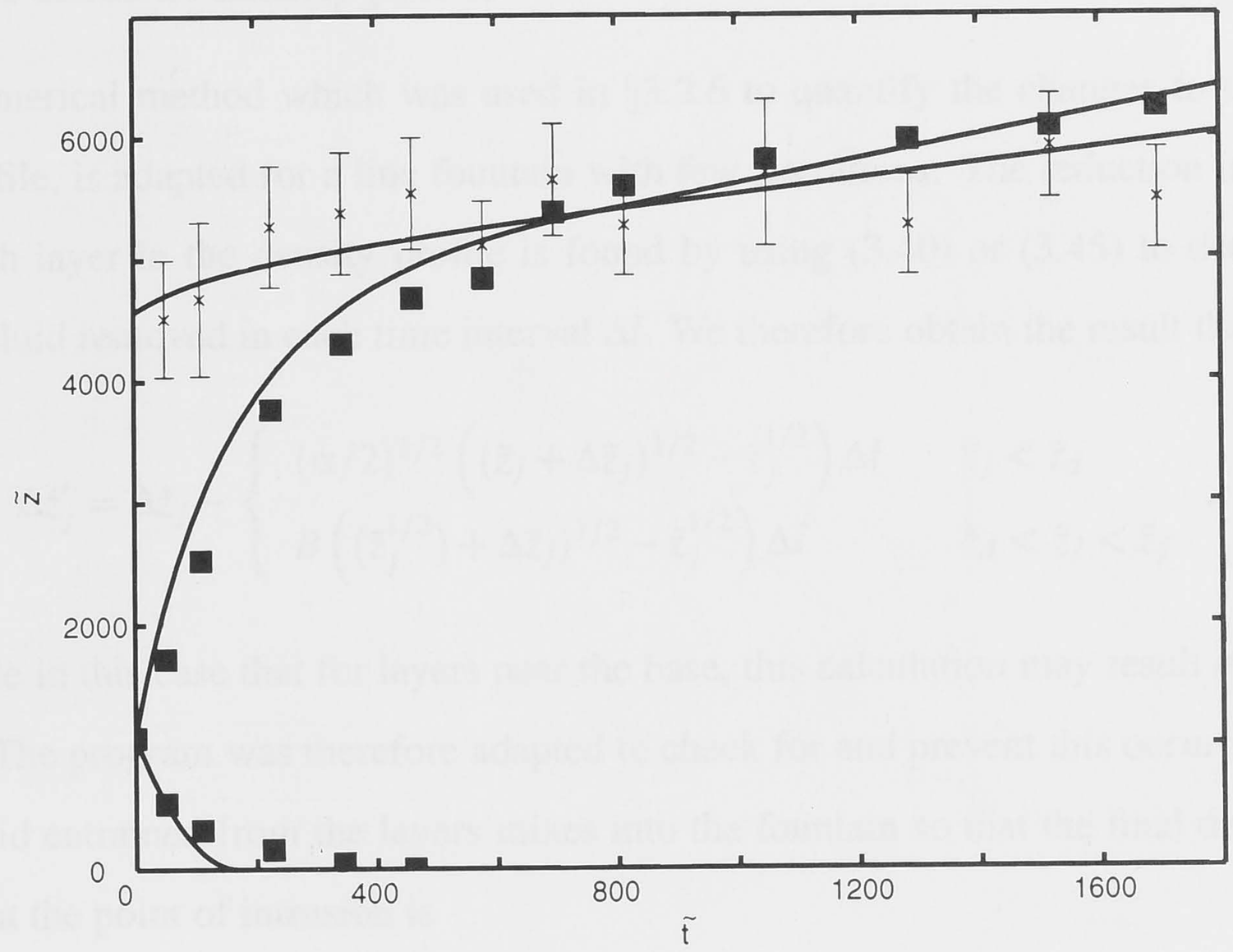

(b)

Figure 3.8: (cont.)

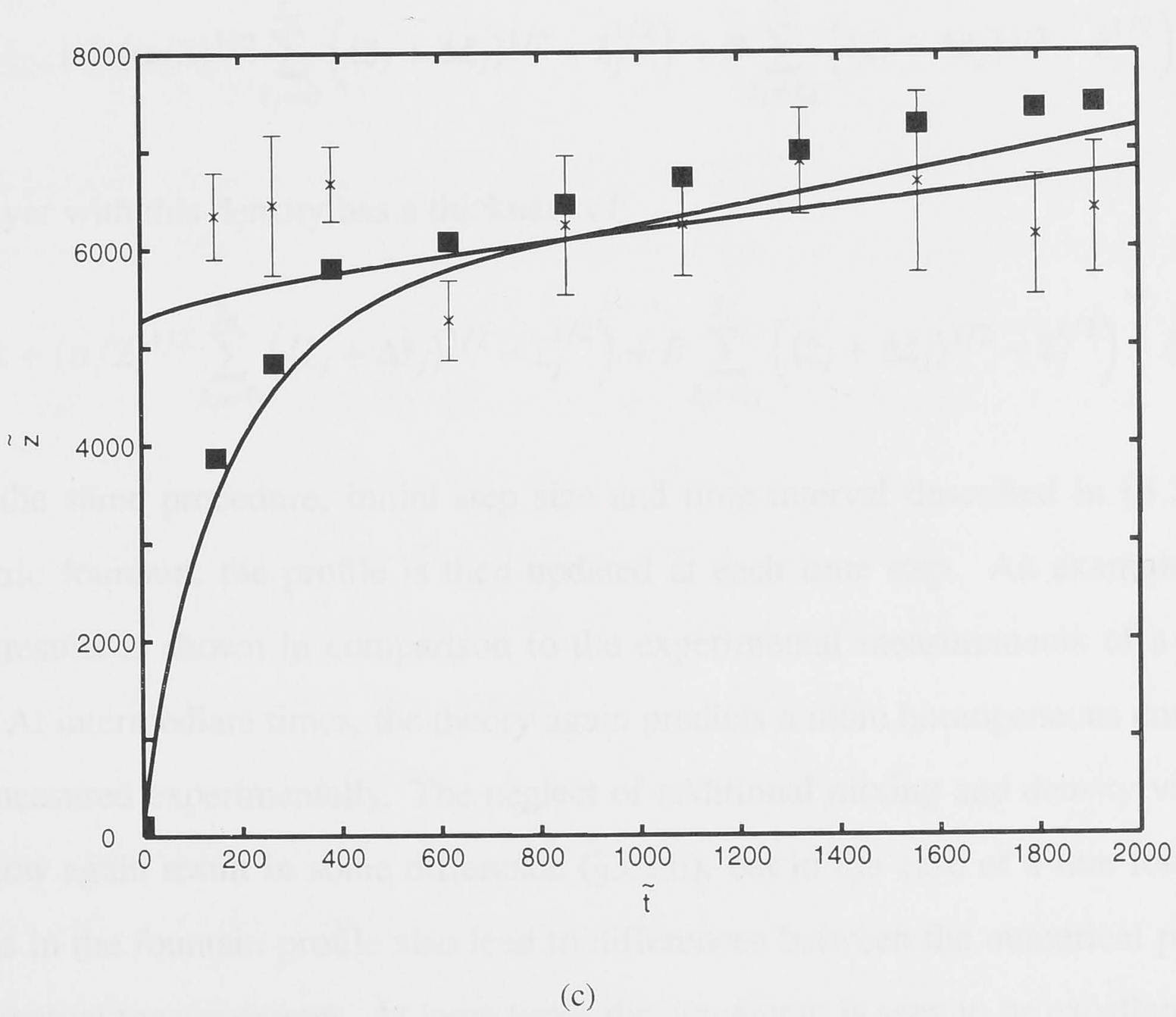

(c)

3.3.6 The ambient density profile

The numerical method which was used in §3.2.6 to quantify the changes to the ambient density profile, is adapted for a line fountain with few alterations. The reduction in the thickness of each layer in the density profile is found by using (3.40) or (3.45) to determine the volume of fluid removed in each time interval $\Delta\tilde{t}$. We therefore obtain the result that

$$\Delta\tilde{z}'_j = \Delta\tilde{z}_j - \begin{cases} (\alpha/2)^{1/2}\left((\tilde{z}_j+\Delta\tilde{z}_j)^{1/2}-\tilde{z}_j^{1/2}\right)\Delta\tilde{t} & \tilde{z}_j < \tilde{z}_d \\ B\left((\tilde{z}_j^{1/2})+\Delta\tilde{z}_j)^{1/2}-\tilde{z}_j^{1/2}\right)\Delta\tilde{t} & \tilde{z}_d < \tilde{z}_j < \tilde{z}_f \end{cases}. \tag{3.59}$$

It is possible in this case that for layers near the base, this calculation may result in a negative thickness. The program was therefore adapted to check for and prevent this occurring.

The fluid entrained from the layers mixes into the fountain so that the final density of the downflow at the point of intrusion is

$$\rho_m = \frac{\rho_i + (\alpha/2)^{1/2}\sum_{\tilde{z}_j=0}^{\tilde{z}_d}\rho(\tilde{z}_j)\left((\tilde{z}_j+\Delta\tilde{z}_j)^{1/2}-\tilde{z}_j^{1/2}\right)+B\sum_{\tilde{z}_j=\tilde{z}_d}^{\tilde{z}_f}\rho(\tilde{z})\left((\tilde{z}_j+\Delta\tilde{z}_j)^{1/2}-\tilde{z}_j^{1/2}\right)}{1+(\alpha/2)^{1/2}\sum_{\tilde{z}_j=0}^{\tilde{z}_d}\left((\tilde{z}_j+\Delta\tilde{z}_j)^{1/2}-\tilde{z}_j^{1/2}\right)+B\sum_{\tilde{z}_j=\tilde{z}_d}^{\tilde{z}_f}\left((\tilde{z}_j+\Delta\tilde{z}_j)^{1/2}-\tilde{z}_j^{1/2}\right)}. \tag{3.60}$$

The new layer with this density has a thickness of

$$\Delta\tilde{z}'_n = \left(1+(\alpha/2)^{1/2}\sum_{\tilde{z}_j=0}^{\tilde{z}_d}\left((\tilde{z}_j+\Delta\tilde{z}_j)^{1/2}-\tilde{z}_j^{1/2}\right)+B\sum_{\tilde{z}_j=\tilde{z}_d}^{\tilde{z}_f}\left((\tilde{z}_j+\Delta\tilde{z}_j)^{1/2}-\tilde{z}_j^{1/2}\right)\right)\Delta\tilde{t}. \tag{3.61}$$

Using the same procedure, initial step size and time interval described in §3.2.6 for an axisymmetric fountain, the profile is then updated at each time step. An example of these numerical results is shown in comparison to the experimental measurements of a profile in figure 3.9. At intermediate times, the theory again predicts a more homogeneous environment than that measured experimentally. The neglect of additional mixing and density variation in the downflow again result in some difference (§3.2.6), but in the case of a line fountain, the fluctuations in the fountain profile also lead to differences between the numerical predictions and experimental measurements. At large times the agreement is seen to be excellent.

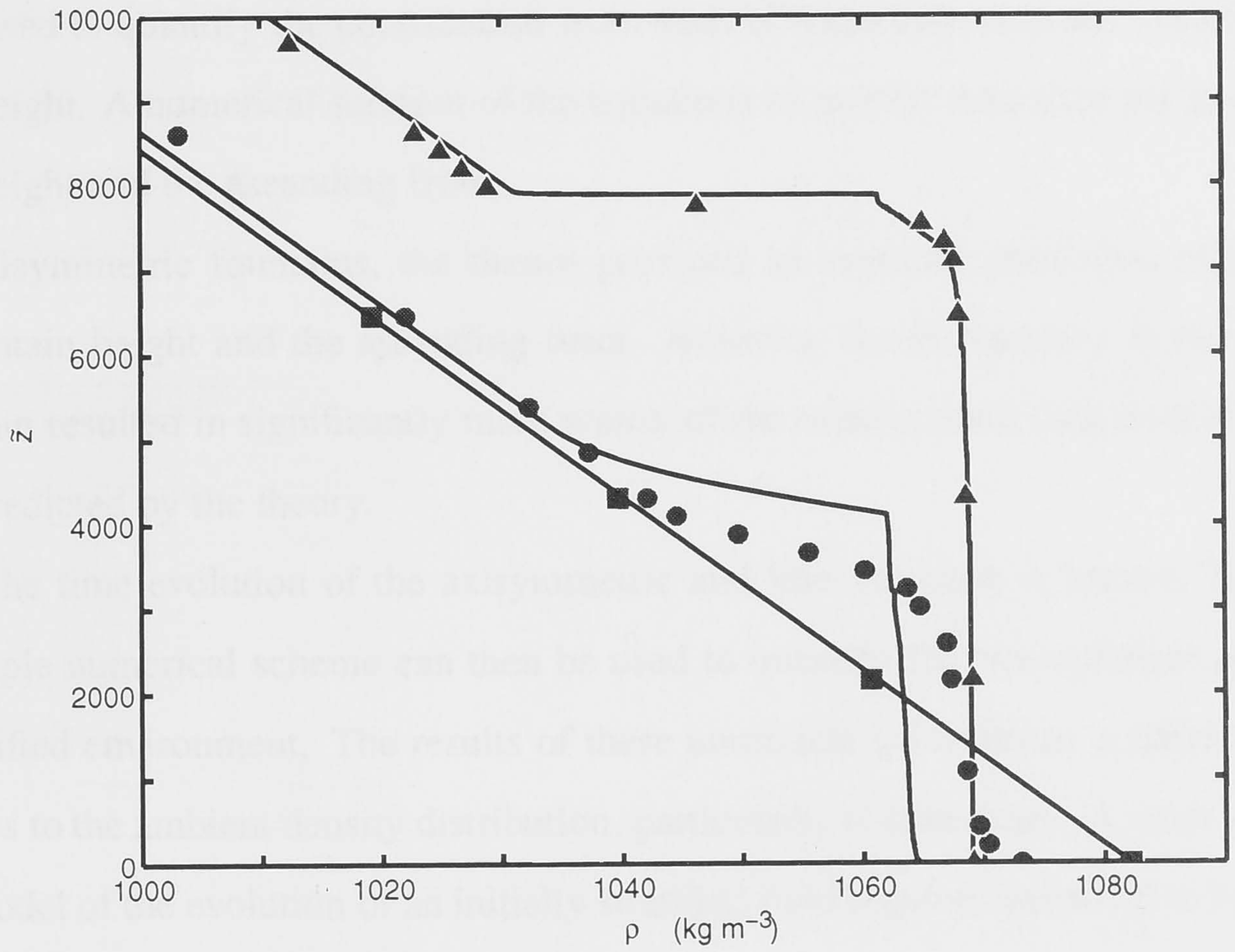

Figure 3.9: Comparison between the numerical results (solid line) and the measured ambient density profiles produced by a line fountain, with $q_o = 2.19 \times 10^{-4}$ m^2 s^{-1}, $N = 1.38$ s^{-1} and $\Delta_o = 0$. Profiles were measured at $t = 0$ (■), $t = 60$ s (•) and $t = 13$ min (▲).

3.4 Conclusions

I have presented an experimental and theoretical investigation into the evolution of turbulent axisymmetric and line fountains, and their effect on an initially stratified ambient density profile. This study has expanded on the work detailed in chapter 2, to show that the evolution of the fountain and the environment depends on whether basal or intermediate spreading occurs, and hence whether one or two fronts, respectively, are observed.

The ambient density profile has been shown to have little effect on the motion of the fronts. For the descending front, this assumption was verified after comparing experimental data with analytical predictions for jet-like flow. Similarly, comparison with experimental results for the ascending front lead to the conclusion that the rate of entrainment into the downflow of the fountain can be quantified using the same constant as that determined in a homogeneous fluid. The motion of the ascending front therefore depends directly on only the position of the top of the fountain. To quantify the rise of the fountain height, the individual effects of the decreasing ambient density gradient and the increasing average ambient density were estimated. A simple weighting function based on the thickness of the spreading layer relative to the fountain height

was then used to quantify the contribution from each of these effects to the overall rise of the fountain height. A numerical solution of the equations of motion then gave the position of the fountain height and the ascending front.

For axisymmetric fountains, the theory provided an accurate prediction of the position of the fountain height and the ascending front. However, the fluctuations in the profile of a line fountain resulted in significantly more scatter of the experimental data around the average position predicted by the theory.

Once the time evolution of the axisymmetric and line fountains is known, I have shown how a simple numerical scheme can then be used to quantify the homogenization of the initially stratified environment. The results of these numerical calculations accurately predicted the changes to the ambient density distribution, particularly at later times. A more accurate theoretical model of the evolution of an initially stratified fluid requires quantitative knowledge of the height of a fountain in an arbitrary density profile.

Chapter 4

Theoretical Models of Turbulent Fountains

"The purpose of computing is insight, not numbers."

Richard Hamming (1915 - 1998)

American Mathematician and Computer Scientist

Expressions for the fountain heights have been found in the preceeding chapters by combining experimental measurements with dimensional arguments. In chapter 3, however, it was shown that dimensional arguments are not sufficient to quantify the fountain properties throughout the time evolution of the ambient density profile. Consequently, I aim in this chapter to develop a theoretical model of a turbulent fountain from which the properties in an arbitrary density gradient can be calculated. First, in §4.1, I discuss some previous theoretical investigations of turbulent flows. Then, in §4.2, I develop a set of entrainment equations that include the effects of mixing between the fountain upflow, downflow and homogeneous environment. The numerical predictions are then compared with experimental measurements in §4.2.3. In §4.3, this model is extended to describe axisymmetric fountains in a linearly stratified fluid, and the results are again compared with experimental measurements. Finally, a model of a line fountain in a stratified fluid is developed in §4.4.

4.1 Previous theoretical investigations

The possibility of using the entrainment equations to develop a theoretical model of a turbulent fountain was first raised by Turner (1966), who proposed that it should be possible to set up a detailed theory of the "double" structure of the fountain in the manner suggested by Morton (1962) for coaxial turbulent jets. In that study, Morton (1962) noted that it is not immediately obvious how the simple ideas of entrainment across a jet boundary should be extended to the more complicated double structure of coaxial turbulent jets. Despite this, he proposed one formulation to quantify the mixing between the core jet and the outer, annular jet.

Morton's (1962) ideas about the rate of entrainment between two turbulent flows were subsequently used by McDougall (1981) to develop the first theoretical model of an axisymmetric fountain in a homogeneous fluid. This model was based on a set of new entrainment equations which quantified the mixing between the upflow and the downflow, and between the downflow and the environment. In addition to the effects of mixing between the flows, McDougall (1981) also recognized that the body forces acting on the fluid in the upflow and downflow are "very much an open question". In an attempt to address this question, McDougall (1981) considered the two most reasonable formulations of the body forces acting on the fountain. From the resulting equations he was able to predict the final fountain height as well as the width, velocity and buoyancy in the upflow and downflow. In that investigation, only the predictions of the fountain height were compared with experimental data, as measurements of the internal fountain structure did not become available until the study by Mizushina *et al.* (1982).

The model presented here builds on the ideas developed by McDougall (1981), but also includes an alternative formulation for the entrainment between the upflow and downflow. The model is also extended to quantify fountains in a stratified fluid.

4.2 An axisymmetric turbulent fountain in a homogeneous fluid

Immediately after injecting the heavy source fluid, the fountain has a simple structure in which the rising, jet-like flow mixes directly with the ambient fluid (figure 4.1a). The volume flux, momentum flux and buoyancy flux in the flow at this stage can be quantified using the

entrainment equations (Morton *et al.* 1956; Turner 1973):

$$\frac{\mathrm{d}}{\mathrm{d}z}(b^2u) = 2\alpha bu, \quad \frac{\mathrm{d}}{\mathrm{d}z}(b^2u^2) = b^2\Delta, \quad \frac{\mathrm{d}}{\mathrm{d}z}(b^2u\Delta) = 0, \tag{4.1}$$

where z is the height above the source, b is the flow radius, u is the mean velocity in the flow, $\Delta = (g/\rho_o)(\rho_f - \rho_o)$ is the buoyant acceleration, ρ_f is the density of the fluid in the flow, ρ_o is the ambient density, g is the gravitational acceleration and α is the entrainment coefficient. In these equations, top hat profiles of velocity and buoyancy have been used to represent average quantities across the turbulent flow.

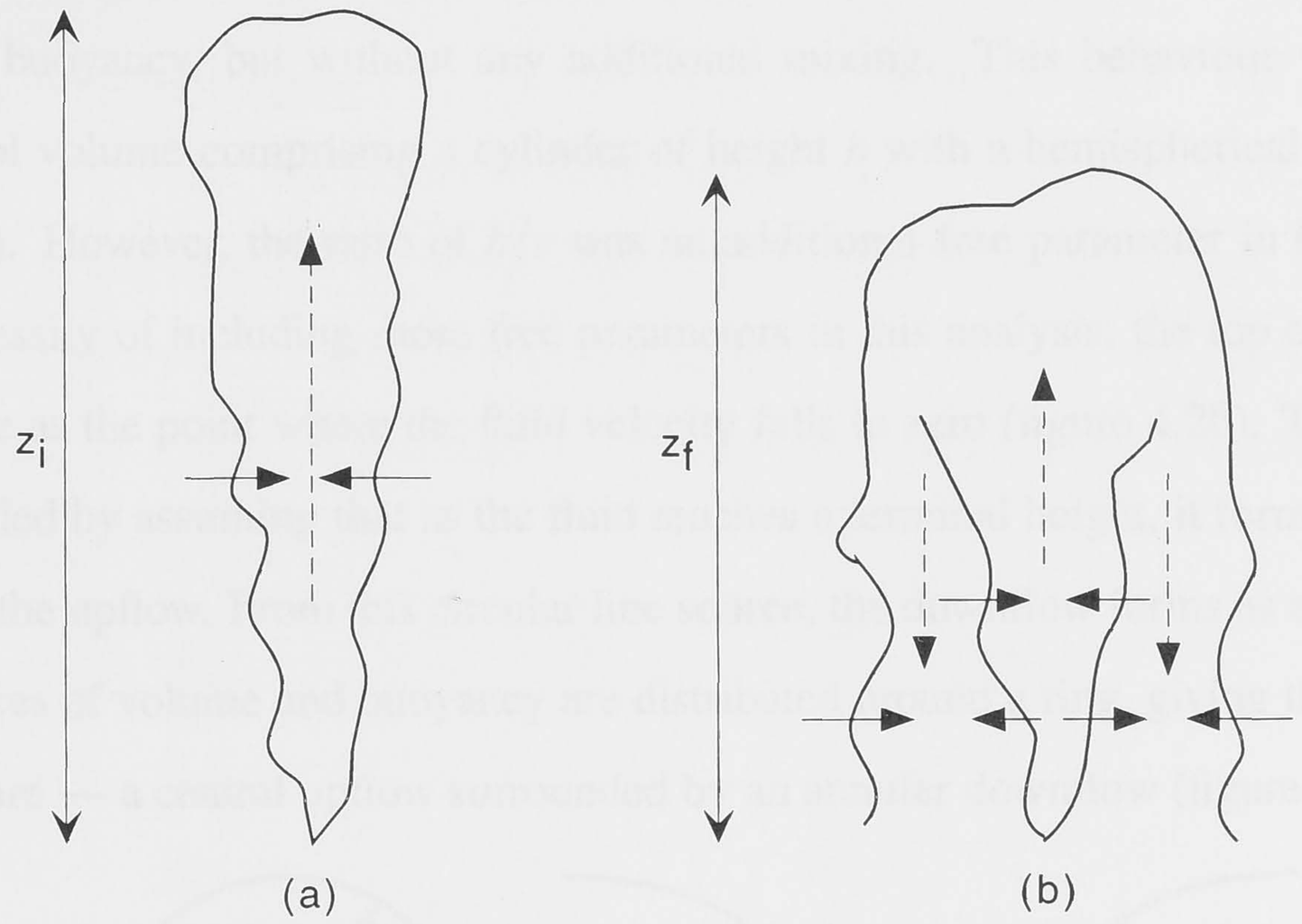

Figure 4.1: Schematic illustration of a turbulent fountain (a) as the flow reaches an initial height and (b) after the fluid has reversed direction to form a downflow, and the initial height is reduced to a final, steady value. The dashed arrows indicate the flow direction, while the solid arrows indicate the directions of turbulent entrainment between the upflow, downflow and environment.

In terms of the fluxes of volume, $Q = b^2u$, momentum, $M = b^2u^2$, and buoyancy, $F = b^2u\Delta$, equations (4.1) become:

$$\frac{\mathrm{d}Q}{\mathrm{d}z} = 2\alpha M^{1/2}, \quad \frac{\mathrm{d}M^2}{\mathrm{d}z} = 2FQ, \quad \frac{\mathrm{d}F}{\mathrm{d}z} = 0. \tag{4.2}$$

For a fountain entering a homogeneous fluid through a point source, the source conditions are defined by a zero volume flux, positive momentum flux and negative buoyancy flux.

The initial height of the fountain, z_i, is determined from the solution of (4.2) to be the

point at which the velocity of the upflow becomes equal to zero. After the initial height has been reached, these entrainment equations are no longer valid, as they do not describe the mixing between the upflow and downflow or the additional entrainment of ambient fluid into the downflow. This mixing can be quantified using similar entrainment assumptions to give a theoretical model of a fountain.

The first complication to be addressed in modelling a fountain is the reversal of the fluid after the initial height has been reached. McDougall (1981) introduced a method of dealing with the fluid reversal in which the numerical solution was terminated when the Froude number of the flow falls to $Fr = 2^{1/2}$. The rising fluid was then assumed to turn around under the action of the buoyancy, but without any additional mixing. This behaviour was modelled using a control volume comprising a cylinder of height h with a hemispherical cap of radius r (figure 4.2a). However, the ratio of h/r was an additional free parameter in his model. To avoid the necessity of including more free parameters in this analysis, the top of the fountain is defined here as the point where the fluid velocity falls to zero (figure 4.2b). The reversal of fluid is modelled by assuming that as the fluid reaches a terminal height, it forms a ring at the outer edge of the upflow. From this circular line source, the downflow forms as a line plume in which the fluxes of volume and buoyancy are distributed around a ring, giving the fountain its typical structure — a central upflow surrounded by an annular downflow (figure 4.1b).

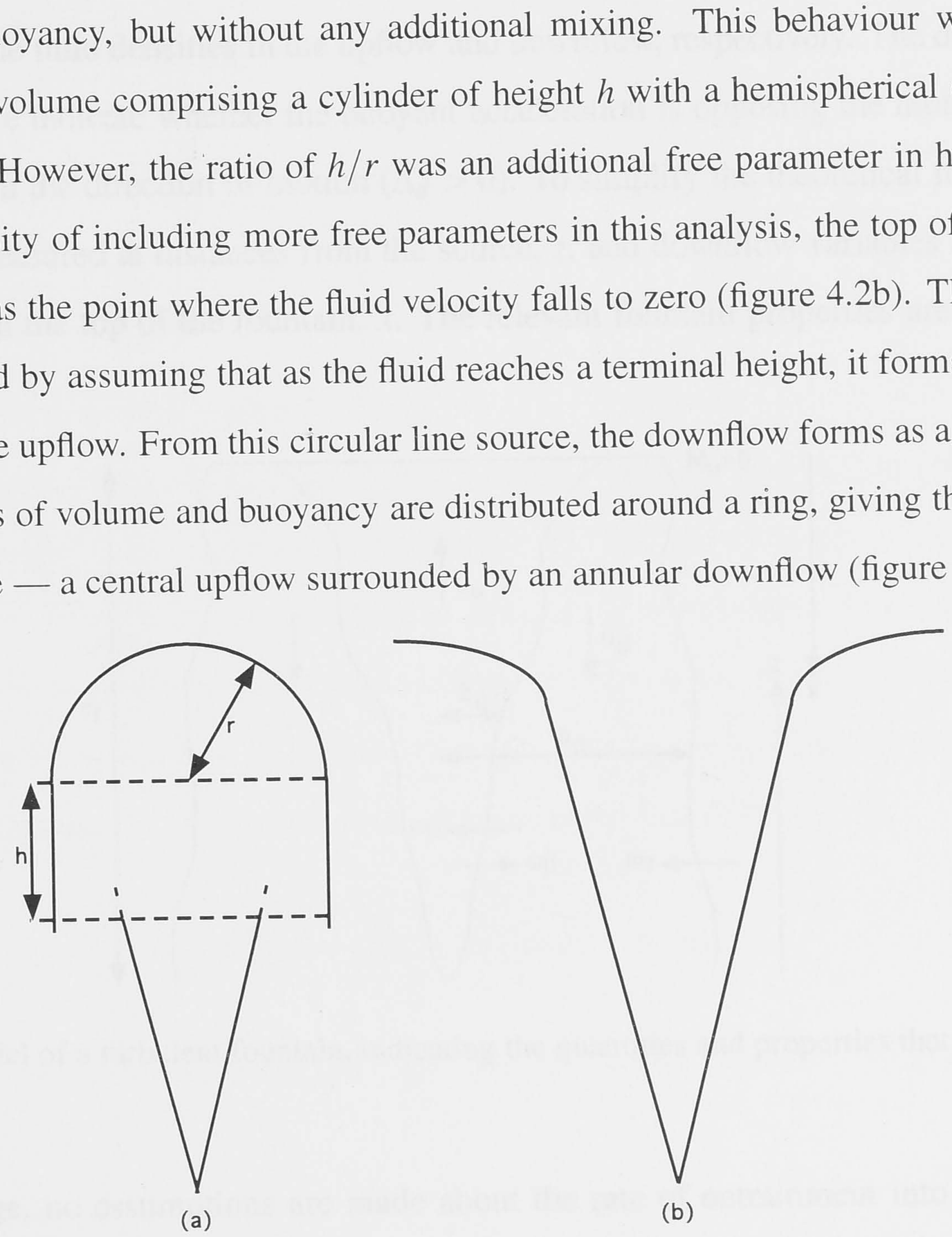

Figure 4.2: Comparison between the two methods of finding the fountain height as outlined (a) by McDougall (1981) and (b) in this study.

Once the downflow has formed, the model must include the mixing that is indicated in

figure 4.1(b) — fluid from the downflow is entrained into the upflow, while fluid is entrained into the downflow from both the upflow and the environment. Separate properties are defined for the upflow and the downflow, indicated by the subscripts u and d, respectively. The fluxes of volume, momentum and buoyancy are therefore:

$$\begin{aligned} Q_u &= b_u^2 u_u \qquad & Q_d &= (b_d^2 - b_u^2) u_d \\ M_u &= b_u^2 u_u^2 \qquad & M_d &= (b_d^2 - b_u^2) u_d^2 \\ F_u &= b_u^2 u_u \Delta_u \qquad & F_d &= (b_d^2 - b_u^2) u_d \Delta_d . \end{aligned} \tag{4.3}$$

The terms for the buoyant acceleration are $\Delta_u = (g/\rho_o)(\rho_o - \rho_u)$ and $\Delta_d = (g/\rho_o)(\rho_d - \rho_o)$, with ρ_u and ρ_d the fluid densities in the upflow and downflow, respectively. The different signs of Δ_u and Δ_d here indicate whether the buoyant acceleration is opposing the motion ($\Delta_u < 0$), or whether it is in the direction of motion ($\Delta_d > 0$). To simplify the theoretical model, upflow quantities are measured at distances from the source, z, and downflow variables are measured at distances from the top of the fountain, x. The relevant fountain properties are illustrated in figure 4.3.

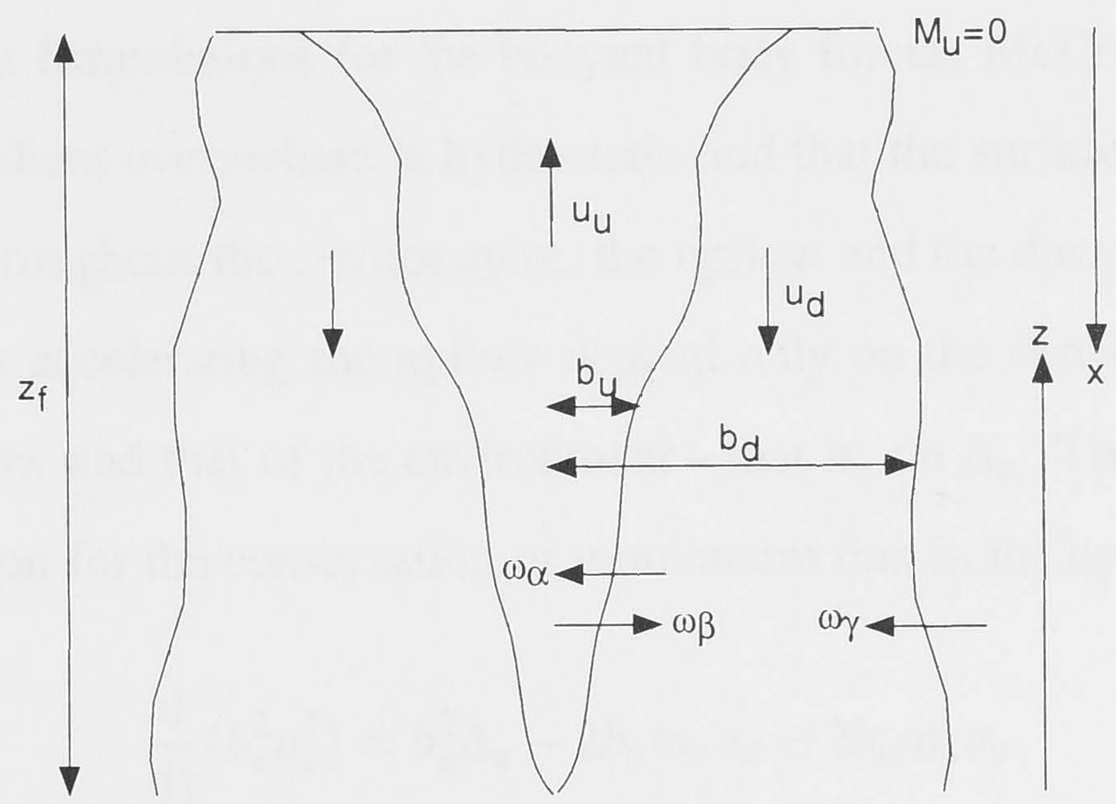

Figure 4.3: Model of a turbulent fountain, indicating the quantities and properties that are included in the equations.

At this stage, no assumptions are made about the rate of entrainment into the upflow or downflow of the fountain. Instead, ω_α is defined as the velocity of entrainment into the upflow, ω_β as the entrainment velocity of fluid entering the downflow from the upflow, and ω_γ as the velocity of entrainment for ambient fluid mixed into the downflow (see figure 4.3). The choice of the relevant velocity scales on which to base ω_α, ω_β and ω_γ, and the consequences of this

decision, are discussed in §4.2.1.

In his theoretical model of a turbulent fountain, McDougall (1981) derived two sets of entrainment equations, based on two different assumptions about how the body forces affect the upflow and downflow. In both formulations, the equations for the conservation of volume and buoyancy fluxes were given by

$$\frac{\mathrm{d}}{\mathrm{d}z}(b_u^2 u_u) = 2b_u\omega_\alpha - 2b_u\omega_\beta, \tag{4.4}$$

$$\frac{\mathrm{d}}{\mathrm{d}x}([b_d^2 - b_u^2]u_d) = 2b_d\omega_\gamma - 2b_u\omega_\alpha + 2b_u\omega_\beta, \tag{4.5}$$

for the upflow and downflow volume fluxes, respectively, and

$$\frac{\mathrm{d}}{\mathrm{d}z}(b_u^2 u_u \Delta_u) = -2b_u\omega_\alpha\Delta_d - 2b_u\omega_\beta\Delta_u, \tag{4.6}$$

$$\frac{\mathrm{d}}{\mathrm{d}x}([b_d^2 - b_u^2]u_d\Delta_d) = -2b_u\omega_\alpha\Delta_d - 2b_u\omega_\beta\Delta_u, \tag{4.7}$$

for the upflow and downflow buoyancy fluxes.

In the first of his formulations for the buoyant body forces, McDougall (1981) assumed that the pressure gradient everywhere is hydrostatic and that the surfaces of constant pressure remain horizontal throughout the environment, the upflow and the downflow. In that case, the buoyant body forces accelerating the upflow depend only on the density difference between the fluid in the upflow and that of the environment - that is, on Δ_u. This assumption leads to the following equation for the conservation of momentum flux in the upflow:

$$\frac{\mathrm{d}}{\mathrm{d}z}(b_u^2 u_u^2) = b_u^2\Delta_u - 2b_u\omega_\alpha u_d - 2b_u\omega_\beta u_u. \tag{4.8}$$

The assumption was then made that the total momentum flux across the fountain should also be conserved, so that

$$\frac{\mathrm{d}}{\mathrm{d}z}(b_u^2 u_u^2) - \frac{\mathrm{d}}{\mathrm{d}x}([b_d^2 - b_u^2]u_d^2) = b_u^2\Delta_u - [b_d^2 - b_u^2]\Delta_d. \tag{4.9}$$

The expression for the conservation of momentum flux in the downflow is then found from

(4.8) and (4.9) to be

$$\frac{\mathrm{d}}{\mathrm{d}x}([b_d^2 - b_u^2]u_d^2) = [b_d^2 - b_u^2]\Delta_d - 2b_u\omega_\alpha u_d - 2b_u\omega_\beta u_u. \tag{4.10}$$

In the second of his body force formulations, McDougall (1981) included the effect of a non-hydrostatic pressure gradient in the accelerating downflow. An alternative way of viewing this result is to assume that the body forces acting on the upflow arise from the local density difference between the upflow and downflow, $\Delta_u + \Delta_d$, but are measured relative to the accelerating downflow. The acceleration of the frame of reference fixed to the downflow was therefore included in the term for the total body force acting on the upflow. The conservation of momentum flux in the upflow is therefore

$$\frac{\mathrm{d}}{\mathrm{d}z}(b_u^2 u_u^2) = b_u^2\left(\Delta_u + \Delta_d - u_d\frac{\mathrm{d}u_d}{\mathrm{d}x}\right) - 2b_u\omega_\alpha u_d - 2b_u\omega_\beta u_u. \tag{4.11}$$

Again, the corresponding expression for the downflow momentum flux is determined from (4.9) and (4.11) to be

$$\frac{\mathrm{d}}{\mathrm{d}x}([b_d^2 - b_u^2]u_d^2) = [b_d^2 - b_u^2]\Delta_d + b_u^2\left(\Delta_d - u_d\frac{\mathrm{d}u_d}{\mathrm{d}x}\right) - 2b_u\omega_\alpha u_d - 2b_u\omega_\beta u_u. \tag{4.12}$$

McDougall (1981) numerically integrated his entrainment equations to obtain predictions for the height of the fountain, as well as the radius, fluid velocity and density of the upflow and downflow, and compared the results with experimental measurements. Due to the number of arbitrary approximations in his model, McDougall (1981) stated that he could not conclude "with any degree of confidence" which of the two body force formulations correspond closest with experiment. However, he did note that when "best guess" values were used for his free parameters, the second formulation gave a more accurate prediction of the final fountain height. In this study, I will continue to consider both formulations for the body forces.

The set of entrainment equations (i.e. (4.4) – (4.7), together with either (4.8) and (4.10), or (4.11) and (4.12)) are simplified by writing them in terms of the non-dimensional variables

given by:

$$\begin{aligned} \tilde{z} &= M_o^{-3/4} F_o^{1/2} z \qquad \tilde{b} = M_o^{-3/4} F_o^{1/2} b \\ \tilde{u} &= M_o^{1/4} F_o^{-1/2} u \qquad \tilde{\omega} = M_o^{1/4} F_o^{-1/2} \omega \\ \tilde{\Delta} &= M_o^{5/4} F_o^{-3/2} \Delta. \end{aligned} \tag{4.13}$$

After some rearranging, and introducing the dimensionless fluxes of volume, $\tilde{Q} = \tilde{b}^2\tilde{u}$, momentum, $\tilde{M} = \tilde{b}^2\tilde{u}^2$, and buoyancy, $\tilde{F} = \tilde{b}^2\tilde{u}\tilde{\Delta}$, the final equations are,

$$\frac{\mathrm{d}\tilde{Q}_u}{\mathrm{d}\tilde{z}} = 2\frac{\tilde{Q}_u}{\tilde{M}_u^{1/2}}(\tilde{\omega}_\alpha - \tilde{\omega}_\beta) \tag{4.14}$$

$$\frac{\mathrm{d}\tilde{Q}_d}{\mathrm{d}\tilde{x}} = 2\frac{\tilde{Q}_u}{\tilde{M}_u^{1/2}}\left(\left(1+\frac{1}{A}\right)^{1/2}\tilde{\omega}_\gamma + \tilde{\omega}_\beta - \tilde{\omega}_\alpha\right) \tag{4.15}$$

$$\frac{\mathrm{d}\tilde{F}_u}{\mathrm{d}\tilde{z}} = -2\frac{\tilde{Q}_u}{\tilde{M}_u^{1/2}}\left(\frac{\tilde{F}_d}{\tilde{Q}_d}\tilde{\omega}_\alpha + \frac{\tilde{F}_u}{\tilde{Q}_u}\tilde{\omega}_\beta\right) \tag{4.16}$$

$$\frac{\mathrm{d}\tilde{F}_d}{\mathrm{d}\tilde{x}} = -2\frac{\tilde{Q}_u}{\tilde{M}_u^{1/2}}\left(\frac{\tilde{F}_d}{\tilde{Q}_d}\tilde{\omega}_\alpha + \frac{\tilde{F}_u}{\tilde{Q}_u}\tilde{\omega}_\beta\right), \tag{4.17}$$

with

$$\frac{\mathrm{d}\tilde{M}_u^2}{\mathrm{d}\tilde{z}} = 2\tilde{Q}_u\tilde{F}_u - 4\tilde{M}_u^{3/2}\left(B\tilde{\omega}_\alpha + \tilde{\omega}_\beta\right) \tag{4.18}$$

$$\frac{\mathrm{d}\tilde{M}_d^2}{\mathrm{d}\tilde{x}} = 2\tilde{Q}_d\tilde{F}_d - 4\tilde{M}_u^{1/2}\tilde{M}_d\left(B\tilde{\omega}_\alpha + \tilde{\omega}_\beta\right), \tag{4.19}$$

for the first body force formulation, and

$$\frac{\mathrm{d}\tilde{M}_u^2}{\mathrm{d}\tilde{z}} = 2\tilde{Q}_u\tilde{F}_u + 4\tilde{M}_u^{3/2}\left(B\left(1+\frac{1}{A}\right)^{1/2}\tilde{\omega}_\gamma + \frac{AB-1}{1+A}\tilde{\omega}_\beta - B\tilde{\omega}_\alpha\right) \tag{4.20}$$

$$\frac{\mathrm{d}\tilde{M}_d^2}{\mathrm{d}\tilde{x}} = 2\tilde{Q}_d\tilde{F}_d + 4\tilde{M}_u^{1/2}\tilde{M}_d\left(B\left(1+\frac{1}{A}\right)^{-1/2}\tilde{\omega}_\gamma + \frac{AB-1}{1+A}\tilde{\omega}_\beta - B\tilde{\omega}_\alpha\right), \tag{4.21}$$

for the second body force formulation. In these equations,

$$A = \frac{\tilde{Q}_u^2\tilde{M}_d}{\tilde{Q}_d^2\tilde{M}_u} = \frac{\tilde{b}_u^2}{\tilde{b}_d^2 - \tilde{b}_u^2} \quad \text{and} \quad B = \frac{\tilde{Q}_u\tilde{M}_d}{\tilde{Q}_d\tilde{M}_u} = \frac{\tilde{u}_d}{\tilde{u}_u}. \tag{4.22}$$

4.2.1 Entrainment

The entrainment assumption in its general form states that the inflow velocity of entrained fluid at any height scales with some characteristic velocity in the flow at that height (Morton *et al.* 1956). In flows with a "double" structure, such as coaxial jets (Morton 1962), bubble plumes (McDougall 1978; Asaeda & Imberger 1993) or fountains (McDougall 1981), it is not immediately obvious on which velocity scales the entrainment velocities should be based. I present here two alternative formulations for the entrainment.

4.2.1.1 Entrainment formulation I

The first formulation I consider is that proposed by Morton (1962) for coaxial jets, and subsequently used by McDougall (1981) in his theoretical modelling of a turbulent fountain. Morton (1962) argued that the supply of energy to the turbulence in the inner flow arose due to the difference in mean velocities between the inner and outer flows. Consequently, it was this velocity difference on which the rate of entrainment should be based. Similarly, he proposed that the turbulence in the outer flow arose as a result of the shear between this flow and the stationary environment, leading to the prediction that the rate of entrainment into the outer flow should scale with the mean velocity of that flow. In a turbulent fountain, these arguments lead to the prediction that

$$\omega_\alpha = \alpha(u_u + u_d); \quad \omega_\beta = \beta u_d; \quad \omega_\gamma = \gamma u_d, \tag{4.23}$$

with α, β and γ the relevant entrainment coefficients.

In this formulation, the shear between the two flows is assumed to affect only the inner flow. However, it is not obvious why the turbulence generated by the shear should be transferred in one direction only (i.e. inwards). I therefore now introduce a second entrainment formulation in which the shear between the flows affects the turbulence in both inner and outer flows.

4.2.1.2 Entrainment formulation II

In this formulation, it is argued that the total shear, $u_u + u_d$, should be partitioned (c.f. Morton (1962)) so that only the component containing upward velocities, $u_u/(u_u + u_d)$, affects

the turbulence in the upflow, and the remaining component, $u_d/(u_u+u_d)$, feeds the turbulence in the downflow. The entrainment velocities therefore depend on the relevant fraction of the total shear, and are given by

$$\omega_\alpha = \alpha u_u; \quad \omega_\beta = \beta u_d; \quad \omega_\gamma = \gamma u_d. \tag{4.24}$$

Essentially, the entrainment velocity is assumed to scale with a velocity difference, although this time the shear is taken to be the difference between the mean fluid velocity in the flow and the mean velocity on the "edge" of the flow under consideration. This approach is consistent with the commonly stated entrainment assumption in simple flows where the velocity on the edge of the flow is equal to that in the environment. In a fountain, however, the obvious position of the boundary between the upflow and downflow is the point at which the mean velocity is equal to zero (Mizushina *et al.* 1982, figure 7).

4.2.2 The numerical method

The starting conditions for the integration of the upflow equations are defined at a height z_o above the point source. This is necessary to avoid the infinite fluid velocity, $u_o = M_o/Q_o$ that would arise from a theoretical point source ($Q_o = 0$). To determine the values of $\tilde{Q}, \tilde{M}$ and $\tilde{F}$ at a height of $\tilde{z}_o = 0.01$, it is noted that near the source, the upflow is unaffected by either its negative buoyancy or the presence of the downflow (chapter 3). A solution of (4.1) for a jet ($\tilde{Q}_o = 0, \tilde{M}_o = 1, \tilde{F}_o = 0$), gives the result that $\tilde{Q}(\tilde{z}_o) = 2\alpha\tilde{z}_o$ and $\tilde{M}(\tilde{z}_o) = 1$. Since the buoyancy flux in a jet is constant, it is then assumed that at small heights in a fountain, $\tilde{F}$ remains unchanged from its value at the source, and $\tilde{F}(\tilde{z}_o) = -1$.

Initially there is no downflow ($\tilde{Q}_d = \tilde{M}_d = \tilde{F}_d = 0$) so that (4.14) and (4.16) together with either (4.18) or (4.20) reduce to the standard entrainment equations. These equations for the upflow are solved numerically using a routine based on a fourth-order Runge-Kutta scheme. The point at which the upflow momentum flux becomes equal to zero gives a value of the initial fountain height, $\tilde{z}_i$ (Morton 1959a). The values of the upflow volume flux, $\tilde{Q}_T$, and buoyancy flux, $\tilde{F}_T$, at this initial height are the starting conditions for $\tilde{Q}_d$ and $\tilde{F}_d$ at $\tilde{x} = 0$ ($\tilde{x}$ is measured from the top of the fountain). The conservation equations for the downflow ((4.15), (4.17) and either (4.19) or (4.21)) are then integrated from the top of the fountain to the starting point

at $\tilde{z}_o$, using the previously determined values of $\tilde{Q}_u$, $\tilde{M}_u$ and $\tilde{F}_u$ at each height. These newly determined values for the fluxes in the downflow are then used in the next integration of the upflow equations. The point at which $\tilde{M}_u = 0$ in this iteration gives the first estimate of the reduced final height, $\tilde{z}_f$. This procedure is continued until the estimate of $\tilde{z}_f$ from subsequent iterations converges to a fixed value, which is taken as the evaluation of the final fountain height.

4.2.3 Results and comparison with experiments

The method outlined above was used to determine the initial fountain height, $\tilde{z}_i$, as well as four values of the dimensionless fountain height, $\tilde{z}_f$, for the combinations of two body force formulations (BFI and BFII) and two entrainment formulations (EI and EII). The values obtained for $\tilde{z}_i$ and $\tilde{z}_f$ correspond to the experimentally determined constants in the expressions relating the fountain heights to the intrinsic length scale of $M_o^{3/4} F_o^{-1/2}$ (Turner 1966).

In the first iteration of the upflow equations, α is the only free parameter. Using a value of $\alpha = 0.085 \pm 0.010$ results in a numerical estimate of $\tilde{z}_i = 2.49 \pm 0.15$, which coincides with the average experimental value of $\tilde{z}_i = 2.49 \pm 0.18$ (§2.2.3). As expected, this value of α is close to the jet value of $\alpha = 0.076 \pm 0.04$, and lies between the jet value and the plume value of $\alpha = 0.117 \pm 0.006$ (List 1982a).

By modelling the downflow as a line plume which encircles the upflow, the entrainment coefficients β and γ are fixed at the value found for a line plume with top hat profiles of velocity and buoyancy: $\beta = \gamma = 0.147$ (List 1982b). The uncertainty in the entrainment coefficient for a line plume can be calculated from the results of Kotsovinos & List (1977) to be $\beta = \gamma = 0.147 \pm 0.014$. These values of β and γ differ from those used by McDougall (1981), who incorrectly used Gaussian entrainment coefficients in entrainment equations which were developed assuming top hat profiles.

The predictions of the final fountain height obtained from the combination of two entrainment formulations and two buoyant body force formulations (referred to hereon as BFIEI, BFIEII, BFIIEI and BFIIEII) are summarized in table 1, showing the variation in $\tilde{z}_f$ due to the uncertainty in the entrainment coefficients α, β and γ. All the numerical results underestimate the average experimental value of $\tilde{z}_f = 1.77 \pm 0.11$ (§2.2.3). The combination BFIIEII ($\tilde{z}_f = 1.49 \pm 0.11$) gives the result closest to the experimentally determined value.

	Entrainment I	Entrainment II
Body force I	$\tilde{z}_f = 1.07 \pm 0.09$	$\tilde{z}_f = 1.25 \pm 0.09$
Body force II	$\tilde{z}_f = 1.20 \pm 0.10$	$\tilde{z}_f = 1.49 \pm 0.11$

Table 4.1: Calculated results for the final height of an axisymmetric fountain in a homogeneous fluid, using the two body force formulations and two entrainment formulations.

To determine the sensitivity of the results to variations in β and γ, β was first decreased from the value for a plume to that for a jet ($\beta = 0.076$), while keeping γ fixed. This resulted in only a 0.5% decrease in the predicted fountain height. Decreasing β has two effects — first, less of the dense rising fluid is mixed into the downflow, so that the downflow remains lighter and therefore experiences a smaller downward acting buoyancy force. Second, however, the decrease in the interaction with the upflow allows greater acceleration of the falling fluid. As varying β has a negligible effect on the predicted fountain height, it appears that these two effects essentially cancel each other out.

In contrast, when γ was also reduced to the jet value of $\gamma = 0.076$, the numerical estimate for the fountain height dropped by approximately 20%. In this case, mixing with the stationary environment does not affect the momentum of the downflow, so the only effect of decreasing the entrainment from the environment is to give a denser and therefore more accelerated downflow.

In addition to the comparisons for the final fountain height, the numerical predictions of the upflow and downflow properties are also compared with the experimental measurements of Mizushina *et al.* (1982). In figure 4.4(a), the numerical results from all four formulations are compared with experimental measurements of the upflow and downflow radius (Mizushina *et al.* 1982). Despite the numerical results for the upflow and downflow radius becoming unrealistic near the top of the fountain (where r_u and r_d become infinite), the results from all four formulations lie within the range of experimental scatter. The predictions for the outer radius are much better than those obtained by McDougall (1981), who stated that his numerical results for the fountain radius were approximately half of the experimentally measured radius.

Figure 4.4(b) shows that for all four formulations, the numerical results for the upflow velocity are in excellent agreement with the centreline velocities measured by Mizushina *et al.* (1982). Near the top of the fountain, the combination BFIIEII agrees best with the experimen-

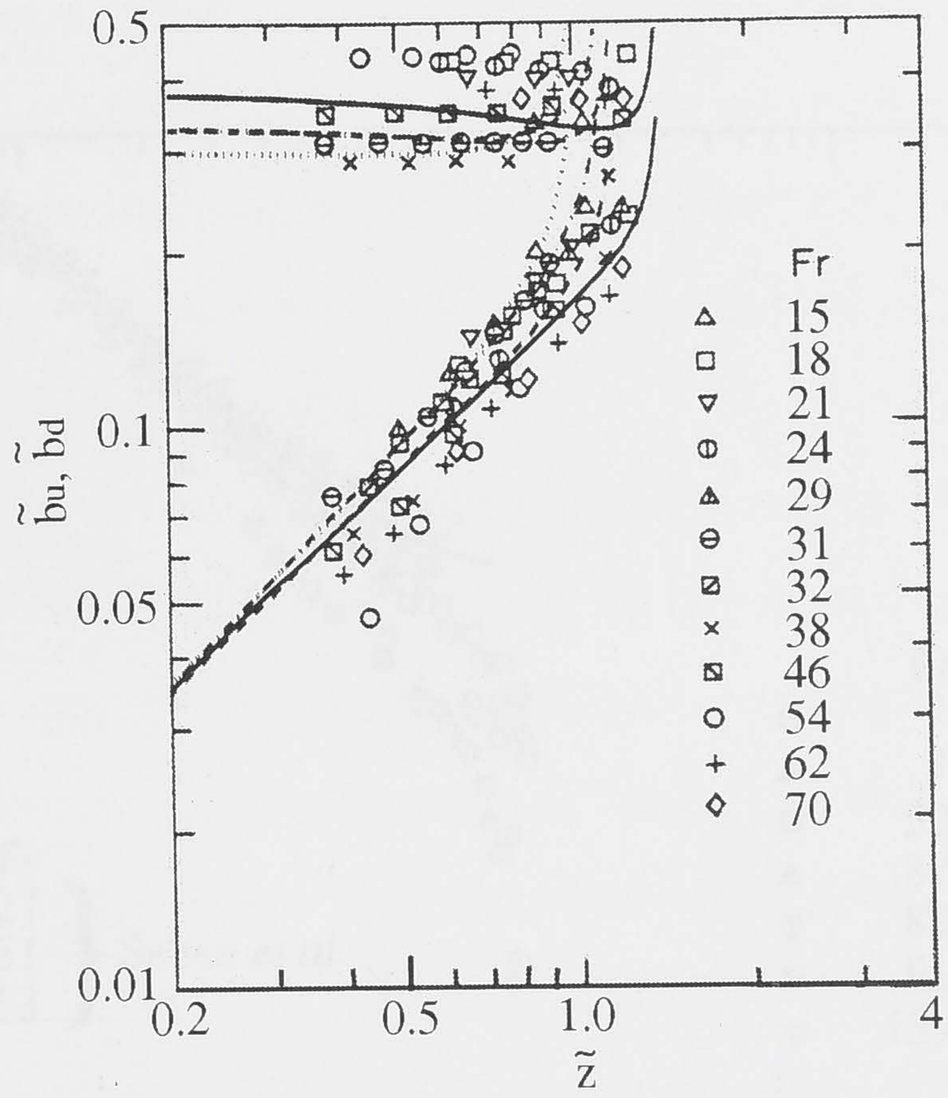

(a)

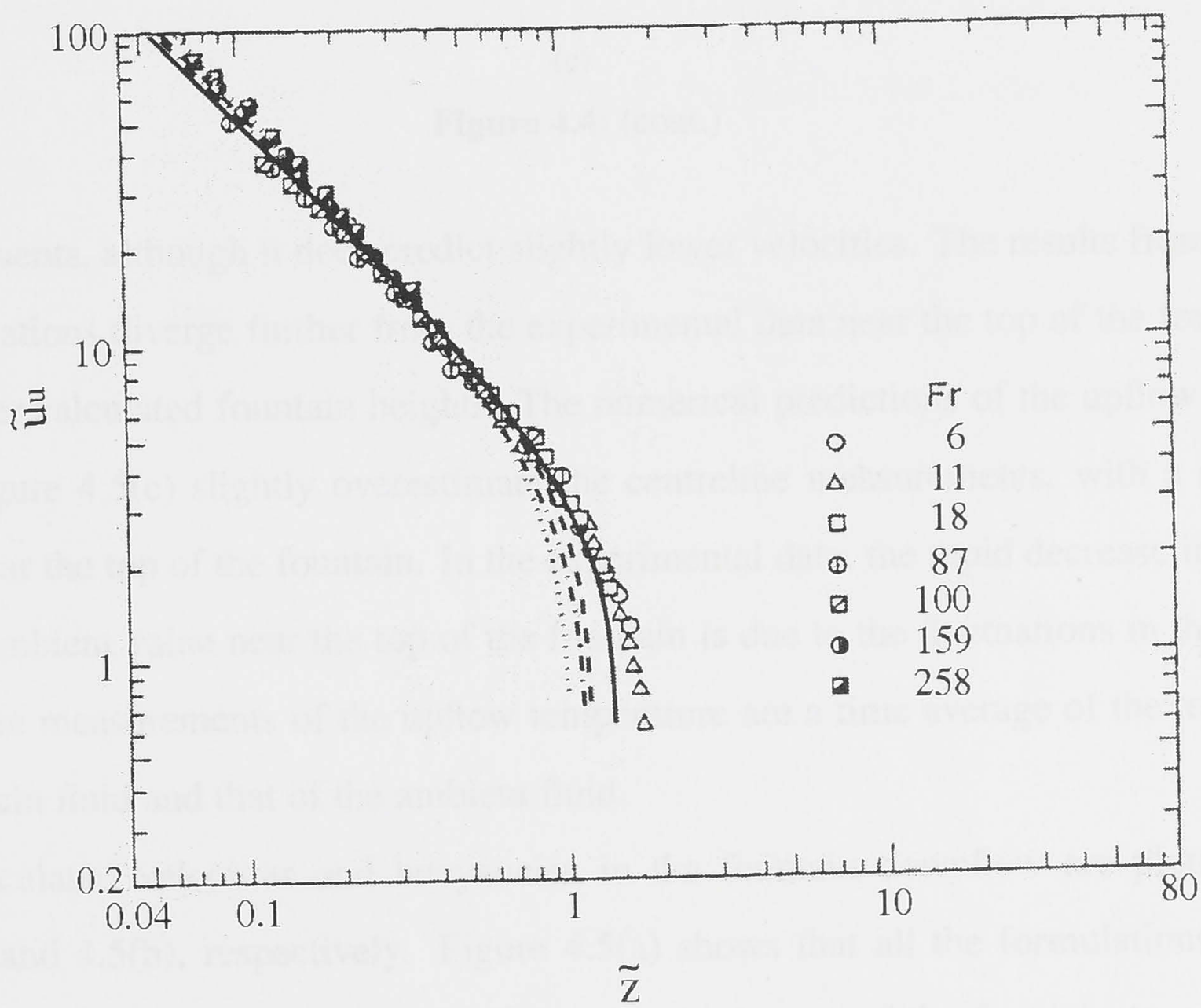

(b)

Figure 4.4: Comparison between the numerical results and the experimental data of Mizushina *et al.* (1982) for (a) the upflow and downflow radius, (b) the upflow velocity and (c) the upflow buoyancy. Shown are the numerical results for the four different formulations: BFIEI (····), BFIIEI (- · - · -), BFIEII (- - -) and BFIIEII (——).

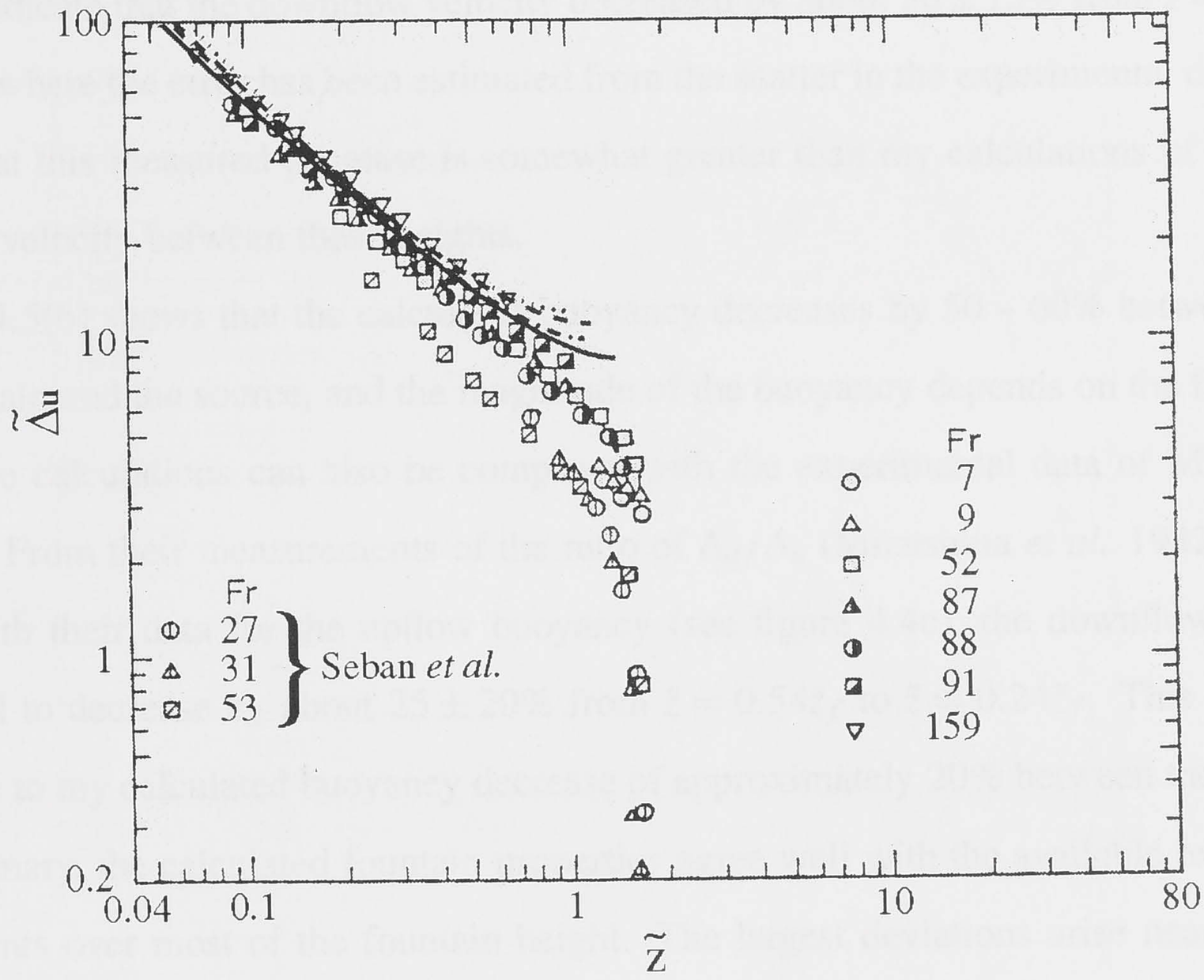

(c)

Figure 4.4: (cont.)

tal measurements, although it does predict slightly lower velocities. The results from the other three formulations diverge further from the experimental data near the top of the fountain due to the smaller calculated fountain heights. The numerical predictions of the upflow buoyancy shown in figure 4.5(c) slightly overestimate the centreline measurements, with a significant deviation near the top of the fountain. In the experimental data, the rapid decrease in temperature to the ambient value near the top of the fountain is due to the fluctuations in the fountain height, where measurements of the upflow temperature are a time average of the temperature of the fountain fluid and that of the ambient fluid.

The calculated velocities and buoyancies in the fountain downflow are plotted in figures 4.5(a) and 4.5(b), respectively. Figure 4.5(a) shows that all the formulations predict a rapid increase in the downflow velocity from zero at the top of the fountain to a maximum near $\tilde{z} = 0.6\tilde{z}_f$, followed by a decrease of 10 – 15% down to $\tilde{z} = 0$. The only experimental measurements of the downflow velocity with which to compare these theoretical results were made by Mizushina *et al.* (1982, figure 7), who measured the ratio of u_d/u_u at two different

heights. These measurements, when combined with their data for the upflow velocity (see figure 4.4b), indicate that the downflow velocity decreased by about $30 \pm 15\%$ from $\tilde{z} = 0.54\tilde{z}_f$ to $\tilde{z} = 0.24\tilde{z}_f$, where the error has been estimated from the scatter in the experimental data. It may be noted that this measured decrease is somewhat greater than my calculations of a 5 – 10% decrease in velocity between these heights.

Figure 4.5(b) shows that the calculated buoyancy decreases by 50 – 60% between the top of the fountain and the source, and the magnitude of the buoyancy depends on the formulation used. These calculations can also be compared with the experimental data of Mizushina *et al.* (1982). From their measurements of the ratio of Δ_d/Δ_u (Mizushina *et al.* 1982, figure 8), together with their data for the upflow buoyancy (see figure 4.4c), the downflow buoyancy is estimated to decrease by about $25 \pm 20\%$ from $\tilde{z} = 0.54\tilde{z}_f$ to $\tilde{z} = 0.24\tilde{z}_f$. This decrease is comparable to my calculated buoyancy decrease of approximately 20% between these heights.

In summary, the calculated fountain properties agree well with the available experimental measurements over most of the fountain height. The largest deviations arise near the top of the fountain, which probably reflects the fact that elements of fluid come to rest at different heights, in contrast to the simple assumption that all the fluid comes to rest at the same height (c.f. figure 4.3).

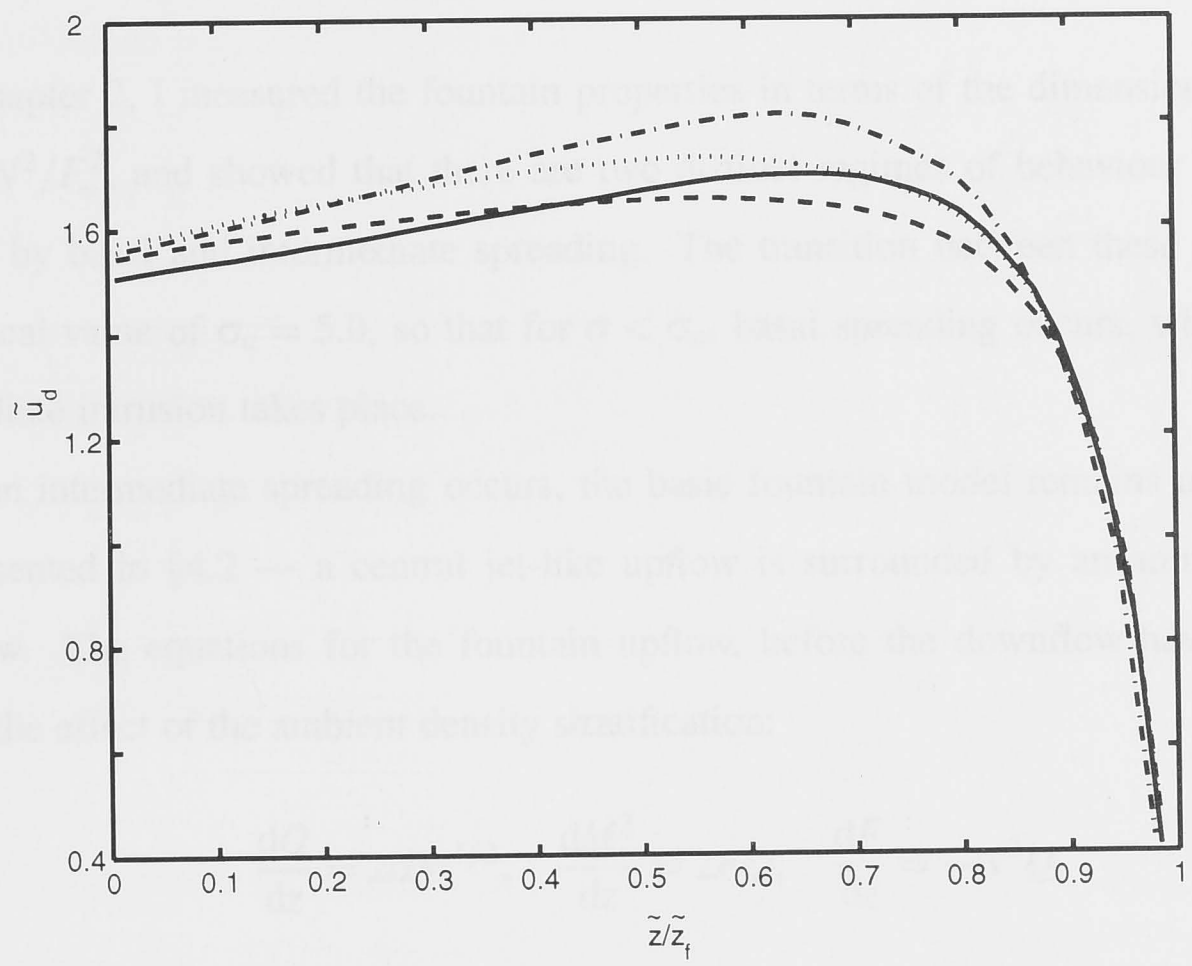

(a)

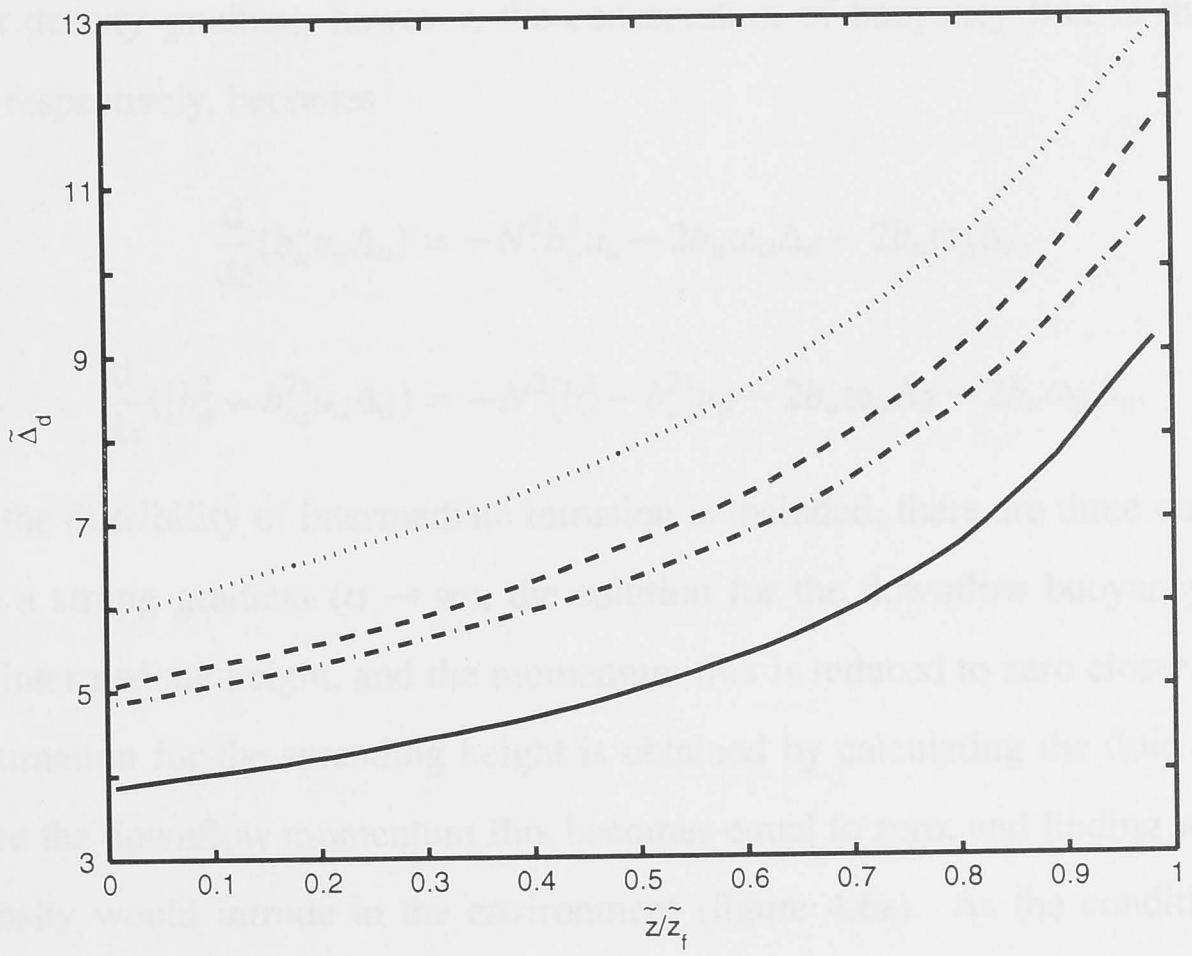

(b)

Figure 4.5: Numerical calculations of the (a) velocity and (b) buoyancy in the downflow for each of the four formulations: BFIEI(····), BFIIEI(- · - · -), BFIEII(- - -) and BFIIEII(——).

4.3 An axisymmetric fountain in a stratified fluid

In chapter 2, I measured the fountain properties in terms of the dimensionless parameter $\sigma = M_o^2 N^2 / F_o^2$, and showed that there are two distinct regimes of behaviour which are represented by basal and intermediate spreading. The transition between these regimes occurs at a critical value of $\sigma_c = 5.0$, so that for $\sigma < \sigma_c$, basal spreading occurs, while for $\sigma > \sigma_c$, intermediate intrusion takes place.

When intermediate spreading occurs, the basic fountain model remains unchanged from that presented in §4.2 — a central jet-like upflow is surrounded by an annular plume-like downflow. The equations for the fountain upflow, before the downflow have formed, now include the effect of the ambient density stratification:

$$\frac{\mathrm{d}Q}{\mathrm{d}z} = 2\alpha M^{1/2}, \quad \frac{\mathrm{d}M^2}{\mathrm{d}z} = 2FQ, \quad \frac{\mathrm{d}F}{\mathrm{d}z} = -N^2 Q. \tag{4.25}$$

The equations for the conservation of volume flux ((4.4), (4.5)) and momentum flux ((4.8) and (4.10) or (4.11) and (4.12)) remain unchanged from those in a homogeneous fluid. In an ambient density gradient, however, the conservation of buoyancy flux in the upflow and downflow, respectively, becomes

$$\frac{\mathrm{d}}{\mathrm{d}z}(b_u^2 u_u \Delta_u) = -N^2 b_u^2 u_u - 2b_u \omega_\alpha \Delta_d - 2b_u \omega_\beta \Delta_u, \tag{4.26}$$

$$\frac{\mathrm{d}}{\mathrm{d}x}([b_d^2 - b_u^2] u_d \Delta_d) = -N^2 [b_d^2 - b_u^2] u_d - 2b_u \omega_\alpha \Delta_d - 2b_u \omega_\beta \Delta_u. \tag{4.27}$$

When the possibility of intermediate intrusion is included, there are three outcomes of the model. In a strong gradient ($\sigma \to \infty$), the solution for the downflow buoyancy flux falls to zero at an intermediate height, and the momentum flux is reduced to zero closer to the source. An approximation for the spreading height is obtained by calculating the fluid density at the point where the downflow momentum flux becomes equal to zero, and finding where the fluid of this density would intrude in the environment (figure 4.6a). As the conditions approach the transition between the two regimes of behaviour ($\sigma \approx \sigma_c$), the buoyancy flux falls to zero above the source but the downflow still has momentum at the base (figure 4.6b). In this case, the density of the downflow as it reaches the base is calculated, and this density used to determine

the spreading height. In the third case ($\sigma \to 0$), neither the buoyancy or momentum fluxes in the downflow reach zero, and basal spreading occurs (figure 4.6c).

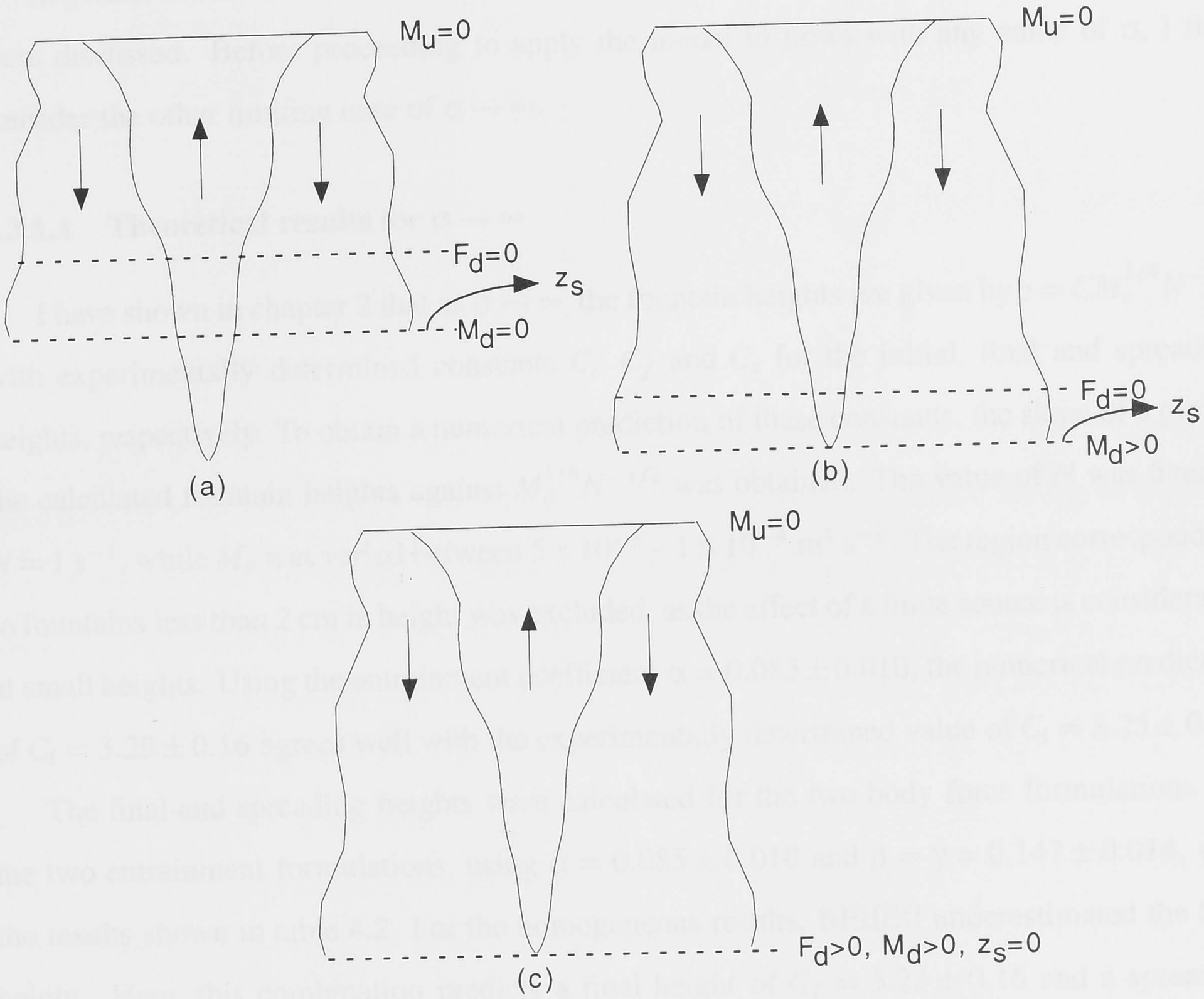

Figure 4.6: To determine the spreading height in a stratified fluid either (a) the density of the downflow is found at the point where the momentum flux falls to zero, and the level where this fluid would intrude is calculated, (b) the density of the now buoyant falling fluid when it reaches the base is determined, and the level where this fluid would intrude is calculated or (c) the downflow reaches the base still heavier than its environment and basal spreading occurs.

In the experimental study of fountains in a stratified fluid (chapter 2), the source characteristics were analysed in detail, and it was found that the flow was turbulent from the source and the virtual point source was located 1 cm below the base of the tank. The numerical integration of the entrainment equations is therefore started at the level of the actual source ($z_o = 0.01$ m) with an effective radius of $r_o = 4.16 \times 10^{-3}$ m and a non-zero volume flux. As the flow is no longer assumed to originate from a point source, the entrainment equations must be solved in their dimensional form ((4.4), (4.5), (4.26), (4.27) together with either (4.8) and (4.10), or (4.11) and (4.12)).

4.3.1 Results

In §4.2.3, the numerical results for the special case of a homogeneous environment ($\sigma = 0$) were discussed. Before proceeding to apply the model to flows with any value of σ, I first consider the other limiting case of $\sigma \to \infty$.

4.3.1.1 Theoretical results for $\sigma \to \infty$

I have shown in chapter 2 that as $\sigma \to \infty$, the fountain heights are given by $z = CM_o^{1/4}N^{-1/2}$ with experimentally determined constants C_i, C_f and C_s for the initial, final and spreading heights, respectively. To obtain a numerical prediction of these constants, the slope of a plot of the calculated fountain heights against $M_o^{1/4}N^{-1/2}$ was obtained. The value of N was fixed at $N = 1\ \mathrm{s}^{-1}$, while M_o was varied between $5 \times 10^{-8} - 1 \times 10^{-4}\ \mathrm{m}^4\ \mathrm{s}^{-2}$. The region corresponding to fountains less than 2 cm in height was excluded, as the effect of a finite source is considerable at small heights. Using the entrainment coefficient $\alpha = 0.085 \pm 0.010$, the numerical prediction of $C_i = 3.29 \pm 0.16$ agrees well with the experimentally determined value of $C_i = 3.25 \pm 0.17$.

The final and spreading heights were calculated for the two body force formulations and the two entrainment formulations, using $\alpha = 0.085 \pm 0.010$ and $\beta = \gamma = 0.147 \pm 0.014$, with the results shown in table 4.2. For the homogeneous results, BFIIEII underestimated the final height. Here, this combination predicts a final height of $C_f = 3.23 \pm 0.16$ and a spreading height of $C_s = 1.60 \pm 0.10$, both of which slightly overestimate the experimentally determined values of $C_f = 3.00 \pm 0.23$ and $C_s = 1.53 \pm 0.10$, respectively (§2.2.4). The closest agreement with the experimental results is obtained using BFIEII ($C_f = 2.98 \pm 0.12$, $C_s = 1.53 \pm 0.06$). However, as all of the formulations predict final and spreading heights which lie within the error bars of the experimentally determined results, these results do not clearly support any particular one of the formulations. This result is not unexpected, as the downflow velocity is smaller when intermediate intrusion occurs, and it was shown in §2.2.5 that the distance over which the upflow and downflow interact clearly affects the amount by which the final fountain height is reduced from the initial value (figure 2.8). In a homogeneous fluid, $\tilde{z}_i/\tilde{z}_f = 1.43$ (Turner 1966), but this ratio falls to $\tilde{z}_i/\tilde{z}_f = 1.05$ as the spreading height reaches a maximum. With such a small difference between $\tilde{z}_i$ and $\tilde{z}_f$, the scope for any differences between the four formulations is similarly reduced.

	Entrainment I	Entrainment II
Body force I	$C_f = 2.80 \pm 0.15$	$C_f = 2.98 \pm 0.12$
	$C_s = 1.43 \pm 0.08$	$C_s = 1.50 \pm 0.06$
Body force II	$C_f = 2.94 \pm 0.15$	$C_f = 3.23 \pm 0.16$
	$C_s = 1.57 \pm 0.08$	$C_s = 1.60 \pm 0.10$

Table 4.2: Calculated values of the constants in the expression $z = C \times M_o^{1/4} N^{-1/2}$ for the final (C_f) and spreading (C_s) heights of an axisymmetric fountain as $\sigma \to \infty$.

4.3.1.2 Theoretical results for $0 < \sigma < \infty$

Of the four possible model variations, those including the second entrainment formulation gave the best results at $\sigma = 0$, while little difference was observed between the formulations at $\sigma \to \infty$. The second entrainment formulation (variations BFIEII and BFIIEII) is therefore now used to model the fountain for the full range of σ.

In chapter 2, I showed that the fountain heights in a stratified fluid are quantified by $z = f(\sigma) M_o^{3/4} F_o^{-1/2}$, where $f(\sigma)$ is different for the initial, final and spreading heights. Numerical predictions for $f(\sigma)$ for the initial, final and spreading heights were obtained for $\sigma = 10^{-1} - 10^4$ by fixing $F_o = 5 \times 10^{-5}$ m^4 s^{-3} and varying M_o from $(0.07 - 3) \times 10^{-3}$ m^4 s^{-2} and N between $0.2 - 1.6$ s^{-1}. Tests of the program showed that for any value of σ, $f(\sigma)$ was independent of the actual values of M_o, F_o and N. The numerical results using BFIEII and BFIIEII with $\alpha = 0.085$ and $\beta = \gamma = 0.147$ are shown in comparison with the experimental results in figure 4.7. The results using BFIIEII (figure 4.7b) give the better prediction of the experimental results over the full range of σ.

From the numerical results, it is also possible to predict the critical value of σ_c which quantifies the transition between basal and intermediate spreading. Using BFIEII gives $\sigma_c = 8.5$, while the prediction of $\sigma_c = 5.2$ obtained using BFIIEII is in much better agreement with the experimentally determined value of $\sigma_c = 5.0 \pm 0.1$.

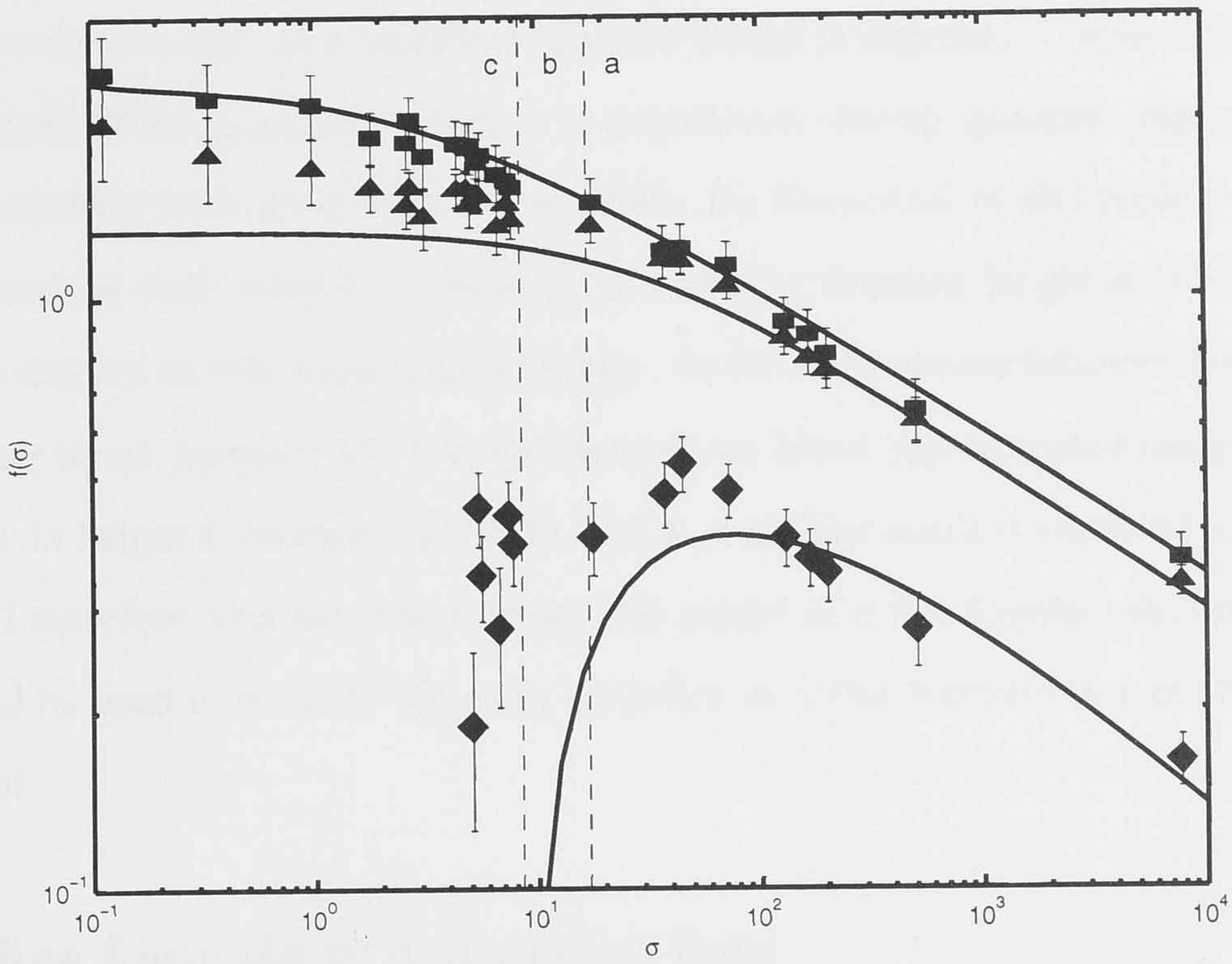

(a)

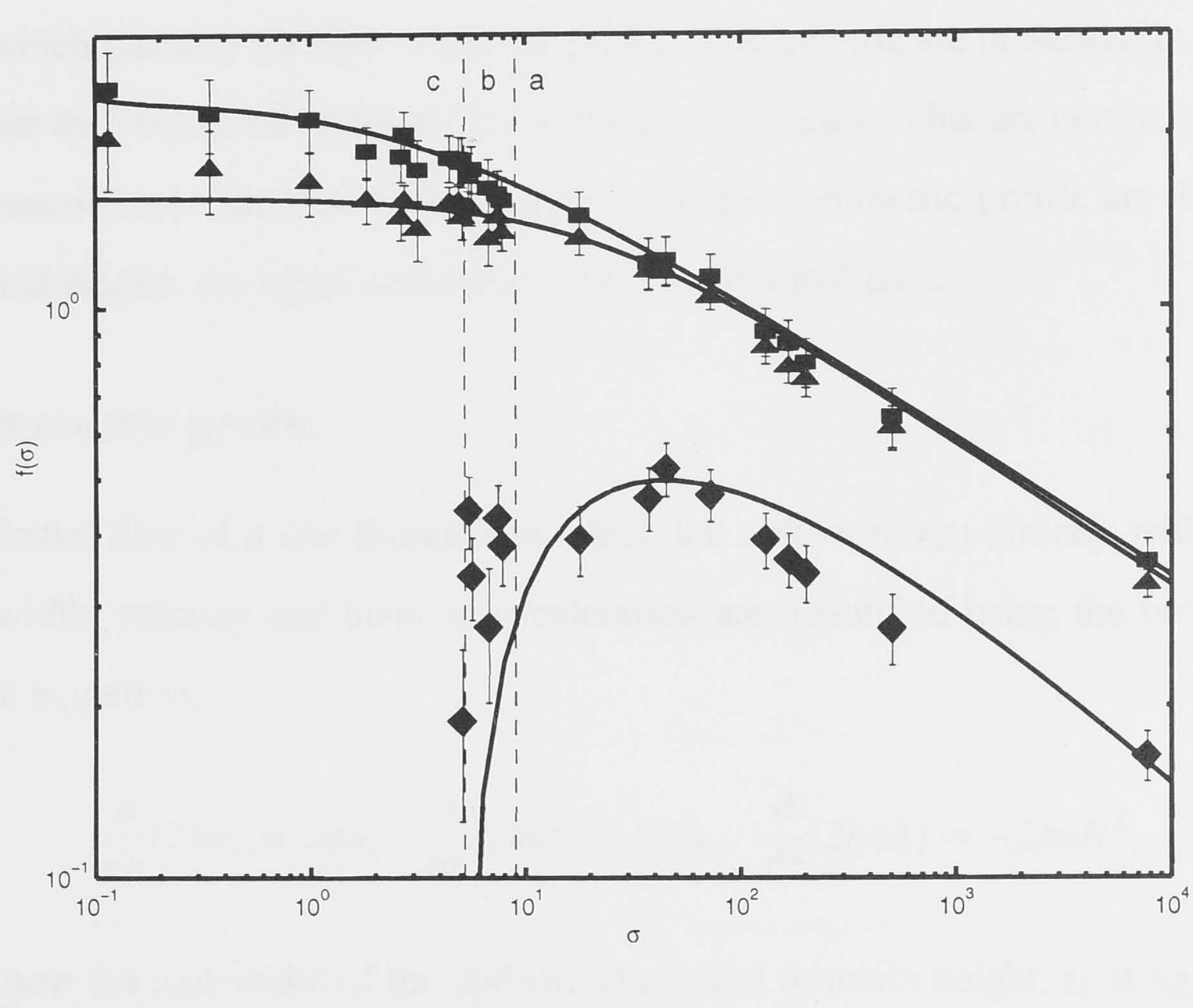

(b)

Figure 4.7: Comparison between the experimental measurements of $f(\sigma)$ for the initial, final and spreading heights and the numerical predictions obtained using $\alpha = 0.085$, $\beta = \gamma = 0.147$ in the formulations: (a) BFIEII and (b) BFIIEII. Also shown on the figures are the three regimes of behaviour corresponding to the different methods of determining the spreading height.

Based on these results in a stratified fluid, the model is expected to give reasonably accurate predictions of the fountain properties in an arbitrary density gradient, especially in cases where intermediate intrusion occurs. In particular, the theoretical model could be applied in a confined stratified environment to quantify the changing fountain height at small times when the ambient density stratification remains strong. As the environment becomes homogeneously mixed at later times, however, the fountain heights are better approximated using the homogeneous fountain height formulation given in §3.2.3. A similar result is expected to apply to line fountains. I therefore now develop a theoretical model of a line fountain in a stratified fluid, which could be used to quantify the early evolution of a line fountain in a confined stratified environment.

4.4 A line fountain in a stratified fluid

In this section, I develop a theoretical model of a line fountain in a stratified fluid. The equations which quantify the flow when the profile is symmetric are presented in §4.4.1. These equations are then integrated numerically and the calculated heights are compared with experimental measurements. In §4.4.2, the equations for an asymmetric profile are developed, and the calculated heights are again compared with experimental data.

4.4.1 Symmetric profile

In the initial flow of a line fountain in which the upflow mixes directly with the environment, the width, velocity and buoyant acceleration are quantified using the two dimensional entrainment equations:

$$\frac{\mathrm{d}}{\mathrm{d}z}(2bu) = 2\alpha u, \quad \frac{\mathrm{d}}{\mathrm{d}z}(2bu^2) = 2b\Delta, \quad \frac{\mathrm{d}}{\mathrm{d}z}(2bu\Delta) = -2buN^2, \tag{4.28}$$

where b is now the half-width of the upflow. The initial fountain height, z_i, is again defined as the height at which the momentum flux falls to zero.

When the profile of a line fountain is symmetric (see figure 4.8), the entrainment equations are derived using the same body force and entrainment formulations as those presented in §4.2 for axisymmetric fountains. The fluxes per unit length of volume, momentum and buoyancy in

the upflow and in the downflow are defined to be

$$\begin{aligned} q_u &= 2b_u u_u \qquad & q_d &= (b_d - b_u)u_d \\ m_u &= 2b_u u_u^2 \qquad & m_d &= (b_d - b_u)u_d^2 \\ f_u &= 2b_u u_u \Delta_u \qquad & f_d &= (b_d - b_u)u_d \Delta_d . \end{aligned} \tag{4.29}$$

As the downflow properties are identical on both sides of the upflow, they are calculated for one side only.

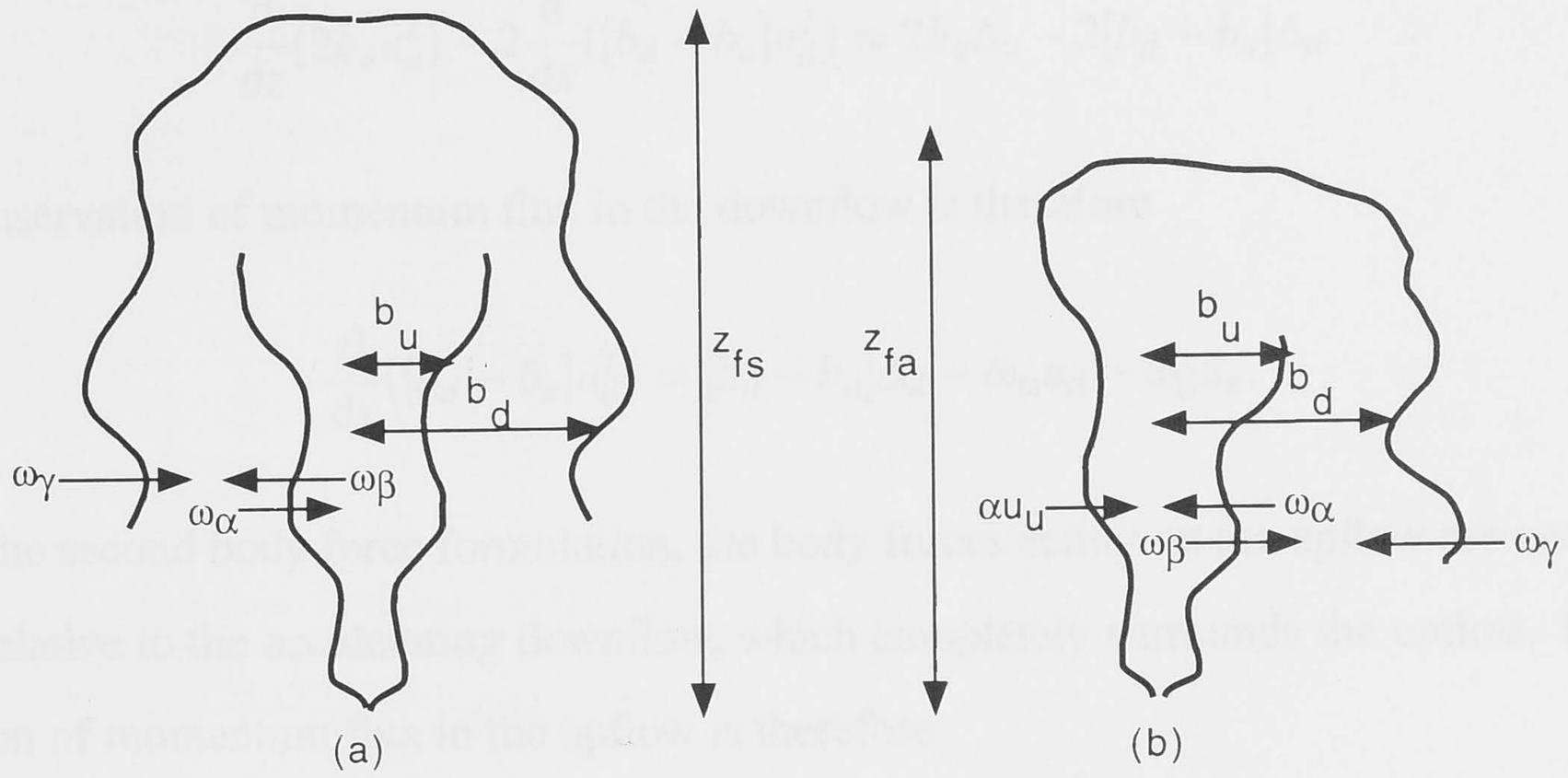

Figure 4.8: Schematic illustration of a line fountain when the profile is (a) symmetric and (b) asymmetric.

The conservation of volume flux in the upflow and each downflow is given by

$$\frac{\mathrm{d}}{\mathrm{d}z}(2b_u u_u) = 2\omega_\alpha - 2\omega_\beta \tag{4.30}$$

$$\frac{\mathrm{d}}{\mathrm{d}x}([b_d - b_u]u_d) = \omega_\beta + \omega_\gamma - \omega_\alpha, \tag{4.31}$$

where ω_α, ω_β and ω_γ are the entrainment velocities, which are given by (4.23) in the first entrainment formulation and (4.24) in the second entrainment formulation. The expressions for the conservation of buoyancy in the upflow and downflow are

$$\frac{\mathrm{d}}{\mathrm{d}z}(2b_u u_u \Delta_u) = -2b_u u_u N^2 - 2\omega_\alpha \Delta_d - 2\omega_\beta \Delta_u \tag{4.32}$$

$$\frac{\mathrm{d}}{\mathrm{d}x}([b_d - b_u]u_d \Delta_d) = -[b_d - b_u]u_d N^2 - \omega_\alpha \Delta_d - \omega_\beta \Delta_u . \tag{4.33}$$

In the first body force formulation, the acceleration of the upflow depends only on Δ_u, and the conservation of momentum flux in the upflow is given by

$$\frac{\mathrm{d}}{\mathrm{d}z}(2b_u u_u^2) = 2b_u\Delta_u - 2\omega_\alpha u_d - 2\omega_\beta u_u, \tag{4.34}$$

while an expression for the conservation of total momentum flux across the upflow and the downflows on both sides is

$$\frac{\mathrm{d}}{\mathrm{d}z}(2b_u u_u^2) - 2\frac{\mathrm{d}}{\mathrm{d}x}([b_d - b_u]u_d^2) = 2b_u\Delta_u - 2[b_d - b_u]\Delta_d. \tag{4.35}$$

The conservation of momentum flux in the downflow is therefore

$$\frac{\mathrm{d}}{\mathrm{d}x}([b_d - b_u]u_d^2) = [b_d - b_u]\Delta_d - \omega_\alpha u_d - \omega_\beta u_u. \tag{4.36}$$

In the second body force formulation, the body forces acting on the upflow are again measured relative to the accelerating downflow, which completely surrounds the upflow. The conservation of momentum flux in the upflow is therefore

$$\frac{\mathrm{d}}{\mathrm{d}z}(2b_u u_u^2) = 2b_u\left(\Delta_u + \Delta_d - u_d\frac{\mathrm{d}u_d}{\mathrm{d}x}\right) - 2\omega_\alpha u_d - 2\omega_\beta u_u, \tag{4.37}$$

which, combined with (4.35) gives

$$\frac{\mathrm{d}}{\mathrm{d}x}([b_d - b_u]u_d^2) = [b_d - b_u]\Delta_d + b_u\left(\Delta_d - u_d\frac{\mathrm{d}u_d}{\mathrm{d}x}\right) - \omega_\alpha u_d - \omega_\beta u_u, \tag{4.38}$$

for the conservation of momentum flux in the downflow.

To model a line fountain in a stratified fluid, I concentrate on the flow when $\sigma^* \to \infty$. In this case, the downflow buoyancy flux becomes equal to zero at an intermediate height, and the momentum flux is reduced to zero closer to the source (as in §4.3). The spreading height is determined by calculating the fluid density at the point where the momentum flux equals zero and finding where fluid with this density would intrude in the environment.

The dimensionless properties are:

$$\begin{aligned} z &= m_o^{1/3} N^{-2/3} \tilde{z} \quad & b &= m_o^{1/3} N^{-2/3} \tilde{b} \\ u &= m_o^{1/3} N^{1/3} \tilde{u} \quad & \omega &= m_o^{1/3} N^{1/3} \tilde{\omega} \\ \Delta &= m_o^{1/3} N^{4/3} \tilde{\Delta} \end{aligned} \tag{4.39}$$

and $\tilde{N}^2 = 1$. Using (4.39), equations (4.30) – (4.33) with either (4.34) and (4.38) or (4.37) and (4.38) simplify to:

$$\frac{\mathrm{d}\tilde{q}_u}{\mathrm{d}\tilde{z}} = 2\tilde{\omega}_\alpha - 2\tilde{\omega}_\beta \tag{4.40}$$

$$\frac{\mathrm{d}\tilde{q}_d}{\mathrm{d}\tilde{x}} = \tilde{\omega}_\beta + \tilde{\omega}_\gamma - \tilde{\omega}_\alpha \tag{4.41}$$

$$\frac{\mathrm{d}\tilde{f}_u}{\mathrm{d}\tilde{z}} = -\tilde{q}_u - 2\tilde{\omega}_\alpha \frac{\tilde{f}_d}{\tilde{q}_d} - 2\tilde{\omega}_\beta \frac{\tilde{f}_u}{\tilde{q}_u} \tag{4.42}$$

$$\frac{\mathrm{d}\tilde{f}_d}{\mathrm{d}\tilde{x}} = -\tilde{q}_d - \tilde{\omega}_\alpha \frac{\tilde{f}_d}{\tilde{q}_d} - \tilde{\omega}_\beta \frac{\tilde{f}_u}{\tilde{q}_u} \tag{4.43}$$

with either

$$\frac{\mathrm{d}\tilde{m}_u^2}{\mathrm{d}\tilde{z}} = 2\tilde{f}_u\tilde{q}_u - 4\frac{\tilde{m}_u^2}{\tilde{q}_u}(B\tilde{\omega}_\alpha + \tilde{\omega}_\beta) \tag{4.44}$$

$$\frac{\mathrm{d}\tilde{m}_d^2}{\mathrm{d}\tilde{x}} = 2\tilde{f}_d\tilde{q}_d - 2\frac{\tilde{m}_u\tilde{m}_d}{\tilde{q}_u}(B\tilde{\omega}_\alpha + \tilde{\omega}_\beta) \tag{4.45}$$

or

$$\frac{\mathrm{d}\tilde{m}_u^2}{\mathrm{d}\tilde{z}} = 2\tilde{f}_u\tilde{q}_u + 4\frac{\tilde{m}_u\tilde{m}_d}{\tilde{q}_d}\left(\frac{A}{2+A}\tilde{\omega}_\gamma + \frac{A-2/B}{2+A}\tilde{\omega}_\beta - \tilde{\omega}_\alpha\right) \tag{4.46}$$

$$\frac{\mathrm{d}\tilde{m}_d^2}{\mathrm{d}\tilde{x}} = 2\tilde{f}_d\tilde{q}_d + 2\frac{\tilde{m}_d^2}{\tilde{q}_d}\left(\frac{A}{2+A}\tilde{\omega}_\gamma + \frac{A-2/B}{2+A}\tilde{\omega}_\beta - \tilde{\omega}_\alpha\right) \tag{4.47}$$

where

$$A = \frac{\tilde{q}_u^2\tilde{m}_d}{\tilde{q}_d^2\tilde{m}_u} \qquad B = \frac{\tilde{q}_u\tilde{m}_d}{\tilde{q}_d\tilde{m}_u}. \tag{4.48}$$

The starting conditions for the downflow are obtained by assuming that the upflow divides evenly at the fountain height so that $\tilde{q}_d(\tilde{x}=0) = \tilde{q}_u(\tilde{z}_f)/2$ and $\tilde{f}_d(\tilde{x}=0) = -\tilde{f}_u(\tilde{z}_f)/2$.

4.4.1.1 Results and comparison with experiment

The initial, final and spreading fountain heights were calculated using the same numerical procedure outlined in §4.2.2. The integration is started at a height $\tilde{z}_o = 0.01$ above the virtual line source with $\tilde{m}_o = 1$, $\tilde{f}_o = -1$ and $\tilde{q}_o = 2(\alpha\tilde{z}_o)^{1/2}$ (where $\tilde{q}_o(\tilde{z}_o)$ was found from a solution of (4.28) for a jet).

First, the upflow equations were integrated numerically using $\alpha = 0.080 \pm 0.015$ to give a value of $\tilde{z}_i = 2.45 \pm 0.16$. This calculated initial height agrees well with the experimental value of $\tilde{z}_i = 2.46 \pm 0.08$. The calculated final and spreading heights for the four formulations are shown in table 4.3. The calculated final heights are lower than the experimental value of $\tilde{z}_{fs} = 2.43 \pm 0.20$, with BFIIEII giving the closest agreement at $\tilde{z}_{fs} = 2.34 \pm 0.08$. This 4% difference between the calculated and experimentally measured heights is comparable to the result obtained from the axisymmetric fountain model (§4.3.1.1).

	Entrainment I	Entrainment II
Body force I	$\tilde{z}_{fs} = 1.84 \pm 0.06$	$\tilde{z}_{fs} = 2.03 \pm 0.06$
	$\tilde{z}_s = 0.53 \pm 0.04$	$\tilde{z}_s = 0.62 \pm 0.03$
Body force II	$\tilde{z}_{fs} = 1.98 \pm 0.07$	$\tilde{z}_{fs} = 2.34 \pm 0.08$
	$\tilde{z}_s = 0.61 \pm 0.04$	$\tilde{z}_s = 0.78 \pm 0.04$

Table 4.3: Calculated results for the final symmetric ($\tilde{z}_{fs}$) and spreading ($\tilde{z}_s$) heights of a line fountain as $\sigma^* \to \infty$.

The calculated spreading heights are between 27% and 50% lower than the experimental value of $\tilde{z}_s = 1.07 \pm 0.05$ (c.f. §4.3.1.1 where the calculated spreading height of an axisymmetric fountain agreed well with experimental measurements). Once again, the formulation BFIIEII gives the closest agreement with experimental results. A number of factors could contribute to the low value of the calculated spreading height. First, a low value of the calculated final height will cause a decrease in the calculated spreading height. In the best of the formulations (BFIIEII), however, the calculated final height is only 4% lower than the experimentally measured final height, while the calculated spreading height underestimates the experimental value by 27%. A second possible cause for the low spreading height is that the model underestimates the amount of mixing into the fountain. If β is decreased to the jet value of $\beta = 0.074 \pm 0.004$, the final symmetric height falls by around 1%, while the calculated spread-

ing height increases by 9%. While this improves the agreement, it still results in a calculated spreading height that underestimates the experimental value by around 18%.

4.4.2 Asymmetric profile

In chapter 2, the observation was made that the profile of a line fountain remains predominantly symmetric in a stratified fluid. It is still of interest, however, to develop a model of a line fountain with an asymmetric profile. When the fountain profile is asymmetric, the second entrainment formulation (§4.2.1.2) is immediately applicable, while it must be noted that in the first entrainment formulation (§4.2.1.1), the entrainment velocity into the upflow, $\omega_\alpha = \alpha(u_u + u_d)$, depends on whether the fluid is being entrained from the environment ($u_d = 0$) or from the downflow ($u_d > 0$) (see figure 4.8). While the first body force formulation can been applied directly, it is not immediately obvious how to quantify the second body force formulation, as the immediate environment of the upflow consists of the stationary ambient on one side and the accelerating downflow on the other. I therefore focus here on using the first body force formulation.

The upflow entrains fluid from the downflow and directly from the environment, while the downflow entrains fluid from both the upflow and environment. The conservation of volume flux in the upflow and downflow is given by:

$$\frac{\mathrm{d}}{\mathrm{d}z}(2b_u u_u) = \omega_\alpha + \alpha u_u - \omega_\beta, \tag{4.49}$$

and

$$\frac{\mathrm{d}}{\mathrm{d}x}([b_d - b_u]u_d) = \omega_\beta + \omega_\gamma - \omega_\alpha, \tag{4.50}$$

where ω_α, ω_β and ω_γ are again given by (4.23) in the first entrainment formulation and (4.24) in the second entrainment formulation. Expressions for the conservation of buoyancy in the upflow and downflow are:

$$\frac{\mathrm{d}}{\mathrm{d}z}(2b_u u_u \Delta_u) = -2b_u u_u N^2 - \omega_\alpha \Delta_d - \omega_\beta \Delta_u, \tag{4.51}$$

and

$$\frac{\mathrm{d}}{\mathrm{d}x}([b_d - b_u]u_d \Delta_d) = -[b_d - b_u]u_d N^2 - \omega_\alpha \Delta_d - \omega_\beta \Delta_u. \tag{4.52}$$

In the first body force formulation, the conservation of momentum flux in the upflow is given by

$$\frac{\mathrm{d}}{\mathrm{d}z}(2b_u u_u^2) = 2b_u \Delta_u - \omega_\alpha u_d - \omega_\beta u_u. \tag{4.53}$$

The conservation of total momentum flux across the upflow and downflow is written as

$$\frac{\mathrm{d}}{\mathrm{d}z}(2b_u u_u^2) - \frac{\mathrm{d}}{\mathrm{d}x}([b_d - b_u]u_d^2) = 2b_u \Delta_u - [b_d - b_u]\Delta_d, \tag{4.54}$$

so that the conservation of momentum flux in the downflow is

$$\frac{\mathrm{d}}{\mathrm{d}x}([b_d - b_u]u_d^2) = [b_d - b_u]\Delta_d - \omega_\alpha u_d - \omega_\beta u_u. \tag{4.55}$$

Using (4.29) to define the fluxes of volume, momentum and buoyancy, and (4.39) to non-dimensionalise the quantities, these equations simplify to

$$\frac{\mathrm{d}\tilde{q}_u}{\mathrm{d}\tilde{z}} = \tilde{\omega}_\alpha + \alpha\tilde{u}_u - \tilde{\omega}_\beta \tag{4.56}$$

$$\frac{\mathrm{d}\tilde{q}_d}{\mathrm{d}\tilde{x}} = \tilde{\omega}_\beta + \tilde{\omega}_\gamma - \tilde{\omega}_\alpha \tag{4.57}$$

$$\frac{\mathrm{d}\tilde{f}_u}{\mathrm{d}\tilde{z}} = -\tilde{q}_u - \tilde{\omega}_\alpha \frac{\tilde{f}_d}{\tilde{q}_d} - \tilde{\omega}_\beta \frac{\tilde{f}_u}{\tilde{q}_u} \tag{4.58}$$

$$\frac{\mathrm{d}\tilde{f}_d}{\mathrm{d}\tilde{x}} = -\tilde{q}_d - \tilde{\omega}_\alpha \frac{\tilde{f}_d}{\tilde{q}_d} - \tilde{\omega}_\beta \frac{\tilde{f}_u}{\tilde{q}_u} \tag{4.59}$$

$$\frac{\mathrm{d}\tilde{m}_u^2}{\mathrm{d}\tilde{z}} = 2\tilde{f}_u\tilde{q}_u - 2\frac{\tilde{m}_u\tilde{m}_d}{\tilde{q}_d}\left(\tilde{\omega}_\alpha + B\tilde{\omega}_\beta\right) \tag{4.60}$$

$$\frac{\mathrm{d}\tilde{m}_d^2}{\mathrm{d}\tilde{x}} = 2\tilde{f}_d\tilde{q}_d - 2\frac{\tilde{m}_d^2}{\tilde{q}_d}\left(\tilde{\omega}_\alpha + B\tilde{\omega}_\beta\right). \tag{4.61}$$

In this case, the starting conditions for the downflow are given by $\tilde{q}_d(\tilde{x}=0) = \tilde{q}_u(\tilde{z}_f)$ and $\tilde{f}_d(\tilde{x}=0) = -\tilde{f}_u(\tilde{z}_f)$.

4.4.2.1 Results and comparison with experiments

The numerical procedure outlined in §4.2.2 was used to calculate the initial, final and spreading heights of an asymmetric line fountain. Using values of $\alpha = 0.080 \pm 0.015$ and

$\beta = \gamma = 0.147 \pm 0.014$, the equations were integrated numerically to give the values for the asymmetric height that are shown in table 4.4.

	$\sigma^* \to \infty$
BFIEI	$\tilde{z}_{fs} = 1.84 \pm 0.05$
	$\tilde{z}_{fa} = 1.84 \pm 0.04$
BFIEII	$\tilde{z}_{fs} = 2.03 \pm 0.05$
	$\tilde{z}_{fa} = 2.04 \pm 0.05$

Table 4.4: Comparison between the symmetric ($\tilde{z}_{fs}$) and asymmetric ($\tilde{z}_{fa}$) heights of a line fountain calculated as $\sigma^* \to \infty$ for the two formulations BFIEI and BFIEII.

The calculated asymmetric heights are 10 – 20% lower than the experimental value of $\tilde{z}_{fa} = 2.27 \pm 0.20$. These calculated values were obtained using the first body force formulation only — if an appropriate second body force formulation could be developed, the agreement between the calculated and experimental values should improve (in the symmetric line fountain model and the axisymmetric fountain model, the best agreement was obtained using BFIIEII).

For the two formulations used, the difference between the calculated asymmetric and symmetric heights is negligible. The asymmetric model therefore does not predict the 7% decrease in height (see §2.3.3) when the fountain profile becomes asymmetric.

One possible reason why the model does not predict a smaller asymmetric height relates to a feature of the experiments that was not modelled theoretically: the line fountain extended across the width of the tank, effectively separating the ambient fluid on either side. Any horizontal flow established in the environment (if, for example, more fluid was entrained into one side of the fountain at any stage) would transport fluid directly through the fountain. In a turbulent jet, the effect of a uniform crossflow is limited to the regions where the velocity of the crossflow is comparable to the axial fluid velocity. In these regions, the velocity of jet decreases at a faster rate than when there is no crossflow present (Fischer *et al.* 1979; List 1982a). In a turbulent line fountain, a more rapid decrease in the upflow velocity as a result of a crossflow would lead to a smaller fountain height. The effect of any crossflow could be examined in the further experiments that are outlined in §6.2.

4.5 Conclusions

I have developed theoretical models of axisymmetric and line fountains, in which sets of entrainment equations are used to quantify the turbulent mixing between the upflow, the downflow and the environment. In this modelling, I have focused on the effects that different formulations of the body forces and entrainment velocities have on the fountain properties. In the two body force formulations considered, the buoyant acceleration of the upflow was measured relative to either the stationary environment (BFI) or to the accelerating downflow (BFII). In the two entrainment formulations, the entrainment into the upflow was quantified using either the velocity difference between the upflow and downflow (EI) or the velocity of the upflow (EII).

For the axisymmetric fountain, all four variations of the entrainment equations were integrated numerically to calculate the initial, final and spreading heights of the fountain, as well as the radius, velocity and buoyancy of the upflow and downflow. In a homogeneous fluid, the calculated final fountain heights were all lower than the experimental measurements, with the differences between theory and experiment ranging from about 40% (using BFI and EI) to about 15% (using BFII and EII). This difference between the model and experimental measurements probably reflects the fact that both the assumed top hat profiles and the model pictured in figure 4.3 are only rough descriptions of the actual behaviour near the top of the fountain. The theoretical model also gave predictions of the velocity and buoyancy in the upflow, as well as the radius of the upflow and downflow. These calculated properties were compared with all available experimental data, and were found to be in good agreement.

In a stratified fluid, the equations for an axisymmetric fountain were integrated to give the initial, final and spreading heights as a function of the dimensionless parameter, σ, as it varies from $\sigma = 0$ (homogeneous fluid) to $\sigma \to \infty$ (stratified fluid with zero buoyancy flux at the source). As the spreading height rises to an intermediate level (at larger values of σ), the interaction between the upflow and downflow decreases, and consequently there is little difference between the four formulations at large values of σ. The best agreement over the full range of σ was obtained using the combination of body force and entrainment formulations that best predicted the fountain heights in a homogeneous fluid (BFII and EII).

The results for the axisymmetric fountain indicated that the model could be used to quan-

tify the height of a fountain in a confined stratified environment during the early stages of the evolution when the ambient stratification is strong. Based on this conclusion, a theoretical model of a line fountain in a stratified environment was developed. Two models were presented: one to quantify the flow when the fountain profile is symmetric, and the other for when the profile is asymmetric.

Using the two body force formulations and two entrainment formulations, the equations for a symmetric profile were integrated numerically to calculate the initial, final symmetric and spreading heights of the fountain. The best agreement between the calculated and experimentally measured final symmetric height was again obtained using the formulations BFII and EII. The calculated spreading height significantly underestimated the experimental measurements.

The equations developed for an asymmetric profile included both entrainment formulations, but only the first body force formulation. The calculated asymmetric final heights were lower than the experimental measurements, and it was noted that there was only a negligible difference between the calculated asymmetric and symmetric heights. This result contrasts experimental measurements, where the asymmetric height was about 7% lower than the symmetric height. The source of this discrepancy could be determined in further experiments (described in §6.2). As for the axisymmetric fountain, the model of a line fountain could be used to quantify the initial fountain evolution in a confined stratified environment.

Chapter 5

Applications

"There are no such things as applied sciences, only the applications of science."

Louis Pasteur (1822 - 1895)
French Microbiologist

Turbulent jets, plumes and fountains arise in a variety of geological, industrial and environmental situations. Some examples of these situations are outlined in §5.1. In §5.2, I use the results from the previous chapters to investigate the dynamics of an axisymmetric fountain which is produced when a room or an aircraft hanger is cooled or heated. Then, in §5.3, I examine the formation and evolution of a turbulent line fountain as it replenishes a magma chamber.

5.1 Introduction

Much of the motivation behind the study of turbulent jets, plumes and fountains has arisen from a need to improve our understanding of a number of flows in both natural and engineered environments. These flows, which arise in a variety of fluids and on a wide range of length scales, include:

- smoke from chimney stacks (Briggs 1969),
- sewerage outfall into the ocean (Koh & Brooks 1975; Fischer *et al.* 1979),
- the disposal of brines from industrial processes into rivers and estuaries (Pincince & List 1973),
- the formation of 'black smokers' from hydrothermal vents on the ocean floor (Campbell, McDougall & Turner 1984),
- columns of smoke and ash from volcanic eruptions (Sparks *et al.* 1998),
- exit snow from snowplows (Lindberg & Petersen 1991),
- mixing in LNG (natural gas) tanks (Germeles 1975),
- enclosure fires (Goldman & Jaluria 1986),
- the forced or natural ventilation of large buildings (Baines *et al.* 1990; Baines, Corriveau & Reedman 1993), and
- the replenishment of magma chambers (Turner & Campbell 1986; Campbell & Turner 1986b; Campbell & Turner 1989).

Provided the effects of viscosity and diffusivity can be considered negligible, the natural length scale in each of these diverse flows depends on the momentum flux at the source, the buoyancy flux at the source and the ambient density stratification. Properties such as the width, fluid velocity or terminal height can then be quantified using the characteristic length scale combined with the experimentally determined constants for the relevant flow (i.e. jet, plume or fountain). This fact was clearly demonstrated by Wilson *et al.* (1978) in their analysis of the height reached by volcanic clouds of ash. By extrapolating laboratory measurements of

plumes in a stratified environment to scales up to five orders of magnitude larger, Wilson *et al.* (1978) used assumed eruption details and atmospheric conditions to accurately predict the 40 km height reached by the cloud of ash released in the 1956 eruption of Bezymianny, Russia.

Two contrasting examples of situations in which turbulent fountains arise are the forced heating or cooling of a room or aircraft hanger, and the replenishment of a magma chamber. In both cases the ambient air or magma may be stratified and, consequently, an understanding of the flow behaviour and evolution requires the analysis presented in the previous chapters.

5.2 Fountains to heat or cool buildings

In an enclosed building, axisymmetric turbulent fountains arise either when hot air is forced down through ceiling vents into a cold room, or when cool air is forced up through floor vents into a hot room. When the ambient air is thermally stratified, the flow dynamics can be described using the stratified fountain filling box model developed in chapter 3. To illustrate the application of the model to building ventilation, I consider in §5.2.1 a small, warm room that is cooled by the injection of cold air through a vent in the floor, and, in §5.2.2 an aircraft hanger heated by the downward injection of hot air through multiple vents in the ceiling. In both examples a closed system is assumed in which air is removed through vents on or near the floor (when heating) or the ceiling (when cooling) at the same rate at which the heated or cooled air is injected again through the other vent as a fountain. This positioning of the outflow vents ensures that the removal of air does not interfere with the dynamics of the fountain.

5.2.1 A fountain of cold air in a warm room

In this example, I consider a small room 5 m $\times$ 5 m in area and 4 m high, in which the ambient temperature increases with height (figure 5.1). This room is cooled by the injection of cold air through a vent in the floor, with air removed at the same rate through an identical vent in the ceiling. The relevant parameters and their assumed values are summarized in table 5.1.

The lower, inhabited region of the room is cooled faster when the cold air forms a fountain which spreads along the floor. This condition requires the parameter σ to be less than $\sigma_c = 5$,

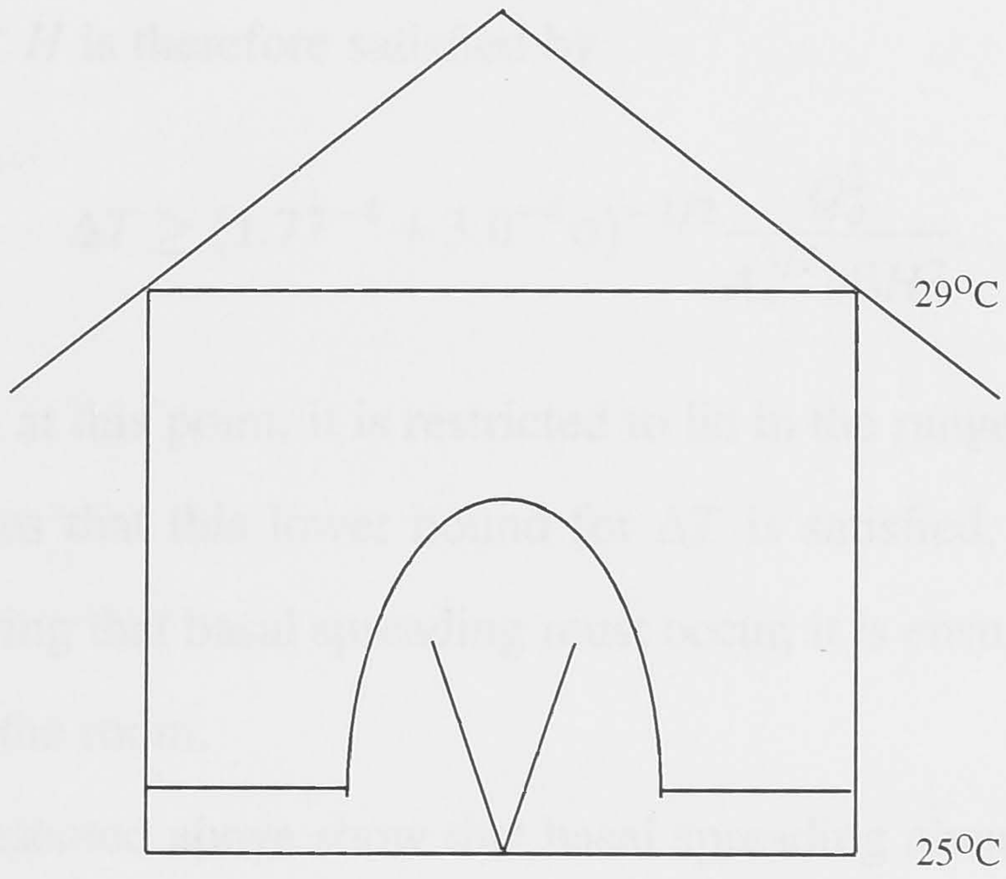

Figure 5.1: Schematic illustration of a room that is cooled by the injection of a fountain of cold air through a vent in the floor.

Property		Value
cross sectional room area	A	25 m^2
room height	H	4 m
ambient temperature at floor	T_f	25°C
ambient temperature gradient	dT/dz	1°C/m
thermal expansion coefficient	β	1/300 K^{-1}
buoyancy frequency	N	0.18 s^{-1}
volume flux at source	Q_o	0.02 m^3 s^{-1}
vent area	A_v	0.01 m^2

Table 5.1: Assumed values of the parameters used in the calculations for a warm room cooled by a fountain of cold air.

so that the temperature difference at the source satisfies

$$\Delta T \geq \frac{Q_o N}{A_v g \beta \sigma_c^{1/2}}, \tag{5.1}$$

where, in the definition of σ, $M_o = Q_o^2/A_v$ and $F_o = g\beta\Delta T Q_o$. The assumed values of Q_o, N and A_v give the result that $\Delta T \geq 4.9°\text{C}$.

An additional restriction on ΔT arises if the fountain height is to remain less than the height, H, of the room. At $t = 0$, the fountain height is found from (2.7) and (2.14) to be

$$z_{fi} = (1.77^{-4} + 3.0^{-4}\sigma)^{-1/4} \frac{Q_o}{(A_v^{3/2} g\beta\Delta T)^{1/2}}. \tag{5.2}$$

The condition that $z_{fi} < H$ is therefore satisfied by

$$\Delta T \geq (1.77^{-4} + 3.0^{-4}\sigma)^{-1/2} \frac{Q_o^2}{A_v^{3/2} g\beta H^2}. \tag{5.3}$$

Although σ is unknown at this point, it is restricted to lie in the range $0 \leq \sigma \leq 5$. Using $\sigma = 0$ in (5.3) therefore ensures that this lower bound for ΔT is satisfied, and gives the result that $\Delta T \geq 2.6°C$. By specifying that basal spreading must occur, it is ensured that the fountain does not reach the ceiling of the room.

The calculations presented above show that basal spreading always occurs for injected air temperatures less than 20°C. The subsequent evolution of the fountain, as well as the changing temperature in the room, is determined using the stratified fountain filling box model developed in chapter 3. Table 5.2 shows how varying the temperature of the injected air affects the height of the fountain at $t = 0$, the time required to establish a layer of cold air 2 m in depth, and the resulting temperature profile within this lower 2 m region. When the temperature of the injected air is $T_i = 20°C$, the air in the lower 2 m of the room is mixed to a homogeneous temperature of $T = 24.9°C$ in only 6 minutes, but little cooling occurs. When the injected air has a temperature of $T_i = 10°C$, it takes nearly 16 minutes to cool the lower 2 m to a temperature of between 19°C at the floor and 23°C at a height of 2 m.

T_i (°C)	σ	$z_f(0)$ (m)	Time when $z_a = 2$ m (mins)	Temperature profile (°C) (floor - 2 m)
20	4.9	2.5	6.0	24.9
15	1.2	1.9	10.3	22.5 – 24.5
10	0.5	1.6	15.7	19 – 23

Table 5.2: Properties of the fountain and the ambient temperature profile produced when a fountain cools an initially stratified room.

5.2.2 Fountains of hot air in an aircraft hanger

Aircraft hangers represent an example of a large building which is heated by injecting hot air downward through a series of vents in the ceiling to form inverted axisymmetric fountains.

In this example, I consider an aircraft hanger 100 m × 100 m in area and 25 m high (large enough to accommodate a 747 or several smaller aircraft), which is heated through an array

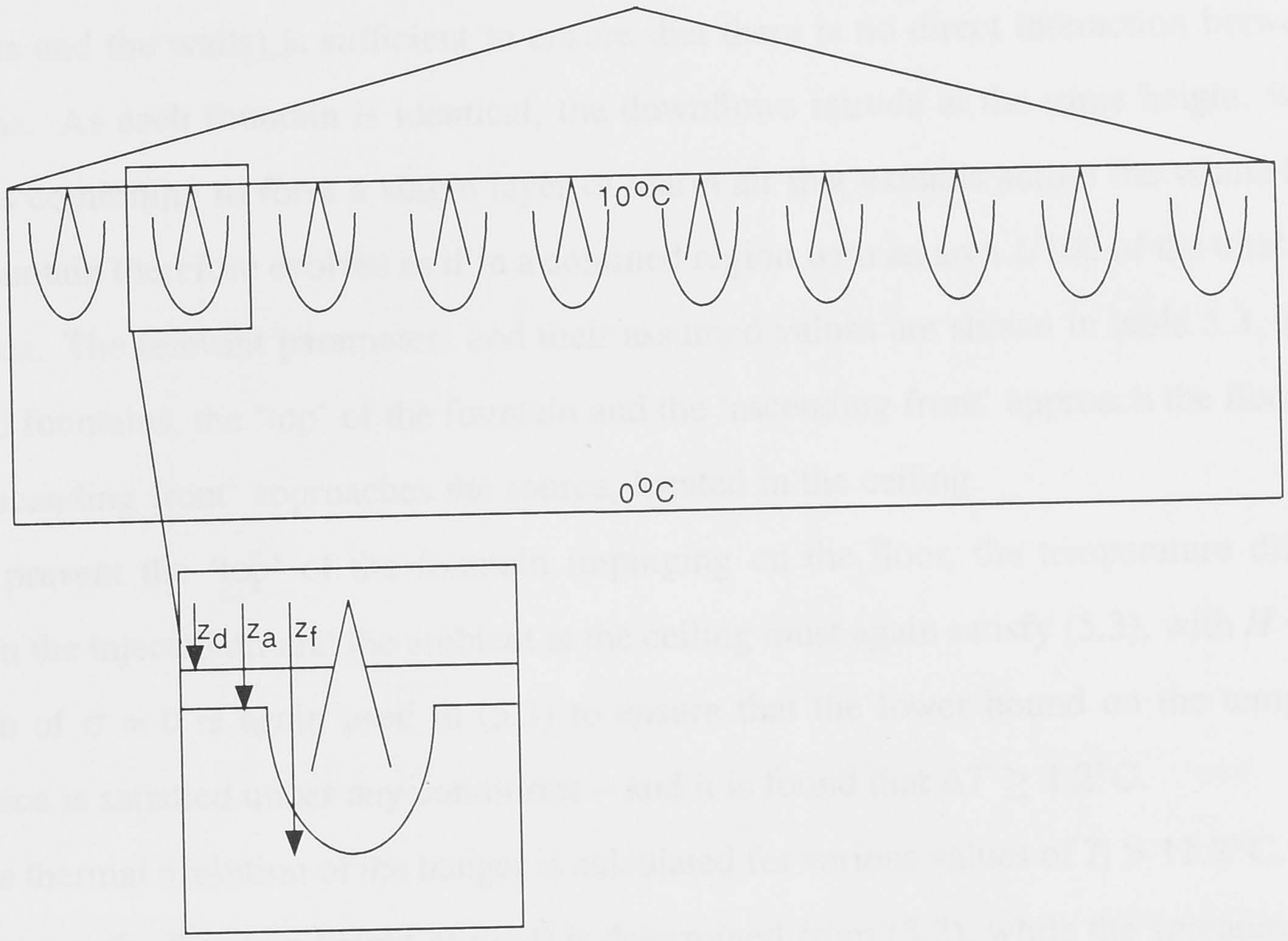

Figure 5.2: Schematic illustration of an aircraft hanger that is heated by the injection of multiple fountains of hot air through vents in the ceiling.

Property		Value
cross sectional hanger area	A	10000 m^2
hanger height	H	25 m
ambient temperature at the floor	T_f	0°C
ambient temperature at the ceiling	T_r	10°C
ambient temperature gradient	dT/dz	0.4°C/m
thermal expansion coefficient	β	1/300 K^{-1}
buoyancy frequency	N	0.11 s^{-1}
volume flux at the source	Q_o	0.5 m^3 s^{-1}
vent area	A_v	0.1 m^2
number of vents		100

Table 5.3: Assumed values of the parameters used in the calculations for a cold aircraft hanger heated by a series of fountains of hot air.

of 10×10 vents (figure 5.2). The 10 m spacing between the vents (and 5 m spacing between the vents and the walls) is sufficient to ensure that there is no direct interaction between the fountains. As each fountain is identical, the downflows intrude at the same height, with the outflows combining to form a single layer of warm air that extends across the whole hanger. Each fountain therefore evolves as if in a confined region with an area 1/100 of the total hanger floor area. The relevant parameters and their assumed values are shown in table 5.3. In these inverted fountains, the 'top' of the fountain and the 'ascending front' approach the floor, while the 'descending front' approaches the source, located in the ceiling.

To prevent the 'top' of the fountain impinging on the floor, the temperature difference between the injected air and the ambient at the ceiling must again satisfy (5.3), with $H = 25$ m. A value of $\sigma = 0$ is again used in (5.3) to ensure that the lower bound on the temperature difference is satisfied under any conditions – and it is found that $\Delta T \geq 1.2°\text{C}$.

The thermal evolution of the hanger is calculated for various values of $T_i > 11.2°\text{C}$. In these calculations, the fountain height at $t = 0$ is determined from (5.2), while the spreading height is estimated from figure 2.9. As illustrated in figure 5.2, the fountain heights are initially calculated as distances from the source (i.e. below the ceiling) before being adjusted to give heights above the floor of the hanger. The position of the 'ascending' and 'descending' fronts and the fountain height are calculated from (3.10), (3.6) and (3.23), respectively. In figure 5.3, the time taken for the 'ascending' front to reach the floor is plotted against the final homogeneous air temperature for values of $T_i = 11.5°\text{C}$, $12°\text{C}$, $13°\text{C}$, $14°\text{C}$, $15°\text{C}$, $17.5°\text{C}$, $20°\text{C}$ and $25°\text{C}$. When $T_i = 11.5°\text{C}$, the ambient air temperature becomes homogeneous on a short timescale (43 minutes), but the temperature is only increased to about $8.5°\text{C}$. In contrast, for $T_i = 25°\text{C}$, it takes 63 minutes for a homogeneous temperature of $20°\text{C}$ to be reached.

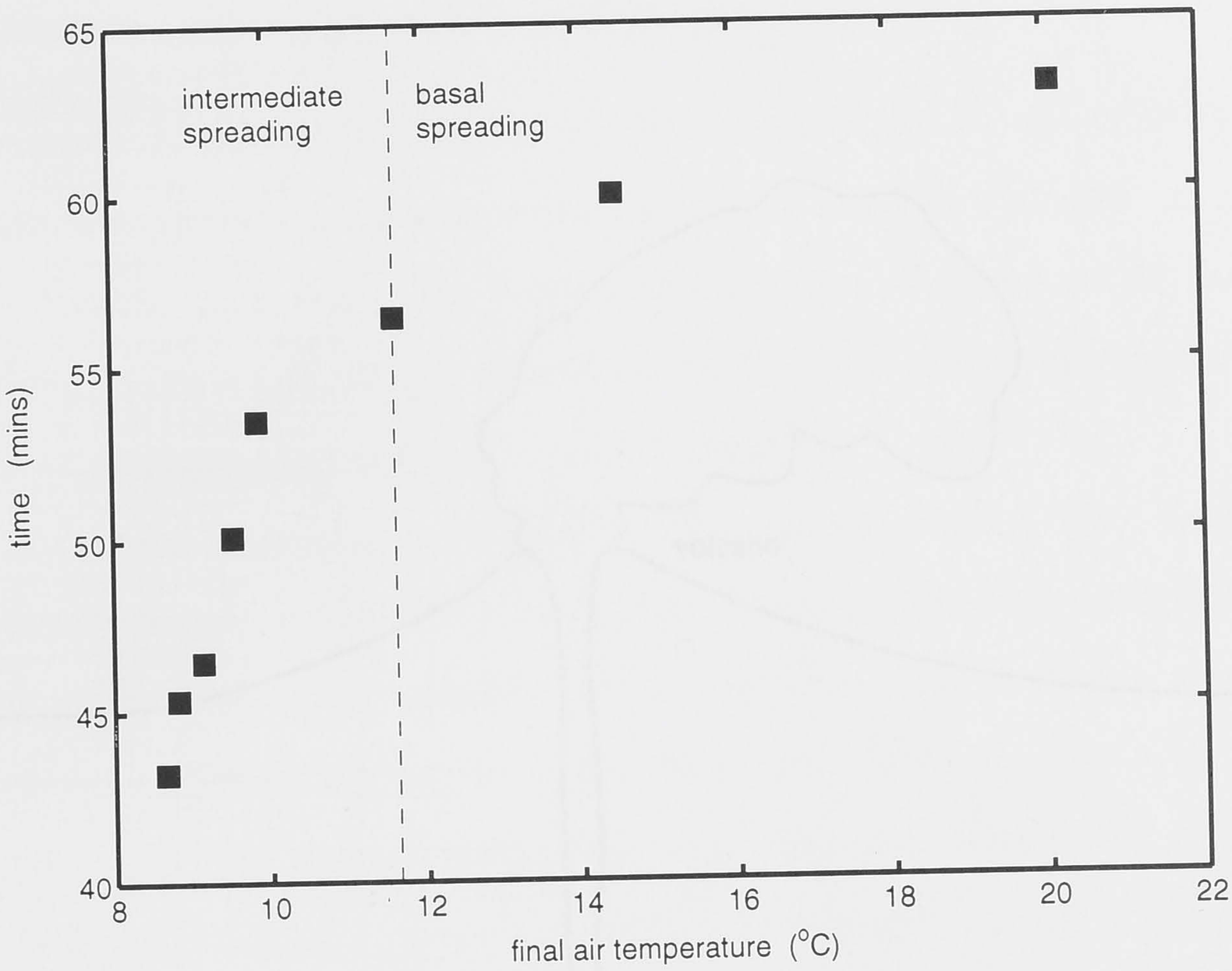

Figure 5.3: Calculated time taken for the ascending front to reach the floor of an aircraft hanger, plotted against the final homogeneous air temperature. The dashed line represents the transition from basal to intermediate spreading.

5.3 Fountains in magma chambers

Magma chambers are large reservoirs of molten rock which form within the Earth's crust (figure 5.4). Geological evidence obtained when solidified chambers are exposed at the surface suggests that many of these chambers do not form in a single phase, but are created over time by the repeated addition of small pulses of parent magma through a feeder pipe or dyke near the base (Turner & Campbell 1986; Campbell & Turner 1989). If these replenishing inputs are denser than the host magma and have sufficient momentum, then a turbulent fountain forms. The properties of these fountains depend on the densities of the injected and host magmas and on the density profile of the host magma. The chemical and physical changes that lead to variations in the density of the host magma are discussed in §5.3.1. Then, in §5.3.2, I present some results for a dense magma that enters a chamber through a narrow fissure to form a turbulent line fountain. These calculations are designed to illustrate the basic fountain behaviour – a discussion of possible double-diffusive effects is presented in §5.3.3, while the effects of viscosity are discussed briefly in §5.3.4.

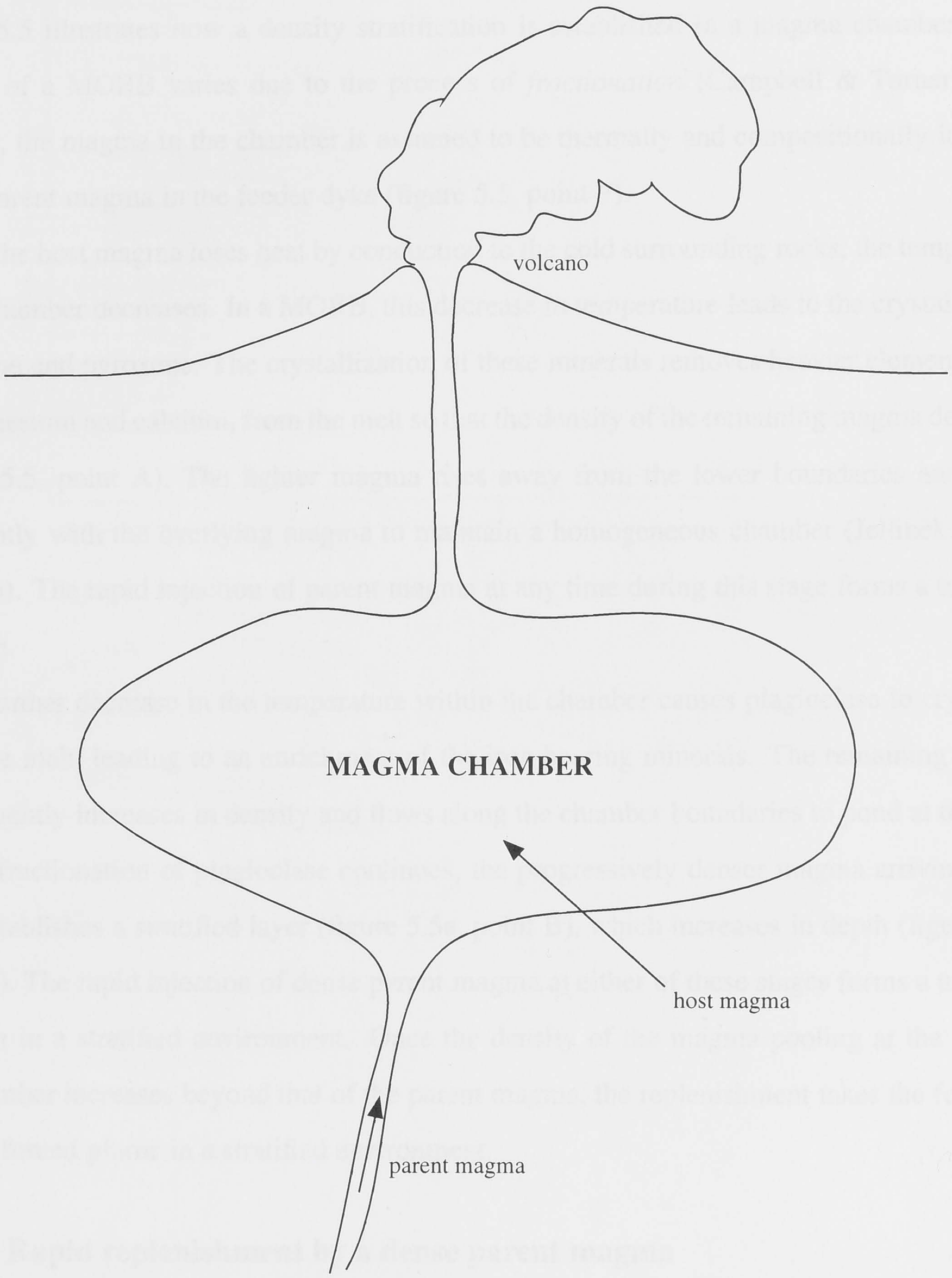

Figure 5.4: Schematic illustration of a magma chamber. The largest known remains of a solidified magma chamber, the Bushveld Intrusions in South Africa, cover an area of 65000 km^2 and are 7 – 9 km deep (Wager & Brown 1968; Eales & Cawthorn 1996).

5.3.1 Magma chamber evolution and replenishment

In this example, I consider the evolution of a Mid Ocean Ridge Basalt (MORB) as it cools. Figure 5.5 illustrates how a density stratification is established in a magma chamber as the density of a MORB varies due to the process of *fractionation* (Campbell & Turner 1989). Initially, the magma in the chamber is assumed to be thermally and compositionally identical to the parent magma in the feeder dyke (figure 5.5, point P).

As the host magma loses heat by conduction to the cold surrounding rocks, the temperature in the chamber decreases. In a MORB, this decrease in temperature leads to the crystallization of olivine and pyroxene. The crystallization of these minerals removes heavier elements, such as magnesium and calcium, from the melt so that the density of the remaining magma decreases (figure 5.5, point A). The lighter magma rises away from the lower boundaries and mixes turbulently with the overlying magma to maintain a homogeneous chamber (Jellinek & Kerr 1999a,b). The rapid injection of parent magma at any time during this stage forms a turbulent fountain.

A further decrease in the temperature within the chamber causes plagioclase to crystallize from the melt, leading to an enrichment of the iron bearing minerals. The remaining magma consequently increases in density and flows along the chamber boundaries to pond at the floor. As the fractionation of plagioclase continues, the progressively denser magma arriving at the floor establishes a stratified layer (figure 5.5a, point B), which increases in depth (figure 5.5a, point C). The rapid injection of dense parent magma at either of these stages forms a turbulent fountain in a stratified environment. Once the density of the magma pooling at the floor of the chamber increases beyond that of the parent magma, the replenishment takes the form of a pure or forced plume in a stratified environment.

5.3.2 Rapid replenishment by a dense parent magma

Some results are now presented to quantify the behaviour of a turbulent line fountain that is formed when parent magma is injected upwards through a fissure at the base of the chamber. The fountain properties are calculated at various stages in the fractionation sequence described in §5.3.1. In these examples, I consider a chamber which is $L = 100$ km in width, several kilometres in depth, and which develops a stratified region approximately 1 km deep. The

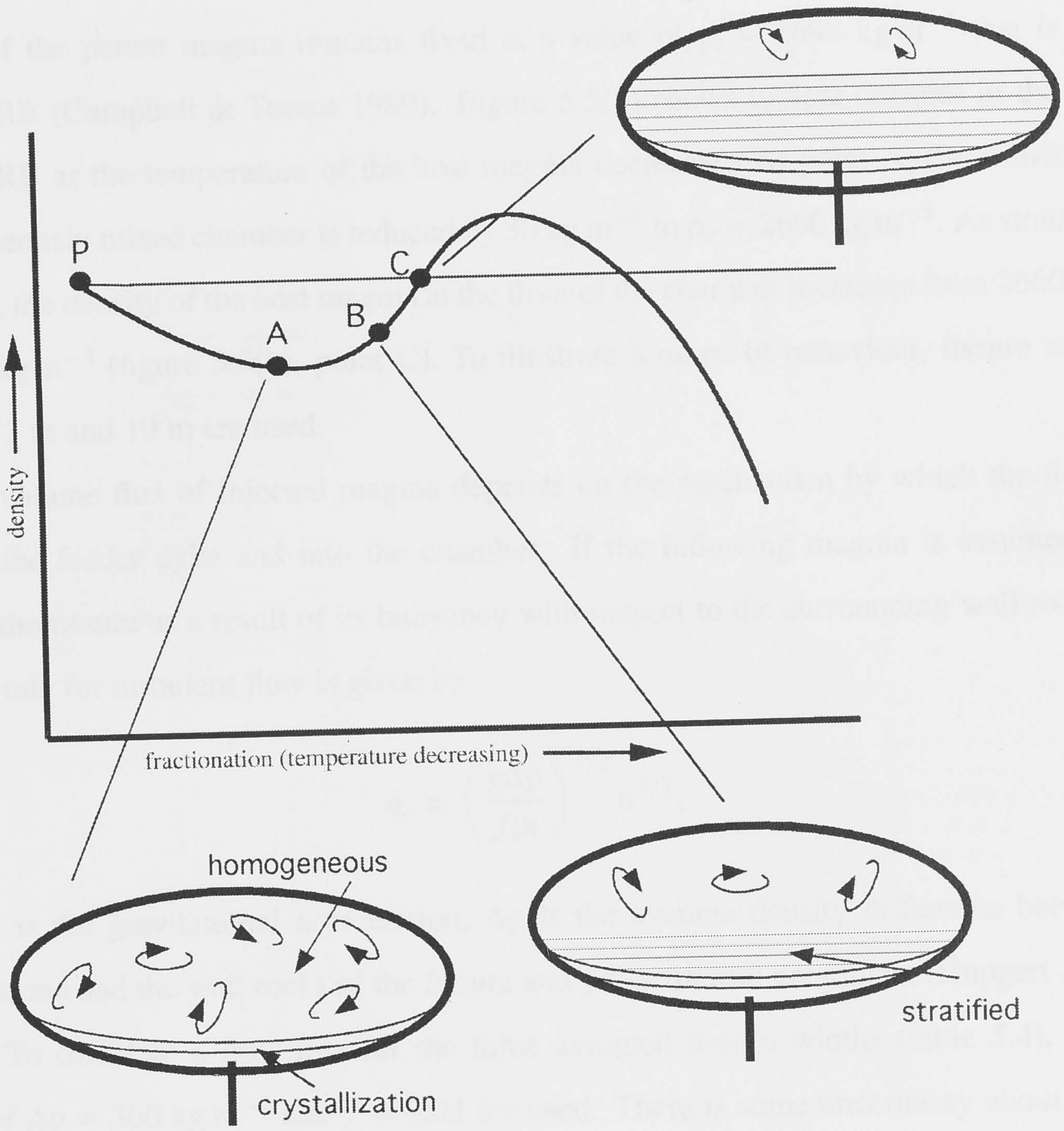

(a)

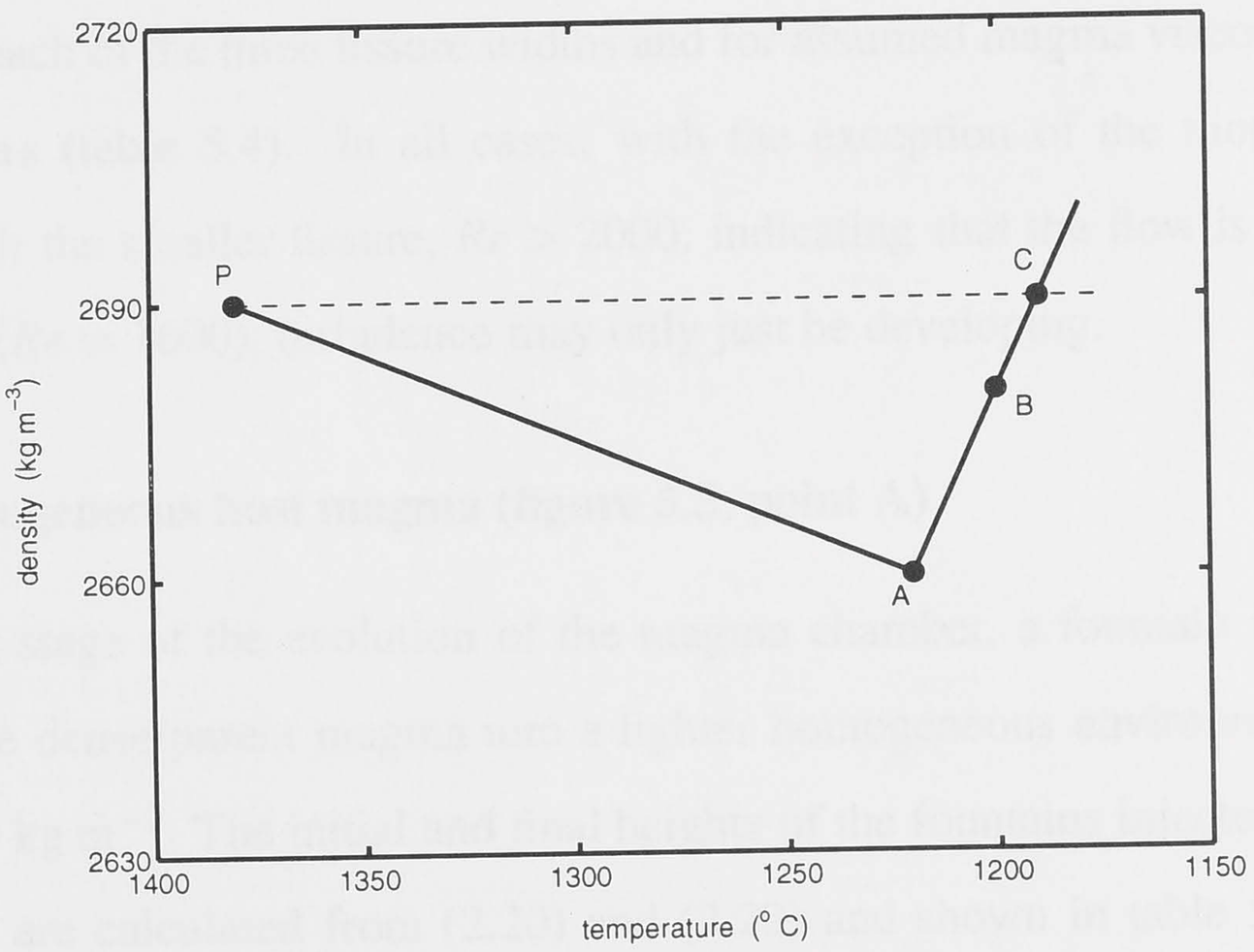

(b)

Figure 5.5: The evolution of a MORB chamber during the process of fractionation, (a) showing how a stable density stratification may be established, and (b) showing typical values of the temperature and density (modified from Campbell & Turner 1989). The plotted densities in (a) and (b) refer to the density of the host magma at the base of the chamber; the homogeneous region overlying the stratified magma remains at a constant density.

density of the parent magma remains fixed at a value of $\rho_i = 2690\ \mathrm{kg\,m^{-3}}$ that is typical of a MORB (Campbell & Turner 1989). Figure 5.5(b) shows typical changes in the density of a MORB as the temperature of the host magma decreases. At point A, the density in the homogeneously mixed chamber is reduced by $30\ \mathrm{kg\,m^{-3}}$ to $\rho_o = 2660\ \mathrm{kg\,m^{-3}}$. As stratification develops, the density of the host magma at the floor of the chamber increases from $2660\ \mathrm{kg\,m^{-3}}$ to $2690\ \mathrm{kg\,m^{-3}}$ (figure 5.5(b), point C). To illustrate a range of behaviour, fissure widths of $d = 1$ m, 3 m and 10 m are used.

The volume flux of injected magma depends on the mechanism by which the flow rises through the feeder dyke and into the chamber. If the inflowing magma is assumed to rise through the fissure as a result of its buoyancy with respect to the surrounding wall rocks, then the flow rate for turbulent flow is given by

$$q_o = \left(\frac{g\Delta\rho}{f\rho_i}\right)^{1/2} d^{3/2}, \tag{5.4}$$

where g is the gravitational acceleration, $\Delta\rho$ is the average density difference between the input magma and the wall rocks of the fissure and f is a friction coefficient (Huppert & Sparks 1985). To calculate a flow rate for the three assumed fissure widths (table 5.4), probable values of $\Delta\rho = 300\ \mathrm{kg\,m^{-3}}$ and $f = 0.03$ are used. There is some uncertainty about the most appropriate values for these quantities, especially f which is known to depend weakly on the flow parameters. To determine if the flow is turbulent, the Reynolds number, $Re = q_o\rho_i/\eta$, is calculated for each of the three fissure widths and for assumed magma viscosities of $\eta = 1$ Pa s and $\eta = 10$ Pa s (table 5.4). In all cases, with the exception of the more viscous magma flowing through the smaller fissure, $Re > 2000$, indicating that the flow is turbulent. For the one exception ($Re = 1600$), turbulence may only just be developing.

5.3.2.1 Homogeneous host magma (figure 5.5, point A)

In the first stage of the evolution of the magma chamber, a fountain is produced by the injection of the dense parent magma into a lighter homogeneous environment with a density of $\rho_o = 2660\ \mathrm{kg\,m^{-3}}$. The initial and final heights of the fountains injected through the three fissure widths are calculated from (2.20) and (2.22) and shown in table 5.4. As the fissure width increases, so does the volume flux of the source magma, resulting in higher fountains.

parameter	$d = 1$ m			$d = 3$ m			$d = 10$ m		
q_o ($m^2\,s^{-1}$)	6.0			31.4			191		
Re ($\eta = 1$ Pa s)	1.6×10^4			8.4×10^4			5.1×10^5		
Re ($\eta = 10$ Pa s)	1.6×10^3			8.4×10^3			5.1×10^4		
	A	**B**	**C**	**A**	**B**	**C**	**A**	**B**	**C**
σ^*	0	2	∞	0	6	∞	0	20	∞
z_i (m)	60	116	171	180	310	355	601	814	792
z_f (m)	34 – 45	70 – 91	157 – 168	103 – 136	203 – 257	327 – 350	344 – 453	610 – 730	731 – 782
z_s (m)	0	0	74	0	0	154	0	249	344
ρ_c ($kg\,m^{-3}$)	-	2684	-	-	2680	-	-	2674	-
$\Delta\rho_e$ ($kg\,m^{-3}$)	-	2.3	5.1	-	6.2	10.6	-	16.3	23.7
t_d (days)	0	0	6.1	0	0	2.9	0	1.1	1.3
t^* (days)	5.6	8.6	14.9	3.2	4.7	6.2	1.8	1.8	2.2
$z_a(t^*)$ (m)	59	109	243	178	303	483	592	804	1008
volume ratio	0.49	0.41	0.32	0.49	0.42	0.34	0.50	0.37	0.36

Table 5.4: Properties of line fountains injected into a magma chamber at points A, B and C from figure 5.5.

For a fissure width of $d = 1$ m, the fountain has an initial height of only 60 m and remains small compared to the height of the chamber. For a $d = 10$ m fissure, the fountain reaches an initial height of 601 m.

When the dense downflow reaches the floor of the chamber, it spreads laterally as a thin layer. The continued influx of magma results in this layer increasing in thickness and becoming stratified. The results of the line fountain filling box model developed by Baines *et al.* (1990) are used to obtain quantitative predictions of the depth of the spreading layer and the time at which the ascending front passes the top of the fountain (table 5.4). These calculations indicate that if $d = 1$ m, it takes 5.6 days to establish a stratified layer 59 m in depth, and if $d = 10$ m, it takes only 1.8 days to establish a layer that is 592 m deep.

5.3.2.2 Stratified host magma (figure 5.5, points B & C)

The dense magma which ponds at the base of the chamber as a result of the crystallization of plagioclase has a density, ρ_b, which may increase from $\rho_b = 2660$ kg m^{-3} to $\rho_b = 2690$ kg m^{-3}. Further increase in ρ_b would then result in the replenishing magma forming plumes rather than fountains (Cardoso & Woods 1993). If $\rho_b = 2680$ kg m^{-3}, for example, the total density variation over a $H = 1000$ m deep stratified region of the chamber is 20 kg m^{-3}. It is then assumed that the stratification is linear (or can be approximated as linear), giving a buoyancy frequency of $N = 8.5 \times 10^{-3}$ s^{-1}. The values of σ^* calculated for each of the three fissure widths correspond to the three regimes of behaviour; $\sigma^* < \sigma^*_c$, $\sigma^* \approx \sigma^*_c$ and $\sigma^* > \sigma^*_c$ (table 5.4). The analytical functions given in (2.21) and (2.23) are used to estimate the initial and final fountain heights, while the spreading heights are estimated from the experimental data (figure 2.14c). For fissure widths of $d = 1$ m and $d = 3$ m, the downflow spreads along the base of the chamber, although the conditions for a $d = 3$ m fissure are close to critical ($\sigma^* \approx \sigma^*_c$). If $d = 1$ m, a small fountain with an initial height of 116 m forms. As d increases, so does the height of the fountain: flow through a fissure width of $d = 10$ m produces a fountain with an initial height of 814 m. The ambient density variation over the initial fountain height, $\Delta\rho_e = z_i(\mathrm{d}\rho/\mathrm{d}z)$, is also shown in table 5.4.

The value of ρ_b which corresponds to the critical conditions between intermediate and basal spreading are also calculated for each of the fissure widths. For this critical density ρ_c,

$N^2 = -(g/\rho_c)(\rho_o - \rho_c)/H$ and $f_o = (g/\rho_c)(\rho_i - \rho_c)q_o$, giving

$$\sigma_c^* = \frac{m_o^2 \rho_c (\rho_c - \rho_o)}{H g q_o^2 (\rho_i - \rho_c)^2}. \tag{5.5}$$

Writing m_o in terms of q_o and rearranging (5.5) results in a quadratic expression for ρ_c with the one realistic root given by

$$\rho_c = \frac{2Hgd^2\sigma_c^*\rho_i - \rho_o q_o^2 - q_o(4Hgd^2\sigma_c^*\rho_i(\rho_i - \rho_o) + \rho_o^2 q_o^2)}{2(Hgd^2\sigma_c^* - q_o^2)}. \tag{5.6}$$

The calculated values of ρ_c for the three fissure widths under consideration are shown in table 5.4. If $d = 1$ m, the critical conditions are reached when $\rho_b = 2684$ kg m^{-3} (strong stratification). For a $d = 10$ m fissure, the density at the floor of the chamber decreases to $\rho_b = 2674$ kg m^{-3} (weaker stratification) before the critical conditions are reached.

When the density at the base has increased to $\rho_b = 2690$ kg m^{-3} (figure 5.5, point C), the fountain has a zero buoyancy flux at the source. The buoyancy frequency of the stratified region is then calculated to be $N = 0.01$ s^{-1}. The initial height, symmetric final height and spreading height are calculated from (2.17). As the assumed fissure width increases from $d = 1$ m to $d = 10$ m, the initial fountain height increases from 171 m to 792 m. For a fissure width of $d = 1$ m, the intruding layer spreads at a height of 74 m, and if $d = 10$ m, the spreading height increases to 344 m.

For magma injected at points B and C in figure 5.5, the subsequent evolution of the stratified magma chamber follows the stratified line fountain filling box model developed in chapter 3. The time taken to establish a homogeneously mixed layer is estimated from the time at which the ascending front passes the top of the fountain, t^*. The values of t_d (the time taken for the descending front to reach the floor of the chamber), t^* and $z_a(t^*)$ in table 5.4 are found from the model detailed in §3.3. Fountains entering the stratified chamber at earlier stages in the fractionation process (figure 5.5, point B) form a homogeneous layer as deep as the fountain in less time than the same fountains injected at later stages (figure 5.5, point C). At any stage, the larger fissures (with the greater volume flux) homogenize the chamber in less time.

Also included in table 5.4 are the calculations of the ratio of the volume of parent magma added to the volume of mixed magma in the nearly homogeneous mixed layer. For all three

fissure widths, and at all stages of the fractionation sequence, this ratio was calculated to be approximately 40%. The importance of this property in a geological context is discussed in §5.3.5.

5.3.3 Double-diffusive fountains

Magma density is a function of both composition and temperature. Apart from the immediate dynamical significance of summing their contributions to the total density difference, the combined effect of compositional and thermal differences lead to a variety of novel convective phenomena known collectively as *double-diffusive convection*. The relative contributions to the total density difference from compositional differences, $\Delta\rho_{\text{comp}}$, and from thermal differences, $\Delta\rho_{\text{temp}}$, are quantified in terms of a quantity R_ρ, where

$$R_\rho = \frac{|\Delta\rho_{\text{comp}}|}{|\Delta\rho_{\text{temp}}|}. \tag{5.7}$$

This quantity, R_ρ, provides a measure of the extent to which a system is double-diffusive; as $R_\rho \to 1$, double-diffusive convection becomes more active. A qualitative discussion of double-diffusive fountains in a homogeneous fluid was presented by Turner & Campbell (1986) (see also Campbell & Turner 1986b and Campbell & Turner 1989). In that experimental investigation, several regimes of behaviour were identified in terms of R_ρ. These experimental observations are used throughout the next section as I present a qualitative discussion of the double-diffusive behaviour that is expected in fountains at various stages in the fractionation sequence shown in figure 5.5.

5.3.3.1 Homogeneous host magma (figure 5.5, point A)

Magma injected at point A in the fractionation sequence in figure 5.5 is 160°C hotter than the homogeneous magma in the chamber, but is 30 kg m^{-3} denser. Using a thermal expansion coefficient of $\alpha = 5 \times 10^{-5}$ °C^{-1} for a basaltic magma (Jellinek & Kerr 1999b), the thermal contribution to the density difference is calculated to be $\Delta\rho_{\text{temp}} = \alpha\Delta T\rho_o = 22$ kg m^{-3}. To maintain the total density difference of 30 kg m^{-3}, therefore, the compositional contribution is 52 kg m^{-3}. At this stage, R_ρ is large, with $R_\rho = 2.4$. Due to the large density differences, the relatively small fountain establishes a strongly stratified layer at the base of the chamber,

in which hot compositionally dense magma underlies cool compositionally lighter magma. Within the stratified layer, the competition between the stabilizing compositional gradient and the destabilizing temperature gradient leads to the formation of several *diffusive convecting layers* (Turner 1973; Turner & Campbell 1986; Campbell & Turner 1986b). The initially smooth gradient therefore evolves to form a stepped profile in which the density difference between successive layers continually increases. Heat is transferred upwards through the diffusive interfaces which separate the layers, but the density differences across the interfaces ensure that the individual layers remain compositionally isolated. No further double-diffusive phenomena are observed at large values of R_ρ.

5.3.3.2 Stratified host magma: $0 < \sigma^* < \infty$ (figure 5.5, point B)

Magma injected at a later stage in the fractionation sequence enters a stratified magma chamber (figure 5.5, point B), in which the net density difference between the parent magma and the host magma at the floor of the chamber is now reduced to 10 kg m^{-3}. As the temperature difference of 180°C gives $\Delta\rho_{\text{temp}} = 24$ kg m^{-1}, the net density difference is maintained by having $\Delta\rho_{\text{comp}} = 34$ kg m^{-1}. At this point, $R_\rho = 1.4$ and double-diffusive effects are more important. To illustrate the types of behaviour that are expected, the three fissure widths are again used. If $d = 1$ m, $\sigma^* < \sigma_c^*$ and the qualitative fountain behaviour will initially be similar to that described in §5.3.3.1 for homogeneous surroundings. However, due to the greater thermal differences, the double-diffusive layers which form in the spreading layer will lose heat rapidly and the density of the spreading layer will begin to increase. Eventually, the density of the weakly stratified spreading layer may become greater than that of the downflow. If this occurs, the downflow will then begin to intrude at an intermediate height in the spreading layer. The outflow has the same density as the environment at the intrusion height, but since the intruding fluid is hotter than its surroundings, it must be compositionally denser. Under these conditions, a diffusive interface will again form at the top of the layer, while *double-diffusive fingers* will form at the base (Turner 1973). These salt fingers create a downward flux of compositionally dense magma that drives convection below the intrusion and hence maintains a well-mixed region. Intermediate intrusion may therefore occur even for fountains with $\sigma^* < \sigma_c^*$.

If magma injected at the same stage in the fractionation sequence enters the chamber through a $d = 3$ m fissure, the conditions are close to critical ($\sigma^* \approx \sigma_c^*$), and the fountain

behaviour is expected to be qualitatively similar to that described above for a $d = 1$ m fissure. The behaviour arising from magma injected through a $d = 10$ m fissure is best described by considering the $\sigma^* \to \infty$ case (§5.3.3.3).

5.3.3.3 Stratified host magma: $\sigma^* \to \infty$ (figure 5.5, point C)

If new magma is injected at point C on figure 5.5, the zero net density difference arises because the density differences due to thermal and compositional effects are equal, and hence $R_\rho = 1$. In such a strongly double-diffusive system, it is expected that the outflow will immediately experience rapid vertical convection and spread laterally as a number of intrusions at different heights (Turner 1978). As each of these layers are hotter and therefore compositionally denser than the surrounding magma, diffusive interfaces will form at the top of the layers and double-diffusive fingers will develop at the base. The subsequent behaviour and evolution of the fountain and environment will then be controlled by the competition between the filling box process (which tends to homogenize the initially stratified environment) and double-diffusive effects (which lead to the formation of layers in the environment).

5.3.4 Effects of viscosity

In the experimental and theoretical analysis of turbulent fountains presented in the previous chapters, it was assumed that the source and ambient fluids have the same viscosity. The effects of differences in viscosity were investigated experimentally by Campbell & Turner (1985, 1986a), who were particularly interested in understanding the behaviour of turbulent fountains entering a more viscous magma chamber.

When a parent magma with viscosity ν_1 is injected into a chamber containing host magma with viscosity ν_2 ($\nu_2 \gg \nu_1$), entrainment is only possible if the turbulent energy is sufficient to distort the bounding interface between the two magmas. Campbell & Turner (1985, 1986a) showed that the limiting conditions at which the viscosity of the host magma inhibits such distortion are defined by $\omega d = k\nu_2$, where k is a constant (a value of $k = 70$ was determined experimentally for axisymmetric fountains), ω is the velocity of the injected magma at the source and d is the width of the source. In terms of the Reynolds number of the upflow, $Re = \omega d/\nu_1 = k\nu_2/\nu_1$. Hence, as ν_2/ν_1 increases, Re must also increase if mixing is to remain

possible.

Campbell & Turner (1985, 1986a) showed that fountains entering a basaltic magma chamber are unlikely to experience any reduction in mixing due to the small ratio of host to parent magma viscosities ($\nu_2/\nu_1 \approx 10$). In contrast, if a basaltic magma is injected into a granitic chamber, the viscosity ratio may be as large as six orders of magnitude ($\nu_2/\nu_1 \approx 10^6$). While the rapid injection of a dense basaltic magma remains turbulent, any mixing of host magma is completely inhibited.

If any reduction in mixing occurs between a fountain and its stratified surroundings, the amount of lighter ambient fluid mixed into the fountain decreases, causing the final density of the downflow to increase towards the density of the injected fluid. In a stratified fluid, the downflow therefore falls further before reaching a height of neutral density, thus increasing σ_c^*. At the extreme conditions under which mixing is completely inhibited, the density of the fluid in the fountain does not change at all, and the downflow always remains heavier than (or equal to) the maximum ambient density.

In their experiments, Campbell & Turner (1985, 1986a) noted that when mixing was inhibited, little difference was observed in the fountain height. In contrast, it was shown in chapter 4 that any reduction in the amount of mixing from the environment into the downflow causes a decrease in the fountain height.

5.3.5 Geological interpretation and implications

As mentioned in §5.3.2.2, the volume ratio of parent magma to that which has accumulated in the mixed layer can be important geologically. When the injected and ambient magmas have different compositions (for example, olivine-saturated and plagioclase-saturated magmas), this mixing ratio is needed to determine the final composition, and hence the properties, of magma in the mixed layer. The mixing ratios of around 40% found in our calculations would result in a mixed magma which is significantly undersaturated in both olivine and plagioclase. This mixed magma would have erosive properties (Kerr 1994), leading to further evolution of the chamber and surrounding rocks. In particular, the level at which this erosive magma contacts the chamber boundaries may be important. When basal spreading occurs, the magma is in contact with the floor of the chamber, which could be eroded and assimilated back into the melt. If intermediate spreading occurs, the only contact between the erosive magma and the

boundaries occurs on the sidewalls at the level of intrusion.

In a number of large magma chambers, *cyclic layering* is observed (Wager & Brown 1968). This geological feature is identified by a number of cyclic units within which the composition of successive layers follows the fraction sequence. The key feature of cyclic layering is that the base of each cyclic unit marks an abrupt return to a more primitive composition. This layering is believed to be caused by phases of replenishment, as the injection of hot, primitive magma increases the temperature and returns the host magma to a previous stage in the fractionation sequence. Cyclic layering is therefore regarded as plausible evidence of the replenishment of a magma chamber by a fountain (Campbell & Turner 1989). In addition, cyclic layering is closely associated with rich deposits of platinum and chromium in two examples of large magma chambers – the Bushveld Complex in South Africa and the Stillwater Complex in the USA. An understanding of the effects of turbulent fountains on magma chambers may therefore also have economic implications.

5.4 Conclusions

I have introduced a number of examples of turbulent fountains, and applied the results of the current study to two specific cases.

The dynamics of a turbulent fountain of air in a thermally stratified room were addressed by considering two examples: a small room which is cooled by the injection of cool air upwards through a vent in the floor, and a large aircraft hanger which is heated by the injection of warm air downwards through a number of vents in the ceiling. I applied the results from chapters 2 and 3 to determine the time required to cool the air in the lower 2 m of a small room, and to calculate the room temperature at this time. The example of injecting hot air down into a cold aircraft hanger through a series of vents showed the relationship between the final ambient temperature and the time taken to reach this temperature.

Finally, I have illustrated the dynamics of a turbulent line fountain which results from the rapid injection of a dense magma into a pre-existing magma chamber. Using results from chapters 2 and 3, I have calculated the timescales required to homogenize an initially stratified magma chamber under a range of conditions which vary depending on the stage of the fractionation sequence.

Chapter 6

Conclusions

"Knowledge is an unending adventure at the edge of uncertainty."

Jacob Bronowski (1908 - 1974)

Polish Mathematician and Philosopher of Science

In this chapter, I summarize the major results and conclusions of this investigation. Finally, I outline some related problems which represent a challenge for the future.

6.1 Summary of results

In this thesis, I have presented the results of an experimental and theoretical study of the dynamics of turbulent fountains in homogeneous and stratified environments.

A study of the behaviour of turbulent fountains in an unbounded stratified environment was reported in chapter 2. Extensive experiments indicated that the behaviour of both axisymmetric and line fountains falls into one of two regimes, identified by basal or intermediate spreading. The initial, final and spreading heights were measured as a function of the dimensionless parameter, σ, and expressions were developed for the heights in the limits of $\sigma = 0$ and $\sigma \to \infty$. The critical value of σ that marks the transition between basal and intermediate spreading was determined for axisymmetric and line fountains.

The effects of confining boundaries on the flow were explored in chapter 3. Expressions were derived to quantify the motion of the ascending and descending fronts as well as the rise of the fountain height as the initially stratified environment becomes homogeneously mixed. In addition, a simple numerical scheme was outlined to quantify the changes to the ambient density stratification.

In chapter 4, I developed theoretical models of axisymmetric and line fountains were developed in which sets of entrainment equations were used to quantify the turbulent mixing between the upflow, the downflow and the environment. These equations were integrated numerically, and it was found that the calculated fountain properties in a stratified fluid compared well with experimental data.

Finally, in chapter 5, the results of this study were used to quantify the behaviour of axisymmetric fountains of air in buildings, and line fountains of magma in magma chambers.

6.2 Further work

The understanding of turbulent fountains represents a continuing challenge – even after this extensive study, there remain a number of further problems which could be explored in more detail.

Inclined turbulent fountains: In many applications, turbulent fountains are inclined at some angle to the vertical when they enter the environment. In their study of fountains in a homoge-

neous fluid, Baines *et al.* (1990) presented experimental measurements of the height reached by a fountain inclined at 7°to the vertical. These preliminary results indicated that an inclined fountain penetrates further into the environment than a vertical fountain, and consequently mixes more extensively with the environment. An experimental study of fountains in a homogeneous fluid, in which the angle of inclination is varied, will identify the angle that optimizes the mixing between the fountain and the environment (some preliminary experiments have already been performed by myself, M. Cooper and R. Kerr). Once the optimum mixing angle has been found in a homogeneous fluid, a similar investigation could proceed in a stratified fluid as $\sigma \to \infty$. If the optimum mixing angle found under these conditions differs from that determined in a homogeneous fluid, then further investigation would be needed to determine the dependence of the angle on the parameter σ. This knowledge of the optimum mixing angle is of practical importance in engineering applications such as building ventilation, as the increased mixing is obtained at no extra cost.

A similar study of inclined line fountains may reveal additional interesting properties. While vertical line fountains were observed to fluctuate between a symmetric and an asymmetric profile, inclined line fountains are forced into an asymmetric profile. By varying the angle of inclination, more insight may be gained into why the profile fluctuates, and why the fountain height decreases when the profile is asymmetric (as opposed to the expected increase due to the reduction in the interaction between the upflow and downflow).

Line fountains with different geometries: In order to investigate the cause of the fluctuations in line fountains, experimental measurements could be made of a line fountain produced from a source that is no longer placed centrally along the length of the tank. This imposed asymmetry would cause the spreading layer to increase in thickness faster on one side of the fountain. The effect of the asymmetric ambient density profile on the fountain dynamics could then be examined experimentally.

Experiments could also be performed in a larger tank in which the source no longer extends across the entire tank width. These experiments would verify whether the presence of a crossflow in the environment is responsible for the decrease in the fountain height when the profile becomes asymmetric. In addition, these experiments could give greater insight into whether the stability of the fountain profile is affected when the ambient fluid on either side of

the fountain is isolated from the other side.

Double-diffusive fountains: In my discussion of fountains in magma chambers, I briefly outlined the expected behaviour of double-diffusive fountains in a stratified fluid. However, there is scope for a detailed experimental study of double-diffusive fountains in both homogeneous and stratified environments. Some experiments were performed in a homogeneous fluid (Turner & Campbell 1986; Campbell & Turner 1986b; Campbell & Turner 1989), although the results were mainly qualitative. A quantitative exploration of double-diffusive fountains may lead to greater insight into the formation of mineral deposits in magma chambers.

Bibliography

ASAEDA, T. & IMBERGER, J. 1993 Structure of bubble plumes in linearly stratified environments. *J. Fluid Mech.* **249**, 35–57.

BAINES, W.D., TURNER, J.S. & CAMPBELL, I.H. 1990 Turbulent fountains in an open chamber. *J. Fluid Mech.* **212**, 557-592.

BAINES, W.D. & TURNER, J.S. 1969 Turbulent buoyant convection from a source in a confined region. *J. Fluid Mech.* **37**, 51–80.

BAINES, W.D., CORRIVEAU, A.F. & REEDMAN, T.J. 1993 Turbulent fountains in a closed chamber. *J. Fluid Mech.* **255**, 621–646.

BATCHELOR, G.K. 1954 Heat convection and buoyancy effects in fluids. *Q. J. R. Met. Soc.* **80**, 339–358.

BLOOMFIELD, L.J. & KERR, R.C. 1998 Turbulent fountains in a stratified fluid. *J. Fluid Mech.* **358**, 335–356.

BLOOMFIELD, L.J. & KERR, R.C. 1999a Turbulent fountains in a confined stratified fluid. *J. Fluid Mech.* **389**, 27–54.

BLOOMFIELD, L.J. & KERR, R.C. 1999b A theoretical model of a turbulent fountain. Submitted to *J. Fluid Mech.*.

BRIGGS, G.A. 1969 *Plume Rise*. U.S. Atomic Energy Commission Critical Review Series.

CAMPBELL, I.H. & TURNER, J.S 1985 Turbulent mixing between fluids with different viscosities. *Nature* **313**, 39–42.

CAMPBELL, I.H. & TURNER, J.S. 1986a The influence of viscosity on fountains in magma chambers. *J Petrol.* **27**, 1–30.

CAMPBELL, I.H. & TURNER, J.S. 1986b The role of convection in the formation of platinum and chromitite deposits in layered intrusions. In: Scarfe, C.M. (Ed.) *Mineralogical Association of Canada Short Course in Silicate Melts*, 236–278.

CAMPBELL, I.H. & TURNER, J.S. 1989 Fountains in magma chambers. *J. Petrol.* **30**, 885-923.

CAMPBELL, I.H., MCDOUGALL, T.J. & TURNER, J.S. 1984 A note on fluid dynamic processes which can influence the deposition of massive sufides. *Econ. Geol.* **79**, 1905–1913.

CARDOSO, S.S.S. & WOODS, A.W. 1993 Mixing by a turbulent plume in a confined stratified region. *J. Fluid Mech.* **250**, 277–305.

CAULFIELD, C.P. & WOODS, A.W. 1998 Turbulent gravitational convection from a point source in a non-uniformly stratified environment. *J. Fluid Mech.* **360**, 229–248.

CRAPPER, P.F. 1977 A note on the characteristics of a two–dimensional jet produced by a series of co–planar three–dimensional jets. *J. Indust. Aero.* **2**, 181–183.

EALES, H.V. & CAWTHORN, R.G. 1996 The Bushveld Complex. In: Cawthorn, R.G. (ed.) *Layered Intrusions*, Elsevier Science, 181–229.

FISCHER, H.B., LIST, E.J., KOH, R.C.Y., IMBERGER, J & BROOKS, N.H. 1979 *Mixing in Inland and Coastal Waters*. Academic Press.

GERMELES, A.E. 1975 Forced plumes and mixing of liquids in tanks. *J. Fluid Mech.* **71**, 601–623.

GOLDMAN, D. & JALURIA, Y. 1986 Effect of opposing buoyancy on the flow in free and wall jets. *J. Fluid Mech.* **166**, 41–56.

HUPPERT, H.E. & SPARKS, R.S.J. 1980 The fluid dynamics of a basaltic magma chamber replenished by influs of hot, dense ultrabasic magma. *Contrib. Mineral. Petrol.* **75**, 279–289.

HUPPERT, H.E. & SPARKS, R.S.J. 1985 Komatiites I: Eruption and flow. *J. Petrol.* **26**, 694-725.

HUPPERT, H.E. & TURNER, J.S. 1981 A laboratory model of a replenished magma chamber. *Earth Planet. Sci. Lett.* **54**, 144-152.

HUPPERT, H.E., SPARKS, R.S.J., WHITEHEAD, J.A. & HALLWORTH, M.A. 1986 Replenishment of magma chambers by light inputs. *J. Geophys. Res.* **91**, 6113–6122.

JELLINEK, A.M. & KERR, R.C. 1999a Mixing and compositional stratification produced by

natural convection 1. Experiments and their application to Earth's core and mantle *J. Geophys. Res.* **104**, 7183–7201.

JELLINEK, A.M. & KERR, R.C. 1999b Mixing and compositional stratification produced by natural convection 2. Applications to the differentiation of basaltic and silicic magma chambers and komatiite lava flows *J. Geophys. Res.* **104**, 7203–7218.

KERR, R.C. 1994 Dissolving driven by vigorous compositional convection. *J. Fluid Mech.* **280**, 287–302.

KOH, R.C.Y. & BROOKS, N.H. 1975 Fluid dynamics of waste-water disposal in the ocean. *Ann. Rev. Fluid Mech.* **7**, 187–210.

KOTSOVINOS, N.E. & LIST, E.J. 1977 Plane turbulent buoyant jets. Part I: Integral properties. *J. Fluid Mech.* **81**, 25–44.

LINDBERG, W.R. & PETERSEN, J.D. 1991 Negatively buoyant jet (or plume) with application to snowplow exit flow behaviour. *Transportation Research Record* **1304**, 219–229.

LIST, E.J. 1982 Mechanics of turbulent buoyant jets and plumes. In: Rodi, W. (ed.) *Turbulent Buoyant Jets and Plumes*. Pergamon Press, 1–68.

LIST, E.J. 1982 Turbulent jets and plumes. *Ann. Rev. Fluid Mech.* **14**, 189-212.

MANINS, R.C. 1979 Turbulent buoyant convection from a source in a confined region. *J. Fluid Mech.* **91**, 765–781.

MARSH, B.D. 1989 Magma chambers. *Ann. Rev. Earth Planet. Sci.* **17**, 439–474.

MCDOUGALL, T.J. 1978 Bubble plumes in stratified environments. *J. Fluid Mech.* **85**, 655–672.

MCDOUGALL, T.J. 1981 Negatively buoyant vertical jets. *Tellus* **33**, 313–320.

MERZKIRCH, W. 1974 *Flow Visualization*. Academic Press.

MIZUSHINA, T., OGINO, F., TAKEUCHI, H. & IKAWA, H. 1982 An experimental study of vertical turbulent jet with negative buoyancy. *Wärme-und Stoffübertragung* **16**, 15–21.

MORTON, B.R., TAYLOR, G.I. & TURNER, J.S. 1956 Turbulent gravitational convection from maintained and instantaneous sources. *Proc. Royal Soc. London A* **234**, 1-23.

MORTON, B.R. 1959a Forced plumes. *J. Fluid Mech.* **5**, 151-163.

MORTON, B.R. 1959b The ascent of turbulent forced plumes in a calm atmosphere. *Int. J. Air Poll.* **1**, 184-197.

MORTON, B.R. 1962 Coaxial Turbulent Jets. *Int. J. Heat Mass Transfer* **5**, 955–965.

OSTER, G. 1965 Density Gradients. *Sci. Am.* **213**, 70-76.

PINCINCE, A.B. & LIST, E.J. 1973 Disposal of brine into an estuary. *J. Water Pollut. Control Federn.* **45**, 2335–2344.

SPARKS, R.S.J., BURSIK, M.I., CAREY, S.N., GILBERT, J.S., GLAZE, L.S., SIGURDSSON, H. & WOODS, A.W. 1997 *Volcanic Plumes*. John Wiley & Sons.

TURNER, J.S. 1966 Jets and plumes with negative or reversing buoyancy. *J. Fluid Mech.* **26**, 779-792.

TURNER, J.S. 1973 *Buoyancy Effects in Fluids*. Cambridge University Press.

TURNER, J.S. 1978 Double-diffusive intrusions into a density gradient. *J. Geophys. Res.* **83**, 2887-2901.

TURNER, J.S. 1986 Turbulent entrainment: the development of the entrainment assumption, and its application to geophysical flows. *J. Fluid Mech.* **173**, 431-471.

TURNER, J.S. & CAMPBELL, I.H. 1986 Convection and mixing in magma chambers. *Earth Sci. Rev.* **23**, 255-352.

WAGER, L.R. & BROWN, G.M. 1968 *Layered Igneous Rocks*. Oliver and Boyd.

WILSON, L., SPARKS, R.S.J., HUANG, T.C. & WATKINS, N.D. 1978 The control of volcanic column heights by eruption energetics and dynamics. *J. Geophys. Res* **83**, 1829-1836.